A FRACTURE AND TEXTURE ANALYSIS OF THE BAKKEN FORMATION, MONTANA

by

Eric Joseph Easley

A thesis submitted in partial fulfillment
of the requirements for the degree

of

Master of Science

in

Earth Sciences

MONTANA STATE UNIVERSITY
Bozeman, Montana

November 2014

©COPYRIGHT

by

Eric Joseph Easley

2014

All Rights Reserved

ACKNOWLEDGEMENTS

I first would like to thank my advisor and committee chair, Dr. David R. Lageson, for his tremendous support and advice on this project. I extend my deepest, and sincerest thanks to Dr. Lowell Miyagi. I am indebted to him for his input, inspiration and willingness to always drop whatever he was doing to assist. Without Lowell this project would be greatly lacking in content and perspective. I would also like to thank Dr. David Mogk and Dr. David Bowen for their thoughts, input and critique of this work and for serving as members on my committee.

I would like to thank Jacob Thacker, Jack Borski, Nicholas Atwood, Betsy Kruk, Tom Evans, and the rest of the structure crew for their insight, perspective, help and advice. I also thank Dr. Rudy Wenk and Jane Kanitpanyacharoen for their help and advice with shales, and the folks at the USGS Core Research Center John Rhoades, Dawn Ostyre and Josh Hicks. I would like to extend special gratitude to Steve and Leigh Ann Easley for their moral support and inspiration. Lastly I would like to thank Evan Easley for his motivation and much-needed humor during the course of this thesis. This project would not have been possible without the support of Marathon Oil Corp's Geological Sciences Support Fund and the MSU Department of Earth Sciences.

TABLE OF CONTENTS

1. INTRODUCTION 1

2. GEOLOGIC SETTING 4

The Williston Basin 4
The Bakken Formation and Total Petroleum System 9
Depositional History 14
History of Production 19
Production in the 1950s 19
Production in the 1960s 19
Production since the 1980s 20
Future Production 21
Fractures in the Bakken Formation 22

3. PURPOSE 25

4. CORE FRACTURE ANALYSIS 26

Methods 28
Results and Discussion 32
Fractures in Core 32
Petrographic Analysis 47
A-1 Stark 48
44-24 Vaira 54

5. OUTCROP FRACTURE ANALYSIS 62

Methods 63
Results and Discussion 66
Logan Gulch 72
Antelope Valley 74
Hardscrabble Peak 74
Moose Creek 77
Fracture Analysis 79

6. X-RAY TEXTURE ANALYSIS 87

Methods 87

TABLE OF CONTENTS – CONTINUED

Results and Discussion 102
Preferred Orientation 102
Seismic Anisotropy 110

7. CONCLUSIONS 124

REFERENCES CITED 127

APPENDICES 135

APPENDIX A: Fracture Data Collected in Core 136
APPENDIX B: Fracture Data Collected in the Field 153
APPENDIX C: Seismic Anisotropy Calculations 176

LIST OF TABLES

Table Page

1. Mudrock classification 11

2. Sappington Member outcrop locations 63

3. Synchrotron XRD samples 89

4. Voigt-Reuss-Hill approximations 100

5. P- and S-wave velocities 117

LIST OF FIGURES

Figure Page

1. Williston Basin stratigraphic chart 5

2. Williston Basin tectonic map 7

3. Generalized stratigraphic chart of the Bakken Formation 10

4. Map of structural features within the Williston Basin 12

5. Map of Silurian and Devonian ocean circulation 15

6. Paleogeographic map of the North American craton 17

7. Map of production in the Williston Basin 20

8. Slabbed core of the middle member showing fractures 23

9. Map of core locations 27

10. A-1 Stark core example study interval 29

11. Example of fracture measurements in core 30

12. Timing of diagenesis in the Bakken Formation 33

13. Fractures in the A-1 Stark core 35

14. Rose plots of the A-1 Stark core 37

15. Rose plots of the 44-24 Vaira core 38

16. Pyritization in the A-1 Stark core 40

17. Rose plots of the Flatwillow 1-31H and Watson Flats 1-12-23-7 cores 41

LIST OF FIGURES – CONTINUED

Figure Page

18. Bar graphs of fracture length and aperture 43

19. Bar graph of fracture intensity in all cores 44

20. Fracture intensity in A-1 Stark and 44-24 Vaira cores 46

21. Photomicrograph of the Three Forks Formation 48

22. Porosity within the middle Bakken member 49

23. Re-crystallization around fractures 51

24. Erosional lag in the 44-24 Vaira core 53

25. Fracture propagation in the Three Forks Formation 55

26. Framework grains of the middle member in the 44-24 Vaira core 56

27. Fractures in the middle member in the 44-24 Vaira core 58

28. Thin section scan of the upper shale in the 44-24 Vaira core 59

29. Map of the Sappington Member outcrop locations 64

30. Logan Gulch outcrop 67

31. Antelope Valley outcrop 68

32. Hardscrabble Peak outcrop 69

33. Moose Creek outcrop 70

LIST OF FIGURES – CONTINUED

Figure Page

34. Regional map showing dominant fracture sets 71

35. Rose plots of fractures at Logan Gulch 73

36. Rose plots of fractures at Antelope Valley 75

37. Rose plots of fractures at Hardscrabble Peak 76

38. Rose plots of fractures at Moose Creek 78

39. Geologic map of the area surrounding Moose Creek 80

40. Bar graph of fracture length 81

41. Bar graph of fracture aperture 82

42. Line graph of log length and log aperture 84

43. Regional map showing fracture sets from outcrop 85

44. Map of X-ray diffraction sample locations 90

45. Synchrotron diffraction hutch 92

46. Synchrotron diffraction experiment set-up 93

47. Sample BND1 diffraction profile 94

48. Debye ring figures 95

49. Pole figure coverage 96

50. Diffraction image showing variation in intensity 103

51. Pole figures of sample R311c 104

LIST OF FIGURES – CONTINUED

Figure Page

52. Pole figures of sample R311a 105

53. Sketch of clay platelets 106

54. Pole figures of outcrop samples 107

55. Line graph of clay volume and preferred orientation 109

56. Line graph of clay volume and anisotropy 112

57. Line graph of anisotropy and preferred orientation 113

58. Line graph of quartz volume and anisotropy 114

59. Line graph of carbonate mineral volume and anisotropy 115

60. P- and S-wave velocities with respect to bedding 119

61. Shale anisotropy from around the world 120

62. Diagram of seismic wave propagation in shales 122

ABSTRACT

The Bakken Formation underlies much of eastern Montana, North Dakota and Saskatchewan, with correlative units extending in the subsurface beyond these regions. It is composed of three informal members: an upper shale member, a middle silty limestone/dolostone member, and a lower shale member. The Bakken petroleum system acts as a conventional and unconventional reservoir within the Williston Basin and fractures that occur naturally within the Bakken petroleum system can either help or hinder reservoir characteristics. Unconventional reservoirs, such as the Bakken Formation, rely heavily on fracture enhancement (hydraulic fracturing) to become producible oil plays. Pre-existing fractures and weaknesses open more readily with fracture stimulation than the creation of new fractures, and have been correlated to increased early production in shale plays. To determine the influence of these fractures on the reservoir in the Bakken Formation and its correlative units, fractures in core and outcrop were examined.

Clay-rich shales, such as those within the Bakken Formation, display high intrinsic anisotropy, which can be helpful in interpreting seismic profiles. Despite the importance of shale oil reservoirs, the contribution of preferred orientation of minerals to shales is not well constrained. These constituent clay minerals are phyllosilicates that acquire preferred orientation during sedimentation and early diagenesis. Hard X-rays produced from a synchrotron source are effective at extracting orientation distributions of individual mineral components within a shale.

Crystallographic preferred orientation can be determined through synchrotron X-ray diffraction and the interpretation of three-dimensional images by using a Rietveld refinement method. This method incorporates a least squares approach to produce a calculated model of the degree of preferred orientation. Samples of the Bakken shales from wells in North Dakota and Montana, and outcrops from southwestern Montana were investigated. Individual phyllosilicate minerals such as illite, smectite, muscovite, and chlorite yield individual orientation patterns. The elastic properties of each shale sample were determined by averaging the calculated properties of each mineral phase over their orientation distributions. The presence of specific clay minerals and degree of anisotropy is highly variable from well to well. A better understanding of shale anisotropy could help improve exploration and production of unconventional shale oil reservoirs.

INTRODUCTION

Technological advancements in drilling and geologic understanding have made reservoirs that are not naturally commercially viable economically producible (Zou et al., 2013). These unconventional reservoirs, such as the Bakken Formation in Montana, North Dakota, Alberta and Manitoba, require reservoir stimulation for recovery within portions of the basin. The Bakken Formation is one of the largest conventional, and unconventional, domestic hydrocarbon reservoirs (Sonnenberg and Pramudito, 2009; Sonnenberg et al., 2011; Pollastro et al., 2012). Because of this, it is extremely important to understand the Bakken Formation, how fractures form, and how these fractures can help or hinder production.

The Bakken Formation extends throughout the Williston Basin without interruption, varying in thickness, lithology and fracture density. Fracture geometry, intensity and connectivity are important when evaluating a reservoir. In order to evaluate a fractured, unconventional reservoir, such as the Bakken Formation, a study on multiple scales of observation must be performed.

The aim of this study was to elucidate the fracture characteristics of the Montana portion of the Bakken shales. This was achieved by addressing the questions below:

1. What are the fracture attributes in core, what are the dominant fracture sets, and what is the relationship between fractures and diagenesis?
    a. What are the dominant fractures within core?
    b. How do they relate to lithology?
    c. How do fractures relate to porosity?
2. Are there outcrop equivalents of the Bakken Formation in Montana?
    a. What are the major fracture sets?
    b. What are the fracture attributes?
    c. How do they differ from the Williston Basin?
3. What is the seismic anisotropy of the shales within the Bakken Formation and how does it affect exploration and production?
    a. What causes preferred orientation within the shale members?
    b. What is the seismic anisotropy of the Bakken?
    c. How does seismic anisotropy in the Bakken differ from other oil-bearing shales around the world?

In order to accomplish the above questions, four Bakken cores drilled in Montana were examined. Fracture attributes including length, orientation, aperture and vein fill were measured. Thin sections were taken from the cores in order to determine their relationship with diagenesis. In order to study outcrop equivalents of the Bakken, the Sappington Member of the Three Forks Formation was chosen

based on its exposure in southwestern Montana and its time-equivalence with the Bakken Formation. The main portion of this study was to determine the seismic anisotropic characteristics of the shales within the Bakken Formation. Clay-rich shales, like the Bakken Formation, display intrinsic anisotropy that changes seismic prospecting results. In order to complete this objective, samples taken from core were diffracted with synchrotron X-ray diffraction. They were then imported into Material Analysis Using Diffraction (MAUD) to calculate the mineral orientation distribution functions (ODFs) and then brought into the University of California Berkley texture package BEARTEX to generate a model of seismic anisotropy.

GEOLOGIC SETTING

The Williston Basin

The Williston Basin in Montana, North Dakota, South Dakota, Manitoba and Saskatchewan contains over four kilometers of Cambrian through Tertiary sedimentary cover in an area of approximately 770,000 km^2 (~300,000 mi^2). Starting in the Cambrian period, sedimentation within the basin was controlled by cyclic transgressive sequences (Ahren and Mrckvica, 1984; Crowley et al. 1985; Gerhard et al., 1987; Nelson et al., 1993; Pitman et al., 2001). Ten petroleum systems span the Phanerozoic section (Figure 1), and are actively producing hydrocarbons from predominantly marine Paleozoic rocks and siliciclasitc Mesozoic and Cenozoic rocks (Sonnenberg and Pramudito, 2009; Sonnenberg et al., 2011; Pollastro et al., 2012). The basin has undergone little tectonic deformation since deposition of sedimentary cover.

Originally a craton-margin basin in the Western Canada Sedimentary Basin the Williston eventually evolved into an intracratonic basin after the Superior craton and the Wyoming and Churchill (Hearne) cratons were sutured together by the Proterozoic Trans-Hudson Orogenic belt province (Ahren and Mrckvica, 1984; Crowley et al. 1985; Gerhard et al., 1987; Pitman et al., 2001; Nelson et al., 1993; Sonnenberg and Pramudito, 2009; Pollastro et al., 2012). Intracratonic basins are unlike continental-margin and ocean basins in that the former forms due to

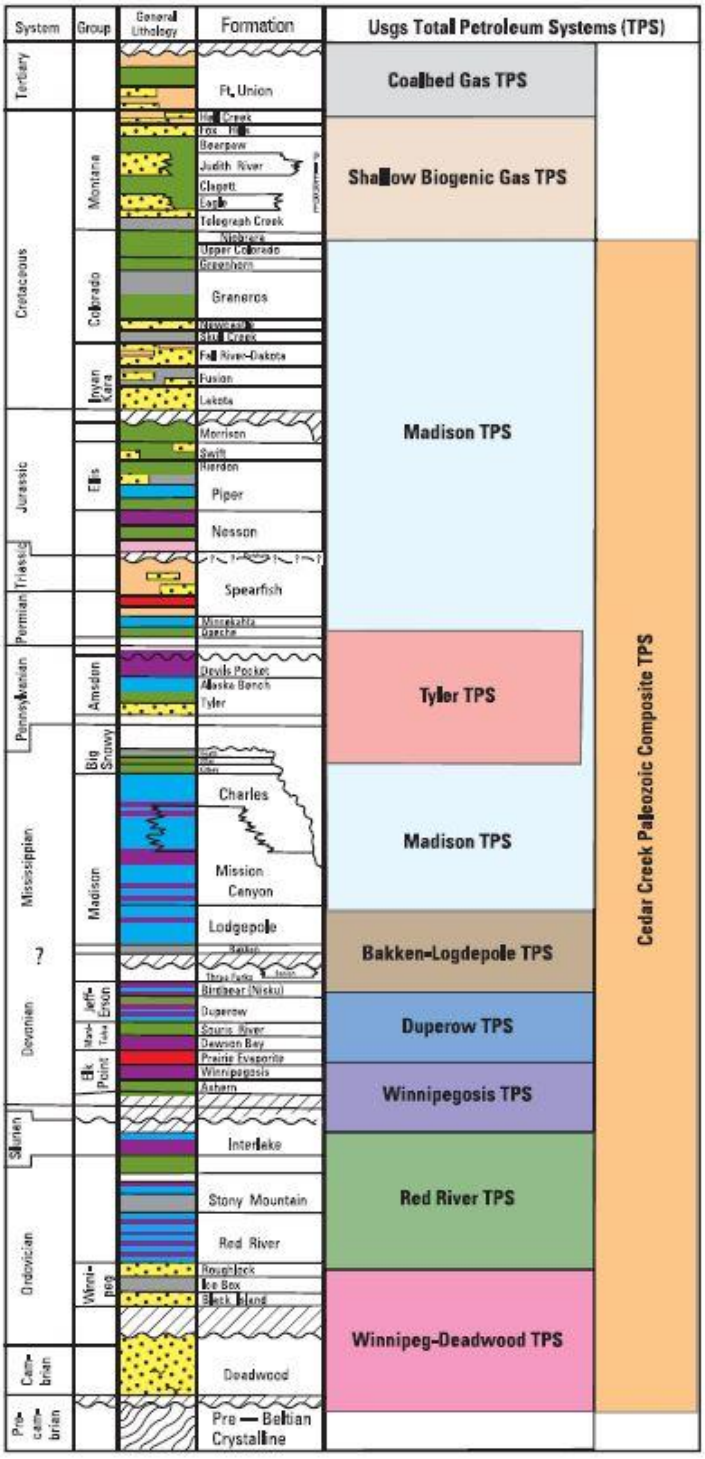


Figure 1. Generalized stratigraphic chart of the Williston Basin in North Dakota and Montana. USGS petroleum systems are shown in the right column (Pollastro et al., 2012).

heated and thinned lithosphere from tectonic processes. In addition, intracratonic basins are not directly affected by tectonic process along plate margins, however thermal anomalies and deformation related to plate boundary tectonics are still observed within these basins (Crowley et al., 1985).

Development of the Williston Basin occurred during the initial subsidence in the Ordovician. Two of the most common mechanisms for the origin of intracratonic basins are conductive cooling of the lithosphere and subsidence from a metamorphic phase change in the lower crust (Baird et al., 1995 and references therein). However, new deep reflection profiles crossing the Williston Basin from the Consortium for Continental Reflection Profiling reveal no distinct reflection Moho under the basin. This phenomenon has been linked to the presence of a collisional crustal root from the Hudsonian collision (ending ~1.7Ga). This remnant consequently transformed to eclogite, creating a shallower, gradational Moho, and causing the subsidence and creation of the Williston Basin (Bensen et al., 2009; Baird, et al., 1995).

The initiation of subsidence is relatively well constrained beginning in the Ordovician period (~495 Ma). A nearly complete sedimentary record within the basin was originally thought to be due to episodic subsidence, but the Williston underwent four major transgressive sequences (Sloss Sequences) during Paleozoic and Mesozoic sedimentation (Porter et al., 1982). The Paleozoic Sauk, Tippecanoe, Kaskaskia and Absaroka sequences occurred during the basin's

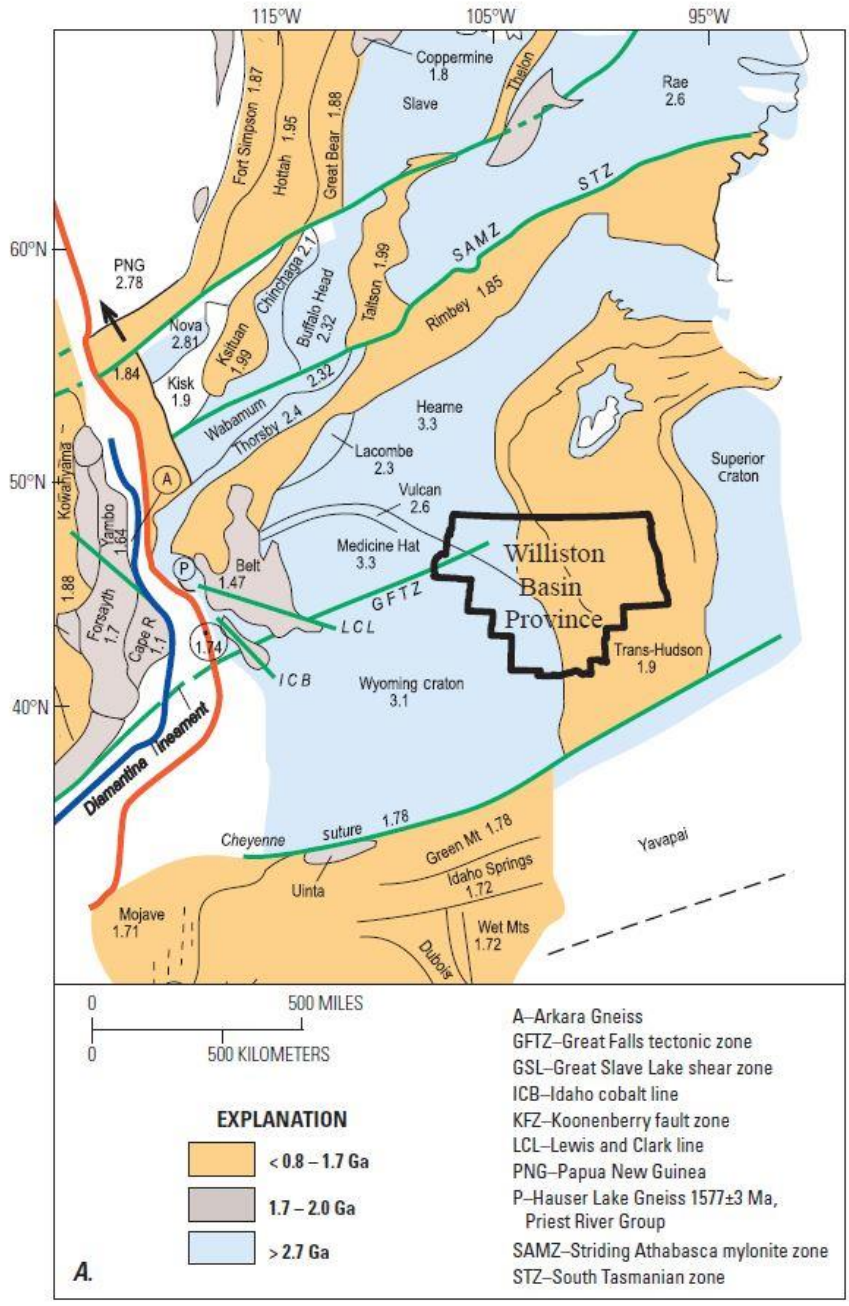


Figure 2. Map showing the Great Falls Tectonic Zone (GFTZ), the Cheyenne Suture Zone and the Precambrian cratons that make up the basement of the basin. The reactivated fault systems are responsible for many of the structural features within the basin (Anna et al., 2010).

evolution and the unconformities within the sedimentary sequence represent periods of global sea level rise. Subsidence was relatively constant throughout the Phanerozoic, allowing for an almost complete sedimentary section to accumulate (Fowler and Nisbet, 1984).

The Williston Basin is structurally simple because of its distal relationship with the Rocky Mountain front. However, the shear systems (Figure 2) are believed to have transferred stress from the western North American plate boundary into the basin, acting as a "stress conduit," throughout the basin's lifetime (Warner, 1978). The majority of the structures in the basin are related to compressive and transpressive deformation. Features such as the Nesson Anticline, Little-Knife Anticline and Billings Anticline trend north/south whereas the Antelope structure, Poplar Dome and Cedar Creek Anticline trend northwest/southeast (Gerhard et al., 1982). As mentioned, wrench fault tectonics from the two Archean shear systems are believed to control the structural framework of the basin and structural features within the Williston Basin are consistent with left-lateral movement. Folding, faulting, salt dissolution and subsidence contribute to the fracture network that allows for unconventional hydrocarbon production within the basin (Pollastro et al., 2012).

The Bakken Formation and TPS

The upper Devonian (Famenian) lower Mississippian (Tournasian) Bakken Formation unconformably overlies the Devonian Three Forks Formation and is overlain by the Mississippian Lodgepole Formation of the Madison Group (Figure 3). It consists of three informal members: a lower organic and carbon-rich siltstone and shale member, a middle calcareous-dolomitic sandstone and siltstone member, and an upper carbonaceous siltstone and shale member (Karma, 1991; Smith and Bustin, 1998; Smith and Bustin, 2000; Kreis and Costa, 2005; Kreis et al., 2006; Sonnenberg and Pramudito, 2009; Pollastro et al., 2012). The Bakken Formation is continuous in the subsurface in the Canadian portion of the basin and is lithostratigraphically consistent with the Exshaw/Banff Formations in Alberta. The name Bakken is given to this series of rocks that only occurs in the subsurface (Pitman et al., 2001).

The classification and nomenclature of mudrocks is not well agreed upon and terms such as shale or mudstone are primarily umbrella terms fine-grained, clay-rich rocks. For clarity purposes, the upper and lower members of the Bakken Formation will be referred to as shales and the Lundegard and Samuels (1980) classification of mudrocks will be used in this work to describe the lithology of mudrocks in core and outcrop (Table 1).

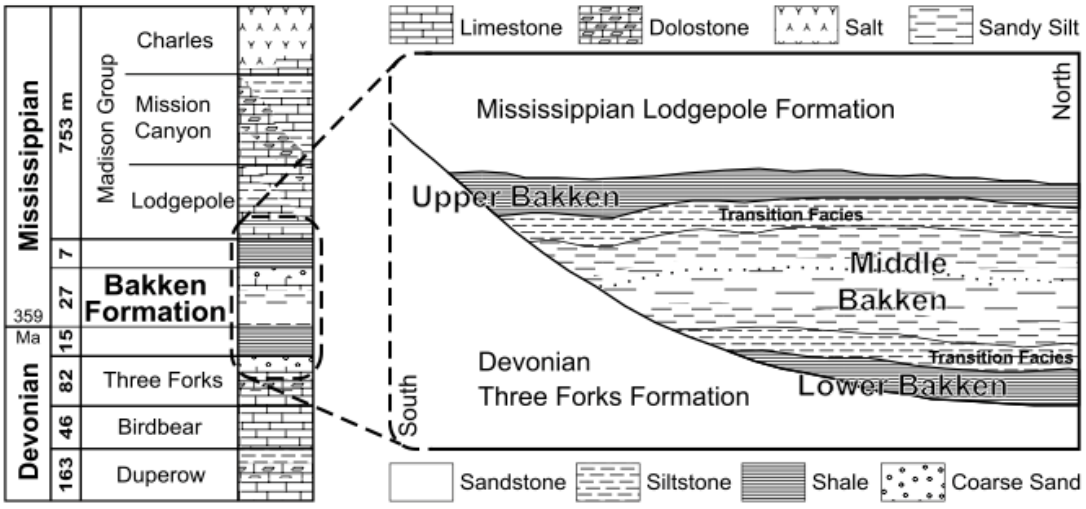


Figure 3. Generalized stratigraphic section of the Bakken Formation. Note the onlapping relationship of the member in the southern and western (not shown) extent of the Williston Basin (Kuhn et al., 2012).

The Bakken Formation is thickest in the center of the basin in North Dakota. Within the deepest portions of the basin, the Bakken system is considered a continuous accumulation of hydrocarbons. Sonnenberg and Pramudito (2009) outlined what is required for a continuous accumulation: extensive hydrocarbon charge, no definitive oil- or gas-water contact, diffuse boundaries, elevated pressure, large in-place resource with a low recovery factor, low water production, geologically-controlled “sweet spots,” reservoirs close to mature source rocks, low matrix permeability, and water occurring up-dip from hydrocarbons. All of these criteria are observed within the deepest portions of the Williston Basin, making it one of the largest continuous accumulations of hydrocarbons in the United States

Silt Content	**> 2/3**	**1/3 - 2/3**	**< 1/3**
Laminated	laminated siltstone	mudshale	clayshale
Nonlaminated	siltstone	mudstone	claystone

Table 1. Modified version of the Lundegard and Samuels (1980) mudrock classification scheme.

(Sonnenberg and Pollastro, 2009).

Marine mudstones that make up the upper and lower members of the Bakken Formation are lithologically consistent throughout the basin and are similar to each other. However the middle member varies in thickness, lithology and petrophysical properties. Lithologies include sandstone, silty limestone, dolomite and siltstone (Karma, 1991; Kreis and Costa, 2005; Kreis et al., 2006; Chen et al., 2009; Pollastro et al., 2012). This variation in lithology is due to proximity of sediment source and diagenesis. The lower shale member averages 3 m in thickness with a maximum of 20 m; the middle member averages a thickness of 13 m with a maximum thickness of 30 m; the upper shale member averages a thickness of 2 m with a maximum of 7 m (Smith and Bustin, 1998; Pitman et al., 2001; Smith and Bustin, 2000; Sonnenberg and Pramudito, 2009).

A total petroleum system (TPS) contains all essential elements and associated processes such as source, seal, trap, reservoir, oil-generation, migration etc. (Magoon and Schmoker, 2000). The Bakken TPS consists of the Bakken Formation, the Sanish Sands Member of the Three Forks Formation and the

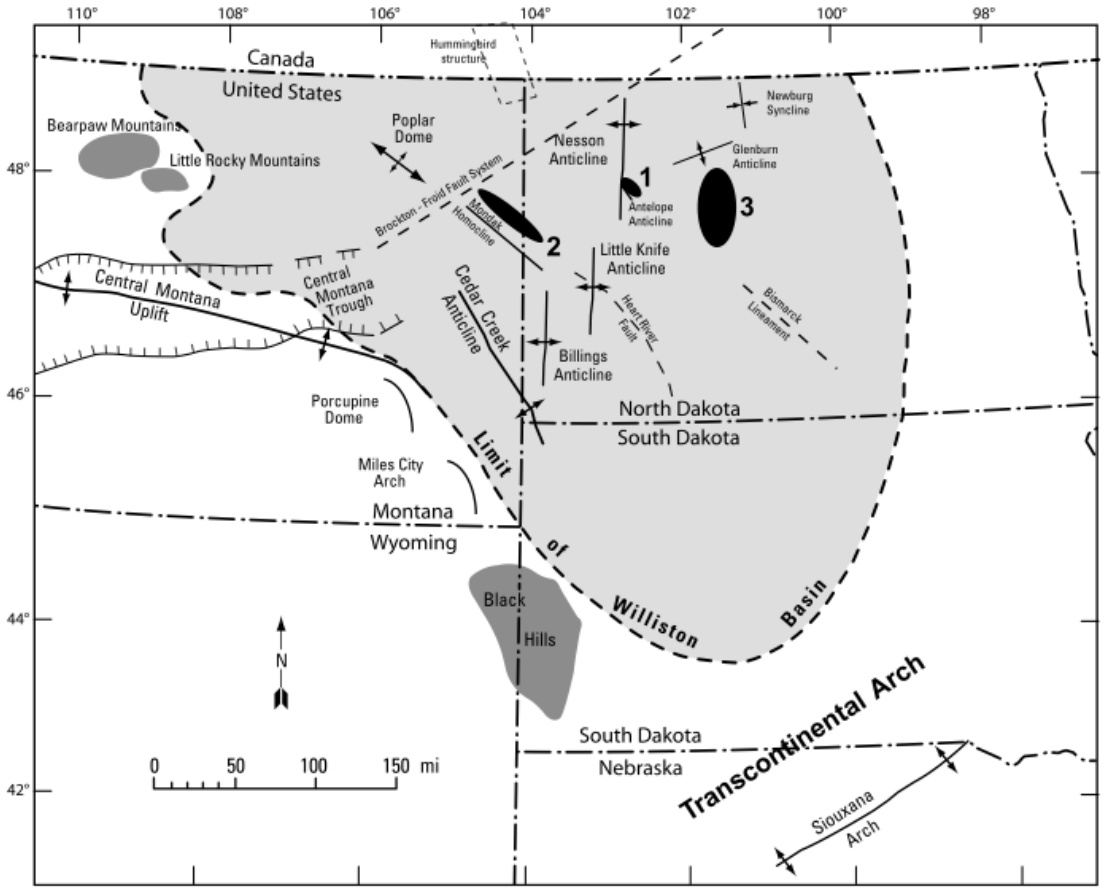


Figure 4. Map displaying the structural features within the Williston Basin. Solid black ovals represent major production regions of the Bakken TPS: 1) Antelope Field, 2) Elm Coulee Field, 3) Parshall and Sanish Sands Field. The majority of the features trend north to northwest (Pollastro et a., 2012).

Scallion Member in the lower Lodgepole limestone (Pollastro et al., 2012; Mark Sonnenfeld, personal communication). The upper and lower shales are extremely similar; they are almost entirely finely laminated, siliceous, slightly calcareous, pyritic, fissile, hemipelagic, organic-rich mudstones that act as sources for hydrocarbons in the system. The dominant organic content within the mudstones is Type II oil-prone kerogen and is distributed evenly throughout the shales

(Meissner, 1978; Hill, 2012). Fossil accumulations and bioturbation are more prevalent within the lower shale (Sonnenberg and Pramudito, 2009). Despite their variation in thickness, the total organic content (TOC) is relatively similar. The lower shale contains an average of 8% TOC and a maximum of 20% TOC whereas the upper shale contains an average of 10% TOC and a maximum of 35% TOC (Smith and Bustin, 2000; Kuhn et al., 2012; Mark Sonnenfeld, Personal Communication).

The middle Bakken member only acts as a conventional reservoir within the system when part of a structural high, such as at the Little Knife and Nesson anticlines (Figure 4). Due to its low porosity (< 8%) and permeability (< 0.1 mD), the middle member sometimes requires horizontal drilling and multi-stage hydraulic fracturing (Meissner, 1978; Smith and Bustin, 2000; Sonnenberg and Pramudito, 2009). The middle member has been dissected into many different units. Smith and Bustin (2000) split the middle member into three different subunits; Pitman et al. (2001) separated it into seven different lithofacies; Canter et al. (2009) split it into eight different facies. Despite the numerous models to accurately represent the entirety of the middle member, the spatial variability within it forces each model to only represent the member locally.

Hydrocarbon generation in the Bakken TPS is considered a closed system, and occurred within the upper and lower shale members, which then migrated into the middle member. However, oil has been produced locally from the Sanish

Sands member of the Three Forks Formation and the Scallion Member within the lower Lodgepole Formation (Pollastro et al., 2012; Sarg, 2012; Sonnenfeld, 2013).

The Mississippian Charles Formation and Middle Devonian Prairie Formation contain salt intervals that act as regional barriers against vertical migration within the Missippian and Devonian petroleum systems. These intervals also contribute to oil-bearing reservoirs acting as seals (Chen et al., 2009). However dissolution within the Prairie Salts has caused collapse within the overlying Mississippian strata, and formed fracture networks allow for oil migration between the Bakken TPS and the Madison TPS (Chen et al., 2009).

Depositional History

During the Late Devonian most of the Williston Basin was exposed to erosion due to sea level drop, allowing the formation of the Acadian unconformity that underlies the Bakken Formation. Following this sea level drop there was a eustatic sea-level rise at the end of the Devonian that resulted in an epicontinental sea that covered a large portion of North America between the Equator and 30° N in a tropical to sub-tropical climate (Smith and Bustin, 1998; Angulo and Buatois, 2011). The uplift of the Transcontinental arch tilted the Williston Basin northward, limiting the interaction between the basin and the Cordilleran shelf to the south (Montana Trough), forcing marine circulation through the Elk Point Basin to the northwest (Figure 5). This restriction was responsible for the deposition of the

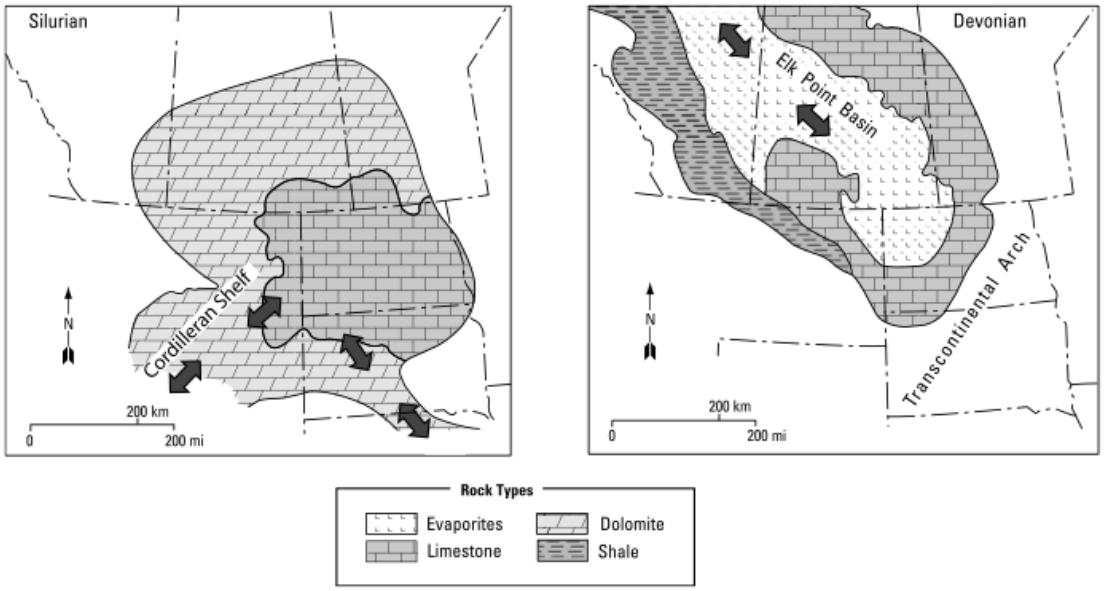


Figure 5. Diagram of the change in deposition patterns and open ocean circulation with the epicontinental sea from the Silurian to the Devonian. Arrows indicate open marine circulation (Pollastro et al., 2012).

organic, black mudstones. The environment is thought to be similar to a modern open marine environment, though there is no modern analog for an epeiric sea (Smith and Bustin, 2000; Pollastro et al., 2012).

The lower shale represents a Late Devonian (365 Ma) transgression, that first accumulated in the deepest portions of the basin in North Dakota and subsequently spread outwards. It has been proposed that the shales in the Bakken Formation represent a deep-marine sediment-starved basin where subsidence exceeded the rate of sedimentation (Karma, 1991; Pitman et al., 2001). Whether continental flooding, increased rates of subsidence, or a combination of both, the lower shale was deposited during a period of sea level rise.

Sediment accumulation rates of ~1-3 m per million years, similar to rates in modern open ocean environments, indicate that sediment most likely originated from fallout of airborne clay- and silt-sized particles (Smith and Bustin, 1998; Hlava et al., 2012). The absence of storm-generated features and erosion of the mudstones implies that deposition was below the storm wave base in > 200 m of water (Smith and Bustin, 2000; Pitman et al., 2001; Pollastro et al., 2012). Three possible conditions can exist in a sediment-starved basin: anaerobic conditions (oxygen depleted), dysaerobic conditions (minimal oxygen) and aerobic conditions (normal levels of oxygen).

These levels of oxygen correlate to depths within the water column. Anything below 150 m of water is considered anaerobic, and displays fine laminations, dark color and high organic content, as seen in the Bakken shales and is consistent with a depth of ~200 m as evidenced by the lack of storm-generated features (Karma, 1991). The water column is believed to have been stratified with estuarian-like circulation and upwelling of nutrient-rich water confined to the upper portion of the water column. The deepest parts of the basin received no circulation resulting in stagnation and anoxic conditions, allowing for preservation of organic material (Smith and Bustin, 1998).

The middle Bakken member has been interpreted as a shallow water marine environment. However, the many lithofacies within the member are variable and each represent deposition in shallow to deep shelf environments (Sonnenberg et

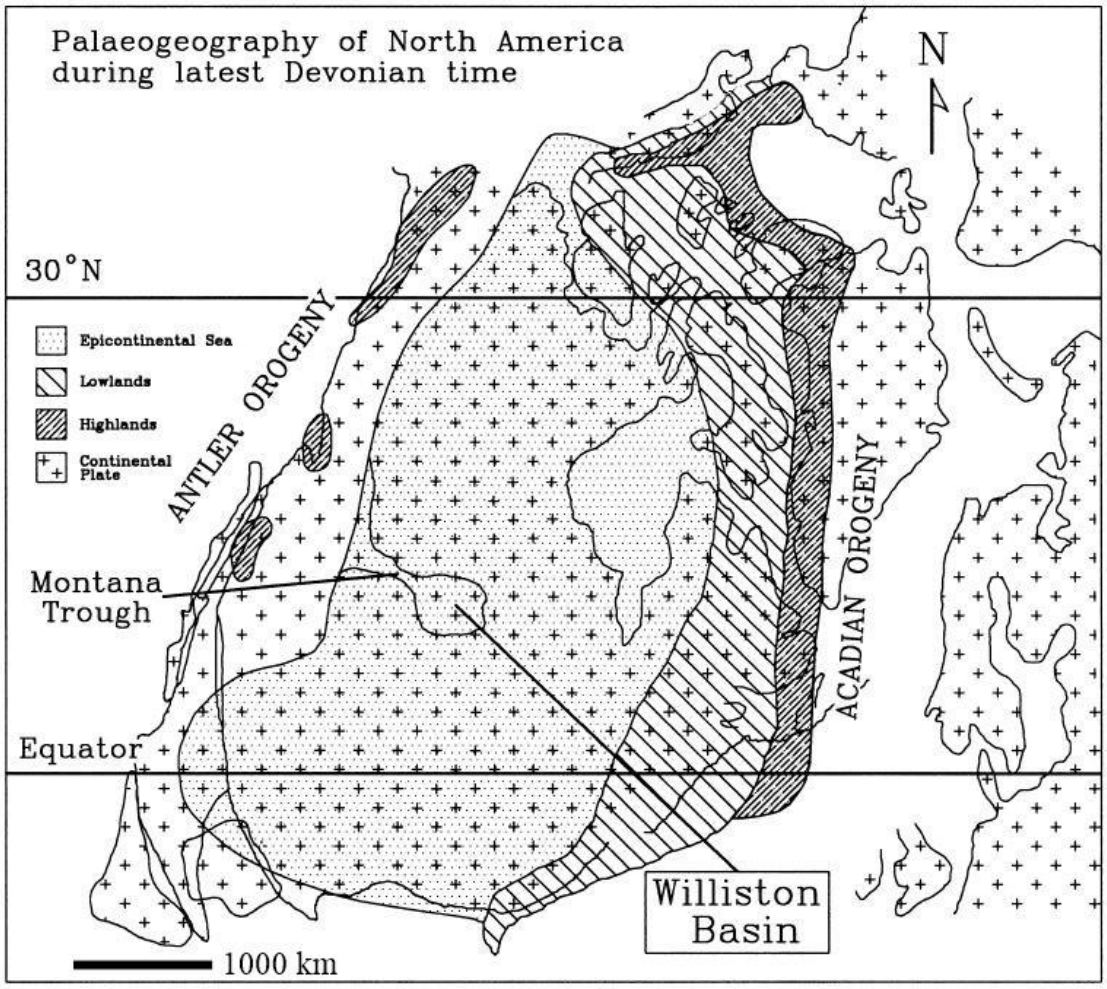


Figure 6. Paleogeographic map of the North American craton during the deposition of the basal shale member of the Bakken Formation. The Williston Basin is far from any orogen. Sediment was sourced from wind-blown sediment (Modified from Smith and Bustin, 1998).

al., 2011; Sarg, 2012). Given its lithologies found within the center of the basin, the member was deposited in less than 10 m of water, resting unconformably above the lower shale member. The basal calcareous siltstone represents the initial sea-level fall, which transferred the basin into a shallow shelf. Sea level rose into a lower shelf environment before drowning and transitioning into the upper deep

marine shale member evidence by a gradation between the bioclast sandstone and the dolomitic siltstone as (Kreis and Costa, 2005; Sonnenberg et al., 2011; Sarg et al., 2012).

The upper shale member is extremely similar to the lower member in lithology and depositional environment, however it is thinner than the lower member and contains higher TOC (Pitman et al., 2001). The upper shale represents a transgression after the fall of sea level during the deposition of the middle member. The basal contact of the upper member with the middle member is abrupt and represents a period of erosion before inundation and deposition onto the continent (Smith and Bustin, 1998; Smith and Bustin, 2000).

During this sea-level rise of North America, the terrestrial sediment sources within the basin were scarce (Smith and Bustin, 1998). The epicontinental sea was bounded on the east by the Acadian Mountains and the north and northeast by the cratonic highlands, which acted as distal sources for sediment, most likely transported by wind (Figure 6). Marginal sediment sources to the west and northwest came from the Antler, Caribou and Ellesmerian Mountains (Smith and Bustin, 1998).

History of Production

Production in the 1950s

The Bakken TPS has undergone multiple cycles of exploration and production beginning in the 1950s (Figure 7). 1953, the first discovery of the Bakken Formation occurred in the Antelope Field in North Dakota as a conventional vertical well. Stanolind Oil was targeting the Mississippian Madison petroleum system, but the lack of success forced them to explore the Bakken Formation. 536 barrels of oil (BO) were produced cumulatively from this well. Most of the wells within this field were drilled in the 1950s and 1960s, and targeted both the Bakken and the underlying Sanish Sands Member of the Three Forks Formation, cumulatively producing 19.4 million billion barrels of oil (LeFever, 2005; Sonnenberg and Pramudito, 2009).

Production in the 1960s

Subsequent discovery did not occur until 1961, when Shell Oil Company used seismic prospecting to locate structures within the Elkhorn Ranch Field in North Dakota. They targeted the Ordovician Red River Formation. This also revealed the depositional limit of the Bakken Formation (Bakken Fairway). The well produced 136 barrels of oil per day (BOPD) until the casing collapsed and the well was abandoned. In 1967 Pan American Petroleum Corporation drilled a well in the Hofflund Field along the Nesson Anticline in North Dakota. This initially

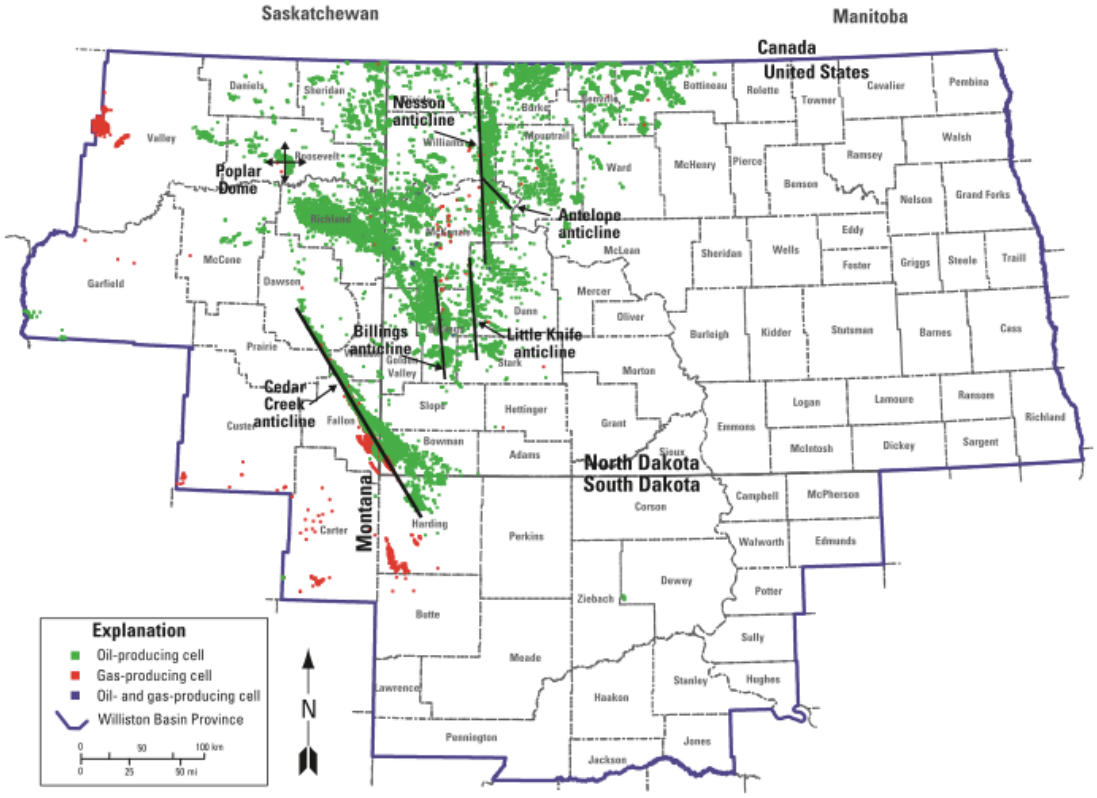


Figure 7. Production within the Williston Basin. Green points are oil-producing wells, red points are gas-producing wells and blue points are oil- and gas-producing wells. The blue outline is the Williston Basin province defined by the USGS (Pollastro et al., 2012).

produced 756 BOPD, and 62,700 BO cumulatively after well perforation until the casing collapsed and was abandoned in 1969 (LeFever, 2005; Sonnenberg and Pramudito, 2009).

Production since the 1980s

In 1987, Meridia Oil, Inc. drilled and completed the first horizontal well in the Billings Nose Field within the Bakken play in North Dakota. The well produced 258 BOPD, and almost 200,000 BO for the first two years until

production dropped off. This discovery spurred on heavy exploration and production through horizontal drilling and fracture enhancement (LeFever, 2005). Production slowed until 2000 when an independent driller discovered oil in the Elm Coulee Field in Richland County, Montana. The well was targeting the middle Devonian Nisku Formation, with the Bakken Formation as a secondary target. The failure of the Nisku target prompted production of the Bakken Formation through horizontal drilling and fracture stimulation. Wells within this field have initially produced between 200 and 1200 BOPD, and projected 300,000 to 750,000 BBO per well (Sonnenberg and Pramudito, 2009).

Future Production

In 2013, the USGS conducted a geologic-based assessment of the total reserves in the Bakken TPS. The assessment included both the Bakken and Three Forks Formations, which in previous assessments had only included the Bakken Formation. The USGS estimated technically recoverable continuous resources to be 7,375 million barrels of oil (MMBO), 6,723 billion cubic feet of gas (BCFG), and 527 million barrels of natural gas liquids (MMBNGL). They also estimated that there is 8 MMBO and 7 BCFG contained within conventional reservoirs (US Department of the Interior, 2013).

Fractures in the Bakken Formation

Fractures play a large role when exploring many unconventional hydrocarbon reservoir like the Bakken TPS, as they contribute to reservoir porosity and permeability and influence fluid migration. Their condition, quantity, length, spacing and porosity (i.e. interconnectivity) all have effects on the reservoir, and the greater these characteristics are the greater production of the reservoir. Even though the reservoir rocks within the Bakken TPS have a measureable matrix porosity (i.e. storage capacity), a fracture network is required for a commercially viable well (Pollastro et al., 2012).

The Williston Basin has been exposed to multiple tectonic processes including wrench faulting, folding, fault-block movement, as well as salt dissolution and induced collapse of overlying rock. All of these processes have contributed to the fracture network that allows the system to be producible (Carlisle et al., 1992; Chen et al., 2009; Pollastro et al., 2012). In addition to fracture formation from the mechanisms discussed above, fractures also form in-situ from the production and maturation of kerogen. This process occurs primarily in the lower and upper members or in regions of high organic material. Each member within the petroleum system contains horizontal and vertical fractures both mineralized and open (Pitman et al., 2001).

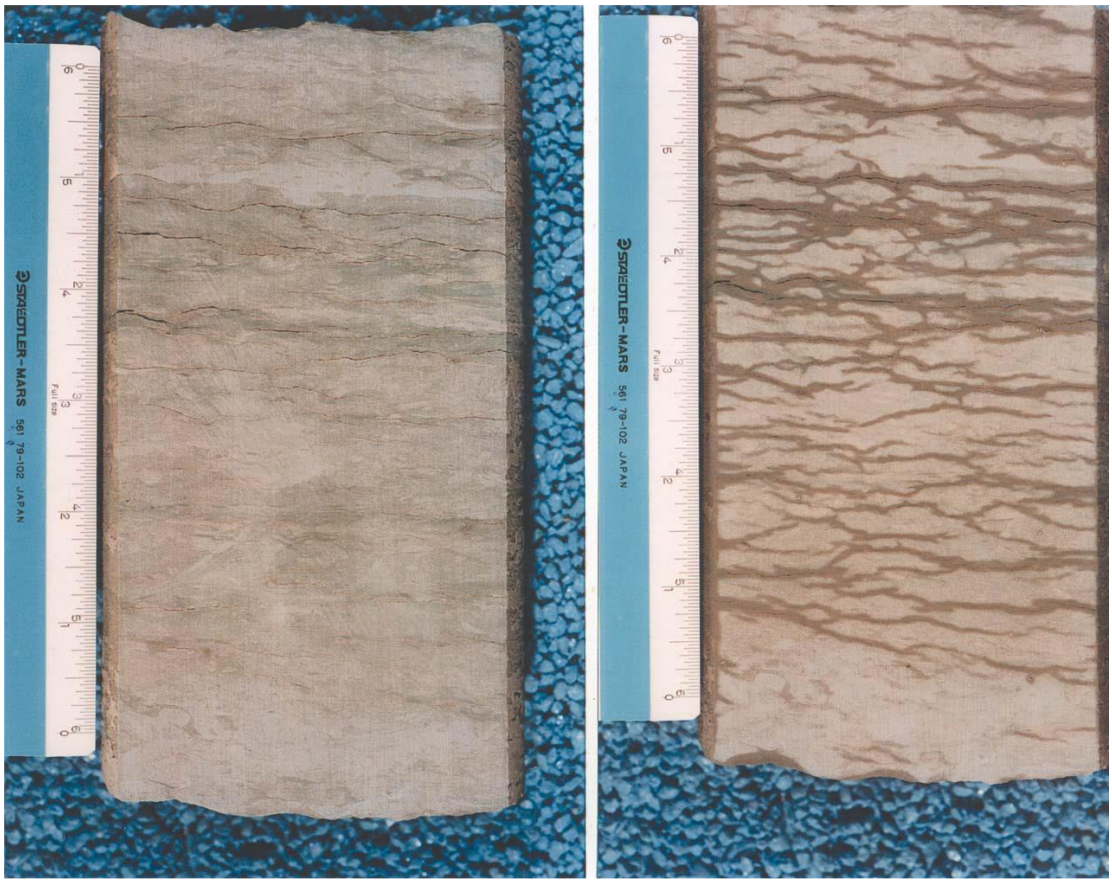


Figure 8. Slabbed core of the middle member displaying a horizontal fracture network on both the wet and dry core. Fractures in core retain water longer than the surrounding rock (Pitman et al., 2001).

Horizontal fracturing within the middle member is believed to have resulted from the expulsion of hydrocarbons from the upper and lower shales into the middle siltstone through overpressurization (Figure 8). However the most extensive fracture networks observed occur in oil-saturated reservoir rocks adjacent to mature shales (Pitman et al., 2001). Beds with high amounts of clay and organic content are the most fractured and provide the most reservoir storage

allowing successful production (Carlisle et al., 1992). The fissility from clay minerals allows for higher fracturing within the shales.

Productivity of the Bakken TPS is directly linked to the maturity of the shales. The greater the maturation the more resources are stored and the greater the interconnectivity of the fracture network becomes (Carlisle et al., 1992; Pitman et al., 2001). The upper and lower members contain sub-horizontal to vertical bitumen filled fractures that are believed to have formed during hydrocarbon generation and large pore systems have been found to form within the shales (Hill, 2012).

PURPOSE

The purpose of this study is to investigate the role that fractures play, of multiple scales, in the Bakken Formation in Montana as well as their relationship to diagenetic processes that can improve and/or degrade reservoir characteristics such as porosity, permeability, reservoir continuity and thermal maturity. This project offers an observational study of fractures in core and outcrop that potentially identifies the timing, orientation and mechanisms of fractures that contribute to the production of oil within the Bakken Formation.

In addition to a study of fractures on multiple scales, this project aims to elucidate the effect of clay minerals on the elasticity of the shales. Seismic anisotropy that is observed in many clay-rich, hydrocarbon-bearing shales is not well constrained, and an understanding of how anisotropy affects seismic wave propagation within one of the largest domestic accumulations of hydrocarbons will improve the understanding of unconventional shale oil reservoirs.

CORE FRACTURE ANALYSIS

Four, non-producing, cores containing Late Devonian to Early Mississippian strata from Montana were observed at the United States Geological Survey Core Research Center (CRC) in Denver, CO. Cores were chosen based on their spatial position within Montana and their spatial relationship with the Williston Basin (Figure 9). Fracture generation, orientation, and relationship to diagenesis were the main focus for core analysis.

The A-1 Stark core located within Fallon County, MT, and operated by Anadarko Productions contains the upper and middle Bakken members and the upper portion of the Three Forks Formation within its 54 foot cored interval. The lower shale member is absent and the middle Bakken member lies disconformably above the Three Forks Formation. This disconformity is consistent with the onlapping relationship observed within the margins of the Williston Basin and the Bakken Formation (Figure 3).

The 44-24 Vaira core in Richland County, MT, operated by Balcron Resources contains the basal member of the Lodgepole Formation, the upper and middle members of the Bakken Formation, and the upper member of the Three Forks Formation. This core, also drilled on the edge of the basin, is missing the lower shale member. The middle Bakken member overlies the upper Three Forks

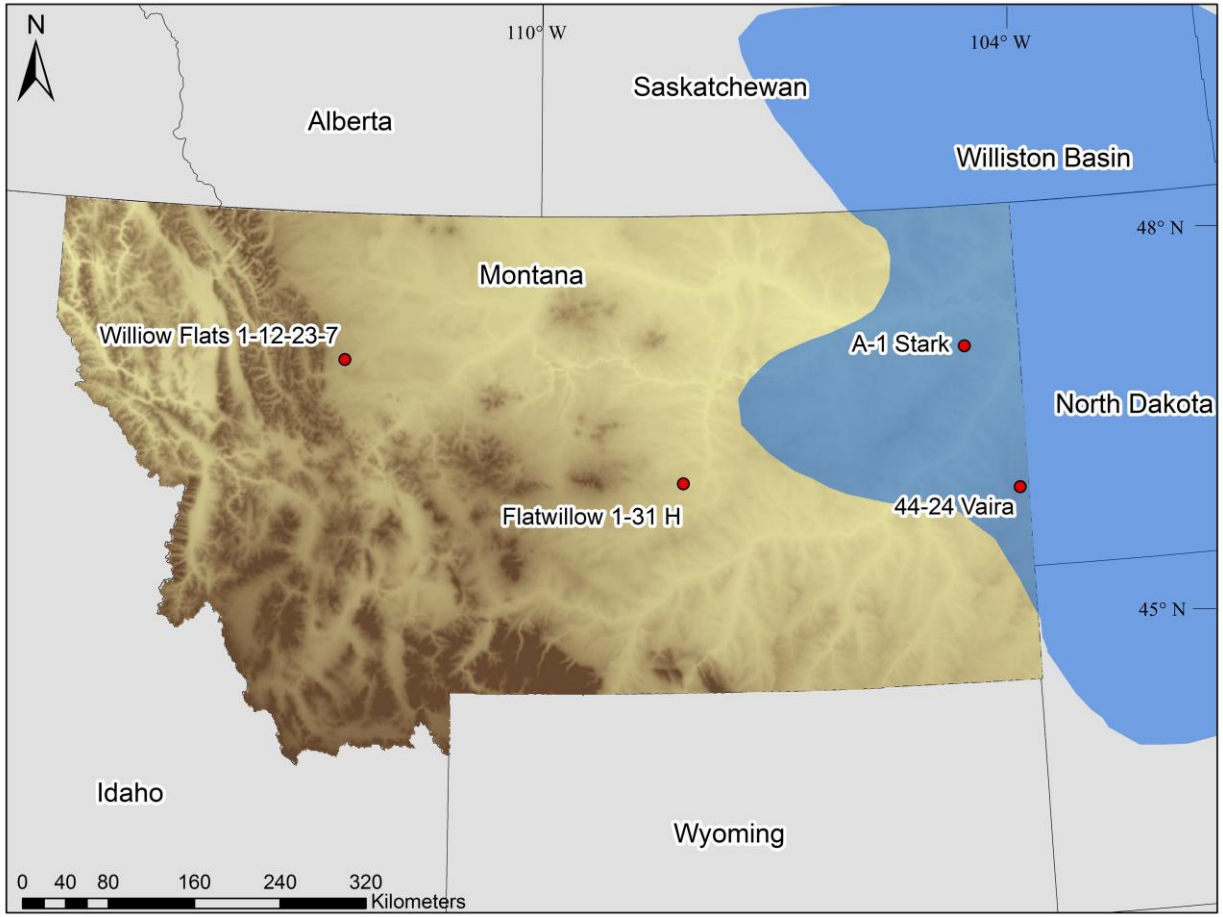


Figure 9. The location of the four cores examined in this study. The blue region represents the extent of the Williston Basin. The A-1 Stark and 44-24 Vaira cores are located within the basin (Williston Basin outline from Angster, 2011).

Formation. The cored interval is 59 feet long.

The Flatwillow 1-31H core, operated by EOG Resources, and the Watson Flats 1-12-23-7 core, operated by Primary Petroleum, located in Petroleum and Teton counties, Montana show an absence of the Bakken Formation entirely. The Flatwillow 1-31H core contains the Lodgepole and the Three Forks Formations. The Watson Flats 1-12-23-7 core only contains the Three Forks Formation. Fractures of the Lodgepole Formation were still recorded. Cored intervals were greater than 100 feet.

Methods

Cores were measured in 6” (15.24) intervals for analysis (Figure 10), and an inventory of fractures was taken within each six-inch interval along the slab face of the core. Fracture characteristics including depth, length, orientation, aperture, vein fill, and vein fabric were measured. Because the cores are un-oriented and there are no formation micro imaging logs available, the actual strikes and dips of the fractures are unknown. The apparent dip was used when generating rose diagrams (Figure 11).

The orientations of fractures were measured with a protractor from horizontal. For example, in a vertical core, a fracture that is horizontal, or

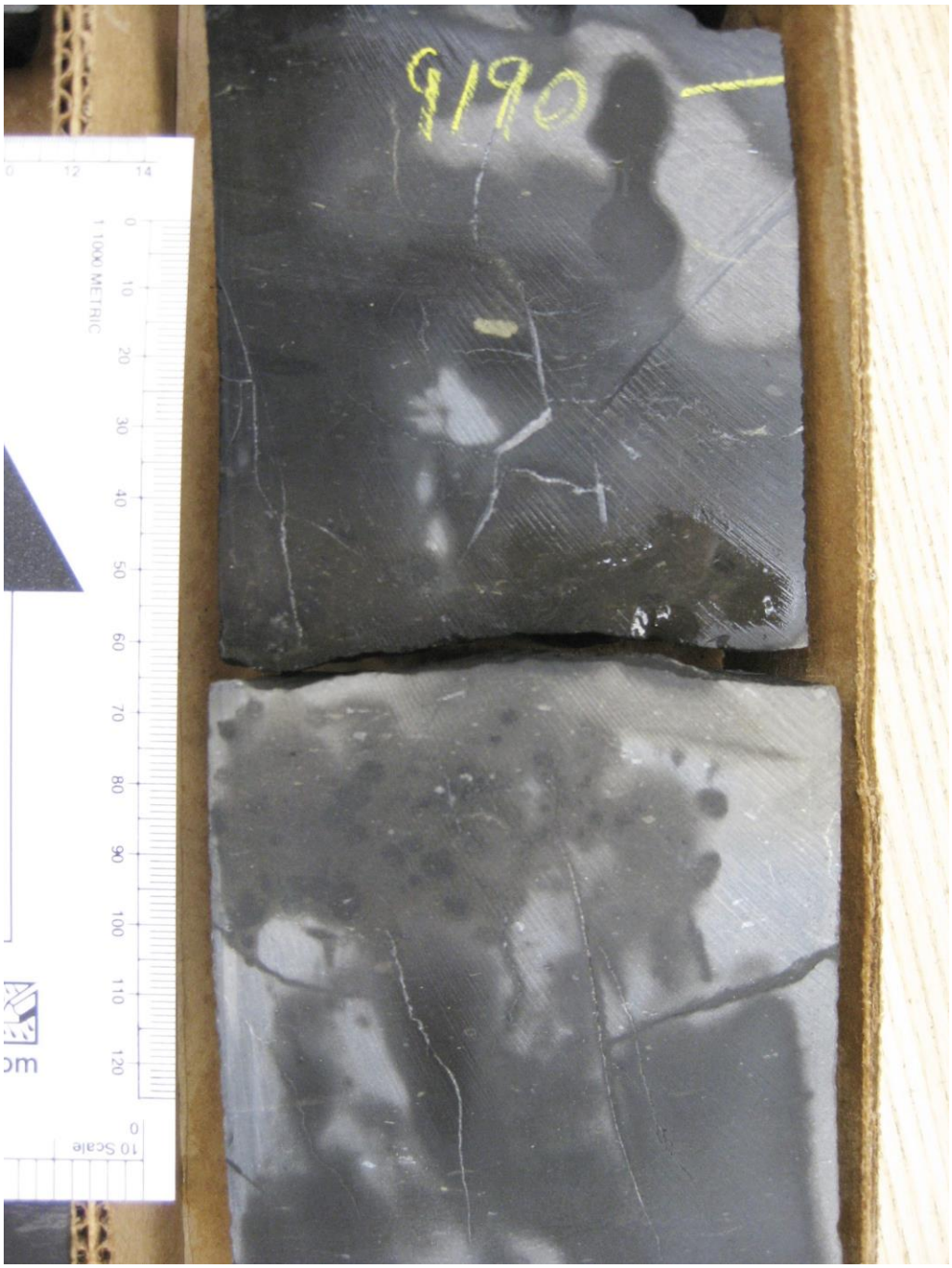


Figure 10. A 6” (15.24 cm) interval of the A-1 Stark core that was described. Fractures were drawn, photographed and their attributes were measured and recorded.

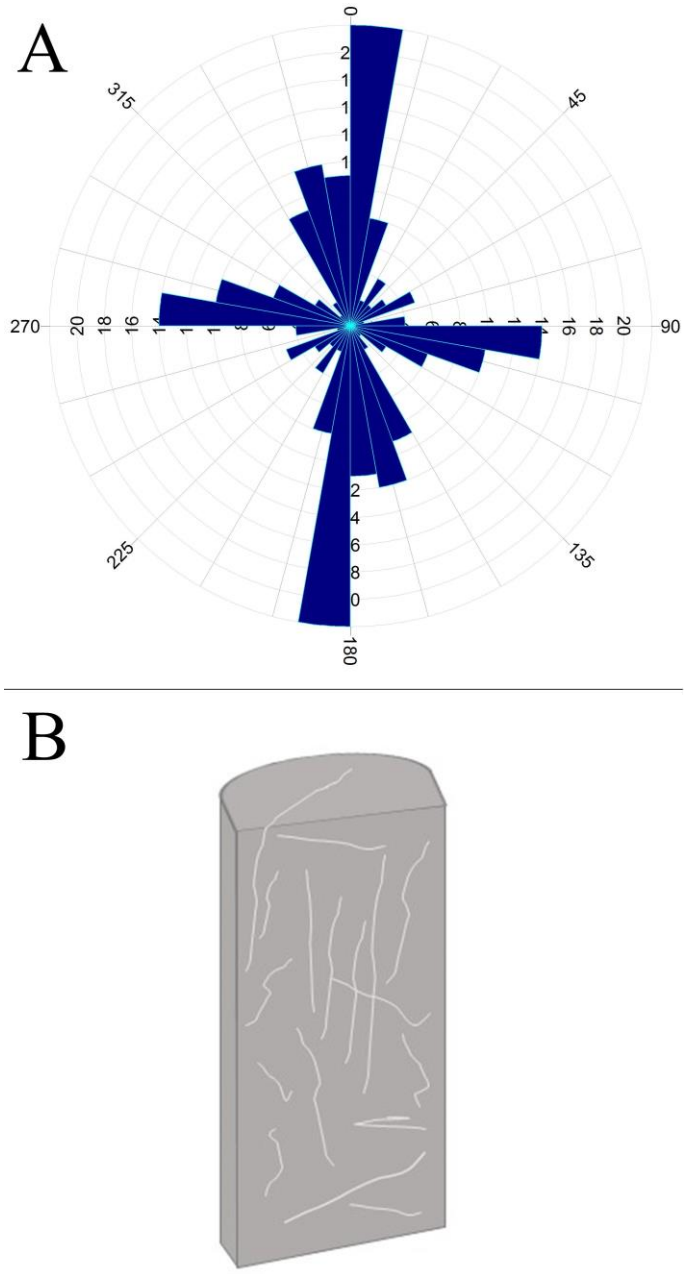


Figure 11. Fracture orientation measurement method. A) Rose plot of A-1 Stark. B) Sketch of fractures within a core corresponding to the above rose diagram. The Apparent dip was measured for every fracture and plotted on a rose diagram. Fractures that are north-south on the rose diagram are vertical within the core.

perpendicular to the length of the core, is at 0° and a fracture that is vertical, or parallel with the length of the core, is at 90°. Curved fractures were measured with a piece of string and their orientation-from-horizontal was estimated with a best-fit line. The spacing of each fracture was measured at first, but due to limited time at the CRC, spacing was not recorded. Fracture aperture were measured at the widest point within the fracture and vein fill composition was identified with a binocular microscope and HCl. Rock fragments, especially within the shale members, were omitted.

Thin section sampling was determined by the amount of macroscopic fracturing observed within each member. Highly fractured and unfractured intervals were sampled. Epoxy was died blue in order to identify pores and nonmineralized, open fractures. Sections were cut and prepared by Spectrum Petrographics Inc.

Fifteen thin sections were made from the middle member and the shales in the A-1 Stark and 44-24 Vaira cores. Twenty-five thin sections available from the CRC were also studied. Thin sections were examined to identify fracture orientation and relationship with diagenesis and the overall reservoir characteristics. Because clay mineral identification is nearly impossible to conduct within a thin section of a shale, clay mineral identification was left to synchrotron X-ray diffraction. However, fractures in thin section were still visible in shale members.

Results and Discussion

Fractures in Core

Unmineralized (open) horizontal fractures are seen within producing intervals of other cores in the Bakken TPS. Horizontal fractures that contribute to reservoir permeability form in the late stages of diagenesis (Figure 12). Two stages of fracturing usually occur within the Bakken TPS. The first stage occurs early within diagenesis, forming fractures during mechanical compaction and are most likely a result of lithostatic stress induced after burial. Most Stage 1 fractures are vertical, but minor amounts are horizontal (Pitman et al., 2001). These fractures are partially to completely healed with either calcite, dolomite or pyrite depending on the surrounding rock mineralogy.

The second stage of fracturing is coincident with the generation of hydrocarbons. Frequency and extent of Stage 2 fractures depends on the level of thermal maturity, the thickness of the source rocks and the distance from them, and the degree of hydrocarbon generation (Pitman et al, 2001). Stage 2 fractures, primarily open and horizontal, within the shale members are due to the presence of kerogen. This process begins when the kerogen absorbs the hydrogen molecules in water, causing a release of oxygen in the form of CO_2. This expulsion of gas allows for the overpressure needed to initiate in-situ horizontal fractures (Price

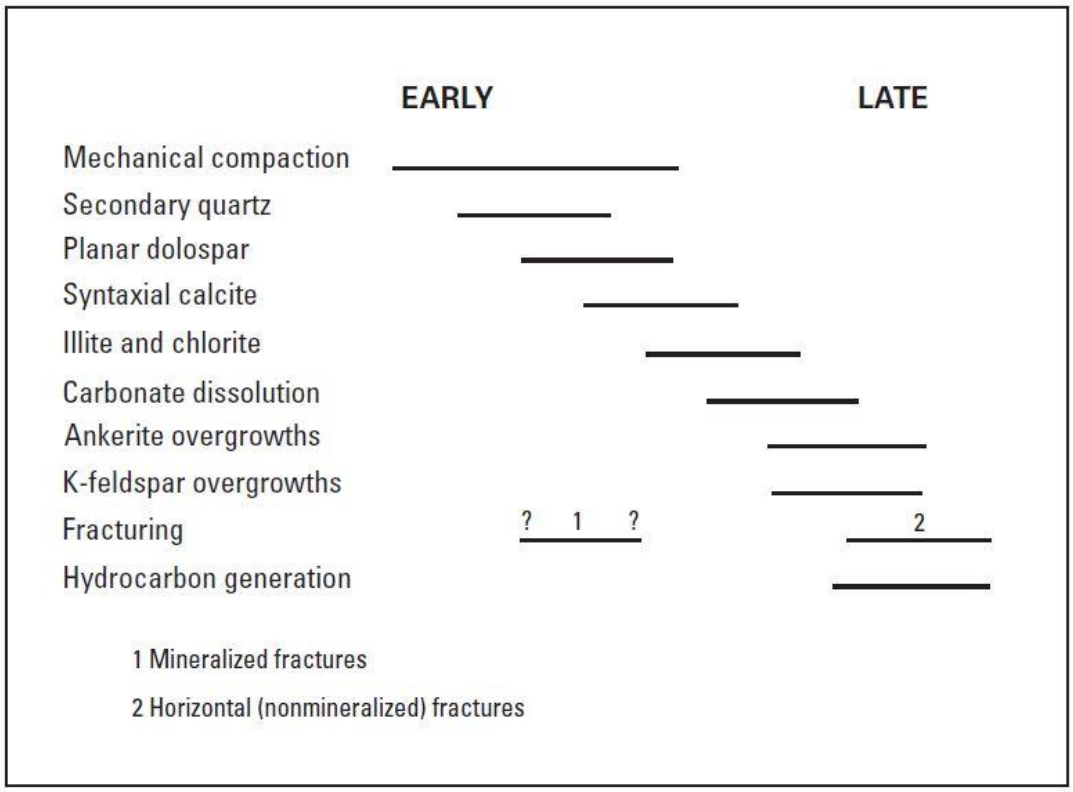


Figure 12. Generalized timing of diagenetic events observed within the middle member of the Bakken Formation (Pitman et al., 2001). This sequence was chosen based on the wide use of this model within the Bakken literature. Note this is only a relative sequence of diagenetic events, not a temporal sequence.

2000; Price and Stolper, 2000; Pitman et al., 2001). However, diverging opinions as to whether these mode-1, horizontal fractures form *in situ* or from the core extraction process.

Cores examined in this study are thermally immature, and the shales are organic-poor. Without large productions of kerogen, it is expected that Stage 1 fractures will be much more prevalent than Stage 2 fractures. Open, horizontal fractures viewed in the shale members within these cores are believed to be from

clay partings inherent in clay-rich mudrocks. Fracture intensity is variable throughout all four cores, indicating that lithology and mineralogy control fracture initiation and propagation.

In general, most fractures originate from "stress raisers" such as abrupt changes in grain size (e.g. erosional surfaces) crinoid stems or other fossil fragments, macro-scale pores (mineralized or unmineralized), and pre-existing fractures or stylolites. Stress concentrations within a rocky body occur from changes in geometry or differences in mechanical characteristics. A crinoid fossil for example has different mechanical properties than the surrounding limestone, and therefore, the concentrated stress around this fossils acts as the origin for a new fracture (Gudmundsson, 2011).

The A-1 Stark core contains the upper and middle Bakken and the upper Three Forks Formations, and is missing the lower shale member. The interval is capped by an organic-poor mudshale with sporadic silty beds present. Some intervals within the upper member show laminations where others appear to be devoid or layering. The upper shale lies disconformably above the middle member, which is primarily limestone and dolomite and lenses of sandstone. The middle member grades into the Three Forks Formation.

Fractures within the A-1 Stark core tend to nucleate in intervals where fossils have accumulated such as crinoid stems or bryozoan fragments. Abrupt changes in grainsize from clay- to silt-sized particles form favorable conditions for

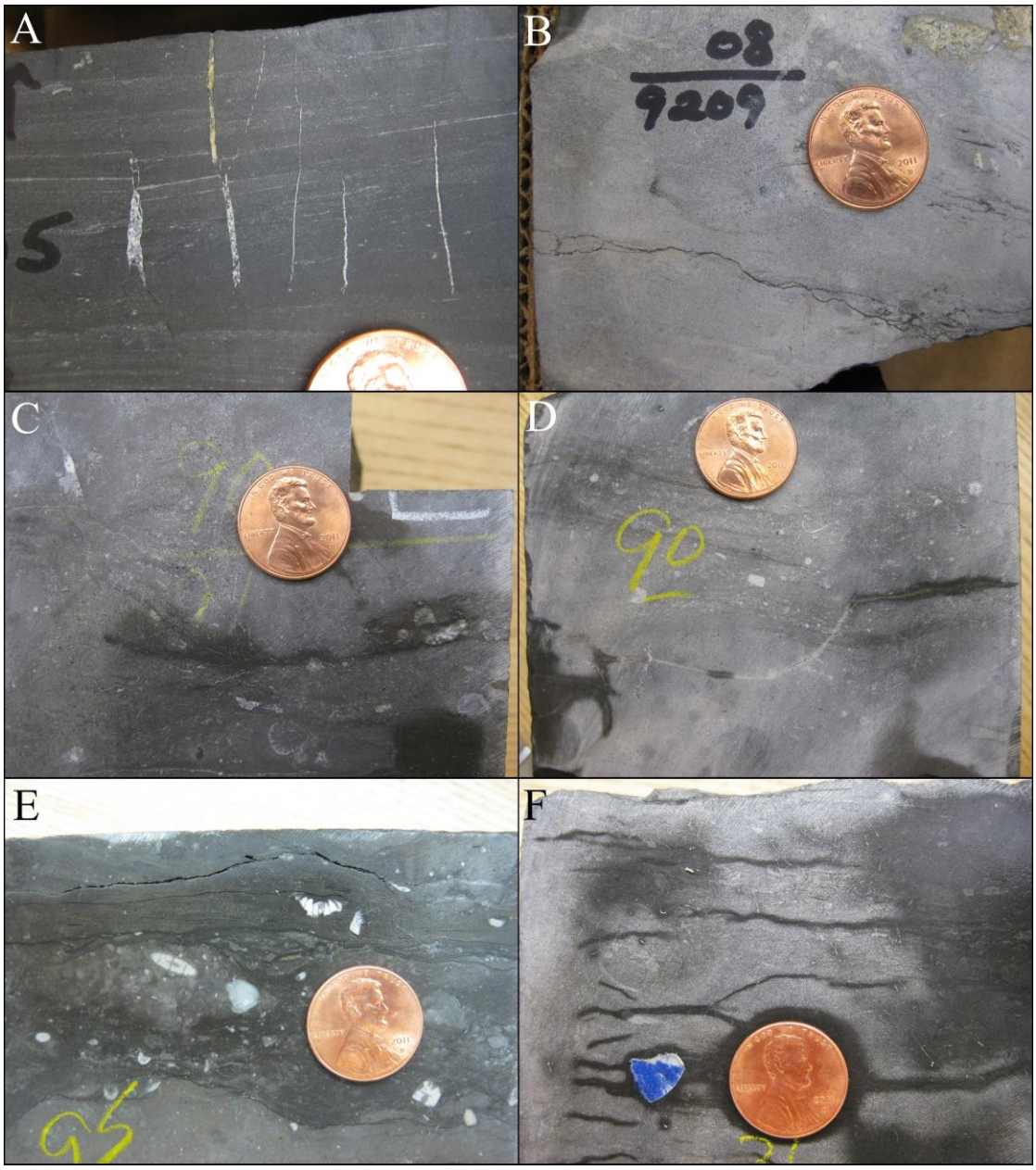


Figure 13. Fractures within the A-1 Stark (A and B) and 44-24 Vaira (C, D, E and F) cores. A) The middle member of the Bakken Formation showing fracture initiation in coarser grain beds, bed offset, and multiple vein-fill events (pyrite and blocky calcite). B) The upper portion of the Three Forks Formation showing a fracture exploiting a stylolite. C) The Lodgepole Formation showing a fracture propagating from a crinoid fragment D) The Lodgpole Formation revealing a fracture originating from a bed of bioclastic material E) A fracture that formed in between the Lodgepole and the upper shale member of the Bakken F) Fractures in the middle member of the Bakken forming from crinoid fragments.

fractures to initiate. Often, biological detritus and siltier layers occur within the same horizons. The presence of bedding-parallel stylolites indicates that chemical compaction did occur within the region. Often, these stylolites are exploited by fractures (Figure 13).

The absence of organic matter in these mudshales suggests that Stage 2 fractures should be scarce within the middle member. This hypothesis is supported by the presence of only two open fractures within the entire cored interval; the rest of the core contains partially to fully healed fractures. Open fractures within this core are believed to have formed through the core extraction and storage process, and are unrelated to in situ fracture formation.

Mineralized fractures within the A-1 Stark core are bimodal with sub-vertical and sub-horizontal fractures (Figure 14). When the apparent fracture strikes are broken down based on the members they occur in, distinct orientations represent each member. The upper shale member of the Bakken Formation shows primarily sub-vertical fractures, whereas the middle member and Three Forks Formation encompass sub-horizontal fractures partially to fully healed with calcite. Due to their orientation and vein fill composition, these fractures are interpreted to be early forming Stage 1 fractures.

The 44-24 Vaira core contains the same interval as the A-1 Stark core. However, the top of the cored interval contains the Lodgepole Formation and the "False Bakken," which is a mudshale that appears to have the same gamma ray

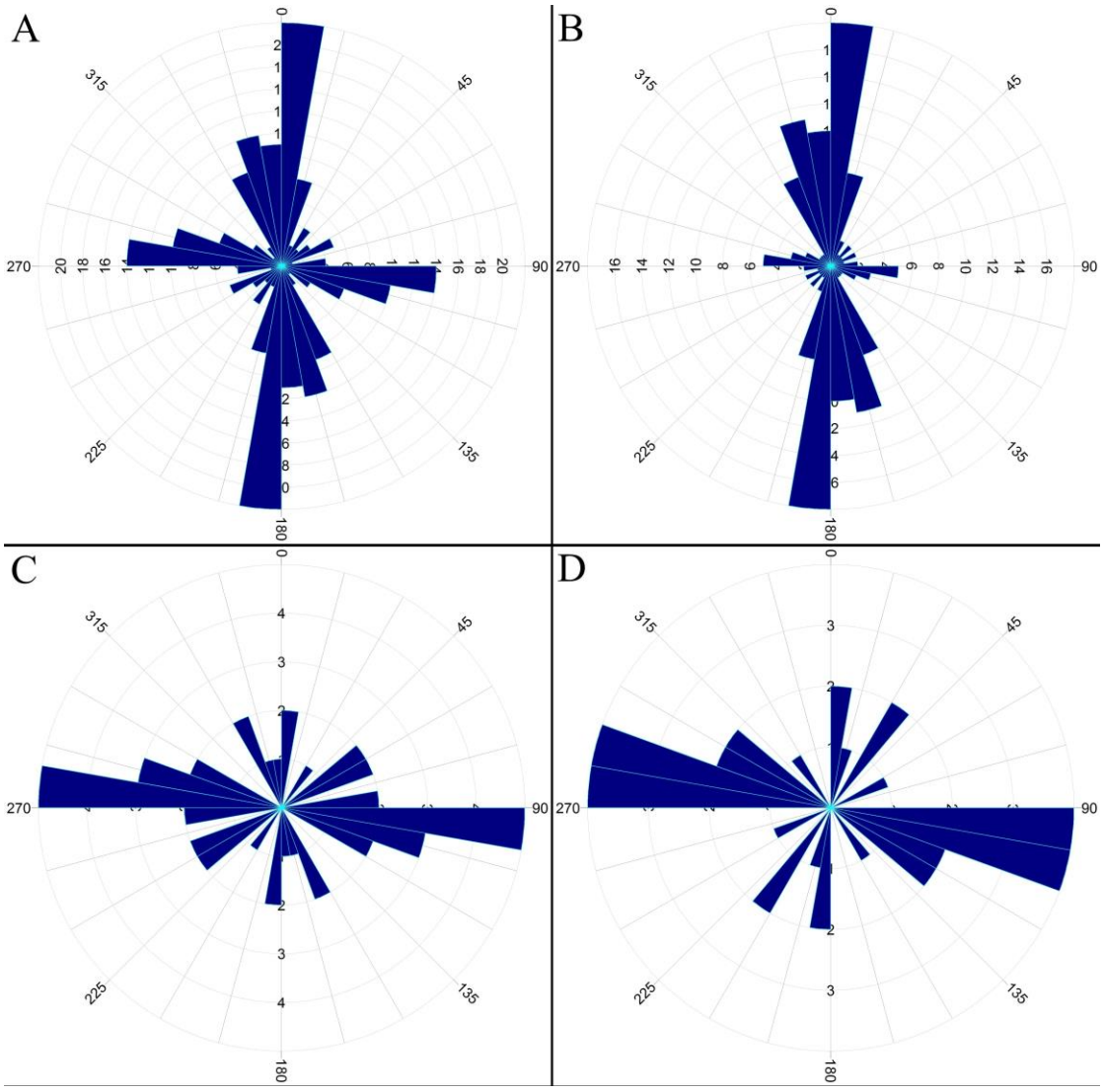


Figure 14. Rose plots from the A-1 Stark core, representing the apparent dip orientation of fractures measured within the core. North (0˚) and south (180˚) represent vertical fractures, and east and west represent horizontal fractures. Petals on the rose diagram represent 10º orientation classes. A) Fractures from the entire core showing a bimodal distribution, n=119. B) Fractures from the upper shale member of the Bakken Formation are primarily vertical, n=79. C) Fractures from the middle Bakken member are dominantly horizontal, n=59. D) Fractures from the upper Three Forks Formation are also dominantly horizontal, n=22.

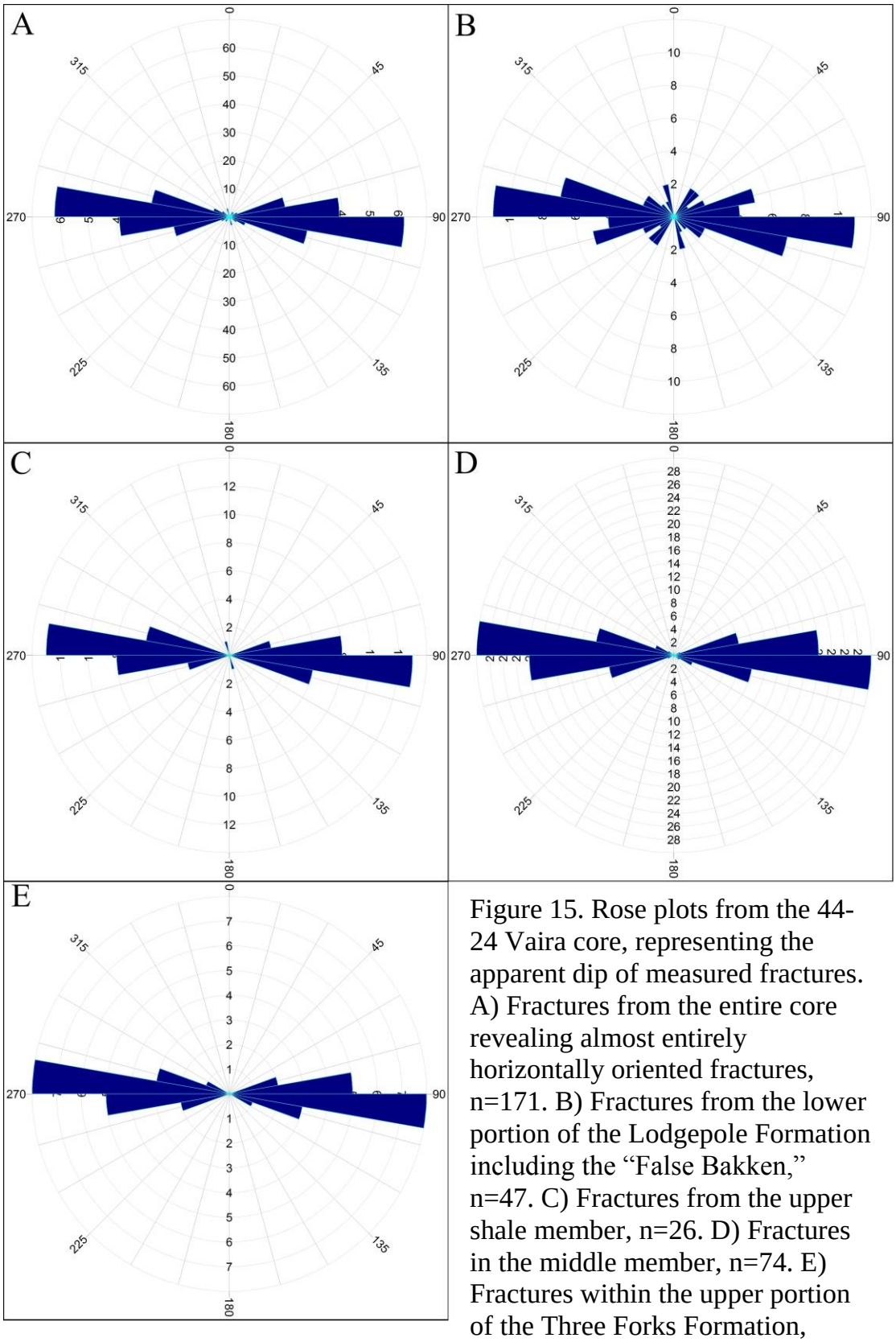


Figure 15. Rose plots from the 44-24 Vaira core, representing the apparent dip of measured fractures. A) Fractures from the entire core revealing almost entirely horizontally oriented fractures, n=171. B) Fractures from the lower portion of the Lodgepole Formation including the "False Bakken," n=47. C) Fractures from the upper shale member, n=26. D) Fractures in the middle member, n=74. E) Fractures within the upper portion of the Three Forks Formation, n=18.

signature on logs as the upper Bakken member. Organic material in the upper shale member is more prevalent than the highly silty upper member in the A-1 Stark core, but less rich than producible shale intervals. The base of the middle member lies disconformably above the Three Forks Formation evidenced by the pyritized erosion clasts at the boundary between formations.

Fractures occur within the upper shale in the 44-24 Vaira core, however, the majority of the upper member fragmented from the extraction process (Figure 15). Pyrite concretions and pyritization are prevalent in both the A-1 Stark and 44-24 Vaira cores, indicative of two processes, 1) sulfur fixation was ubiquitous within the shale and 2) pyrite precipitated early in diagenesis, most likely coeval with mechanical compaction given that beds bend around concretions (Figure 16).

The 44-24 Vaira core contains dominantly sub-horizontal fractures and very few sub-vertical fractures. 18% of fractures inventoried are open. The majority of the fractures are mineralized, however there are more open fractures than present in the A-1 Stark core. The extraction process, and the higher organic content of the 44-24 Vaira core is believed to be the main cause of a greater number of open, horizontal fractures than observed within the A-1 Stark core (Smith et al., 2005a; Smith et al., 2005b).

The Flatwillow 1-31H and Watson Flats 1-12-23-7 cores do not contain the Bakken Formation because they were drilled on an arch that did not contain the Bakken. Both cored intervals contain limestone and dolomite that is interpreted to

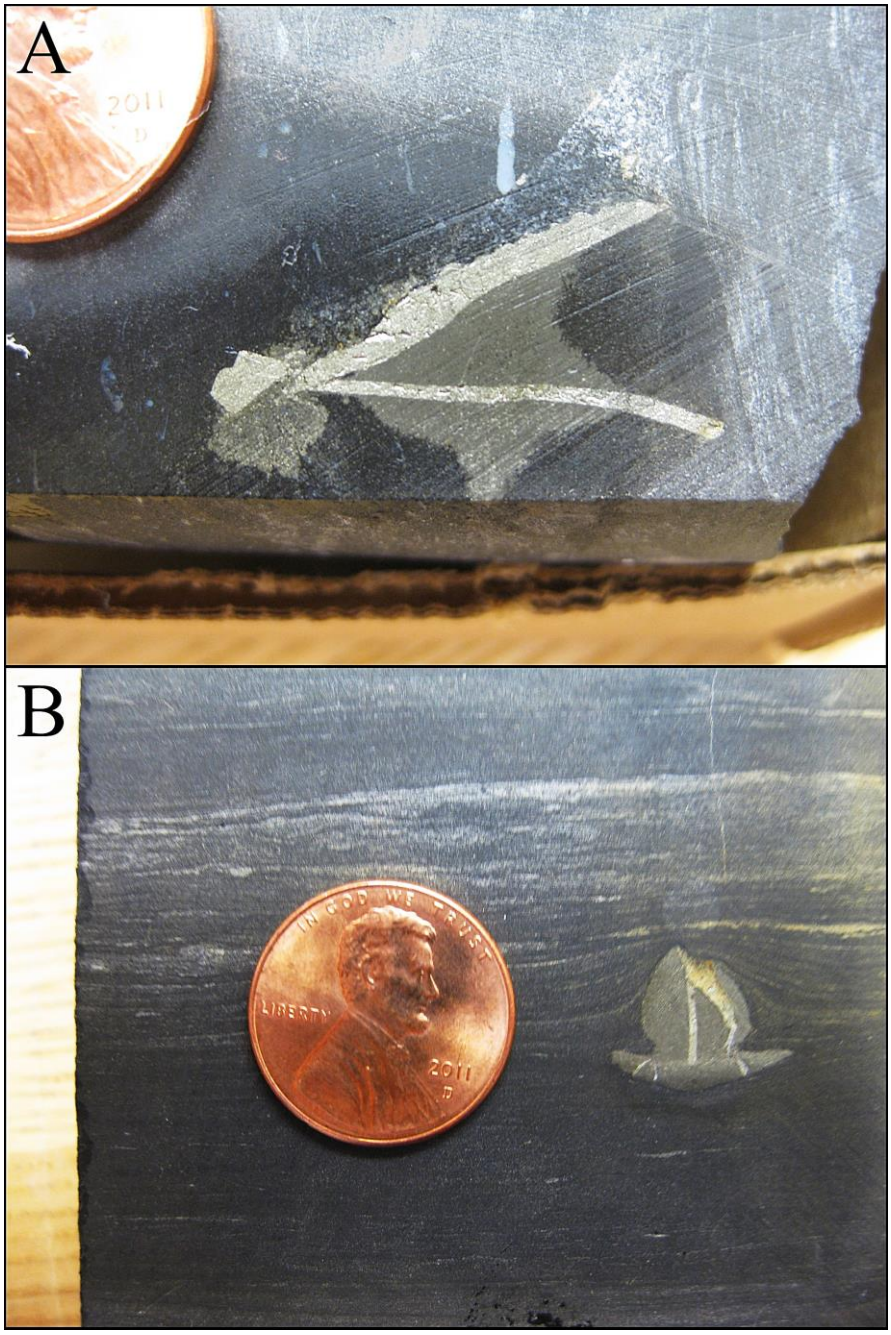


Figure 16. Pyritization within the upper member of the A-1 Stark core. A). A bifurcating fracture filled with pyrite. Fracture-related porosity is visible from the pyritization. Propagation of fluids was quicker through the fractures than the pores as seen by the concave lens of pyrite in between the two arms of the fracture. B). Fractures and fracture-related porosity filled with pyrite. Note the bedding laminations bending around the pyrite structure, indicative of early fracturing and pyritization during diagenesis.

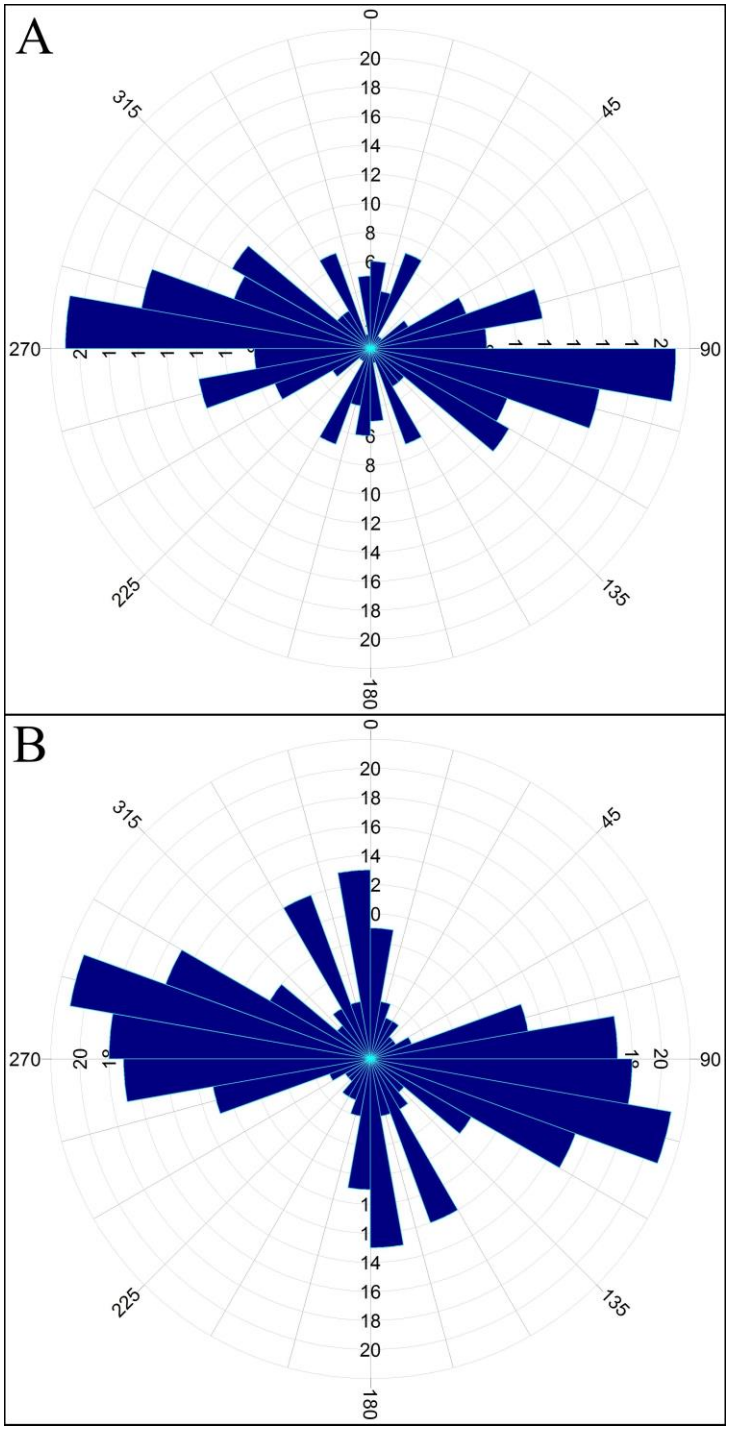
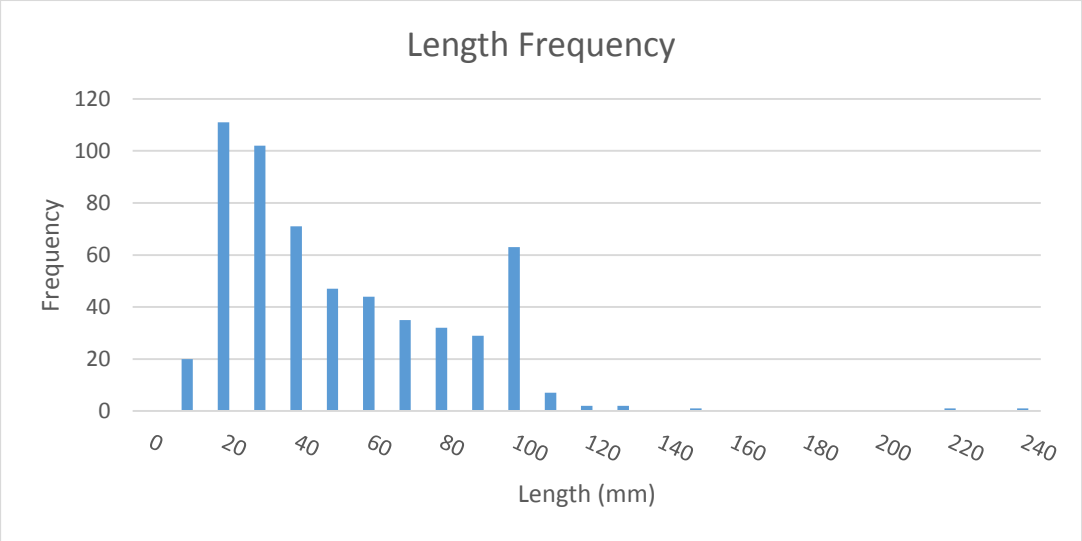


Figure 17. Rose plots of apparent dip of A) Flatwillow 1-31H and B) Watson Flats 1-12-23-7 cores showing a dominantly horizontal orientation.

be part of the Lodgepole and Three Forks Formations. Orientation of fractures in the Watson Flats core are bimodal, but not as strongly oriented the A-1 Stark core (Figure 17). The Flatwillow 1-31H core displays dominantly horizontal, mineralized fractures originating in stylolites and horizons with fossil debris such as crinoids, bryozoans and brachiopods.

The upper shale member in the A-1 Stark and 44-24 Vaira cores have differing fracture orientations. The A-1 Stark fractures are dominantly sub-vertical whereas the Vaira core are almost entirely sub-horizontal. The Stark shale is very silty and organic-poor leading to vertical fracturing by means of the lithostatic load placed upon the rock (Smith et al., 2005a). The Vaira shale is organic- and clay- rich and quartz-poor (Smith et al., 2005b). This discrepancy between the cores is responsible for the change in the dominant fracture orientation observed.

The frequency of length and aperture within a reservoir is very important and was applied to these cores (Figure 18), however, fracture measurements are extremely biased, and only limited to the 3-inch-wide, slabbed core face. Fractures that spanned the entire core were most likely longer than actually measured. The fracture attributes are highly skewed, due to the nature of studying fractures in core. Frequency of fracture length reveals an overwhelming number of short fractures (Figure 18), influenced by two factors: 1) the majority of fractures will be smaller because their propagation under lithostatic stress limits the distance of propagation, 2) unless fractures are vertical (parallel with the length of the core)



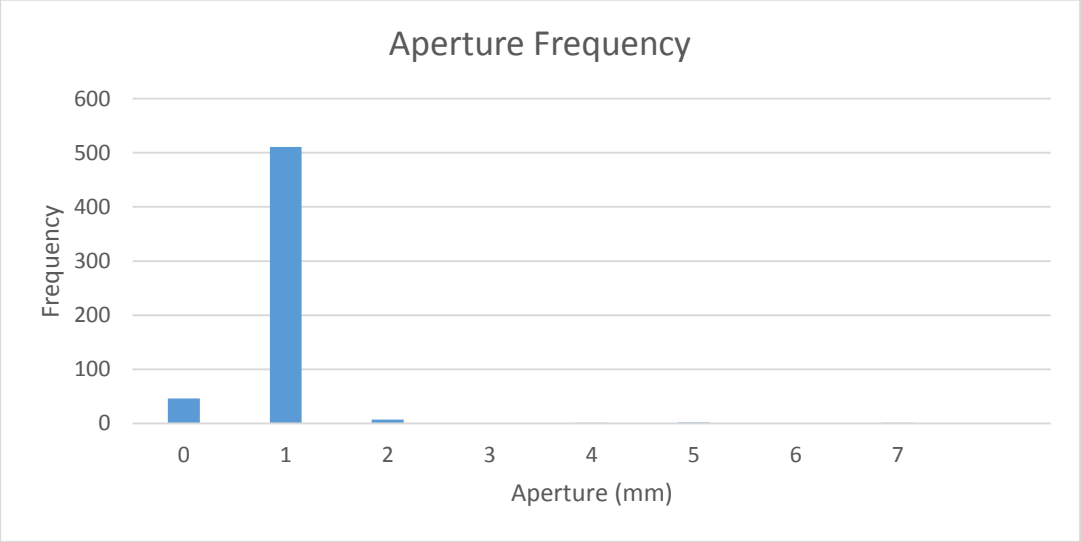


Figure 18. Frequency of length and aperture of all fractures measured in the core analysis. Note the highly skewed frequencies.

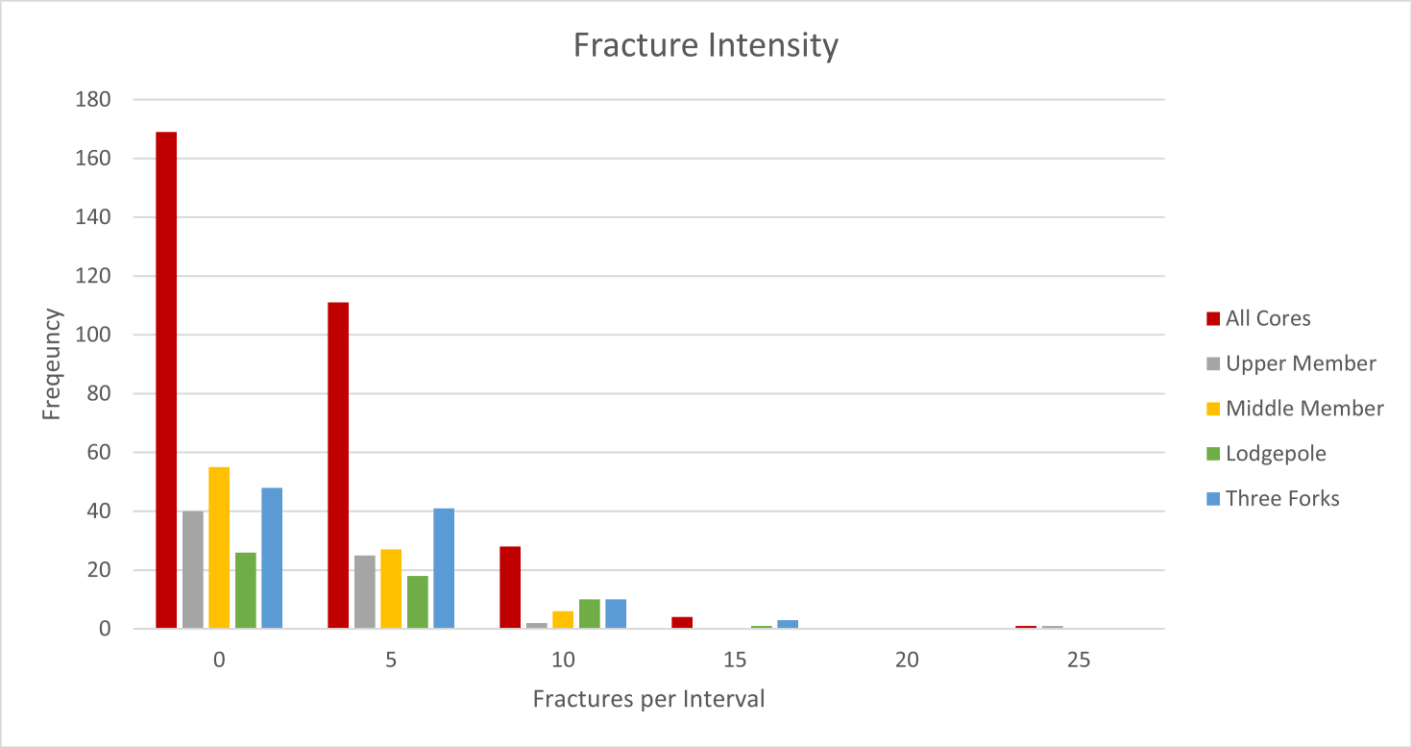


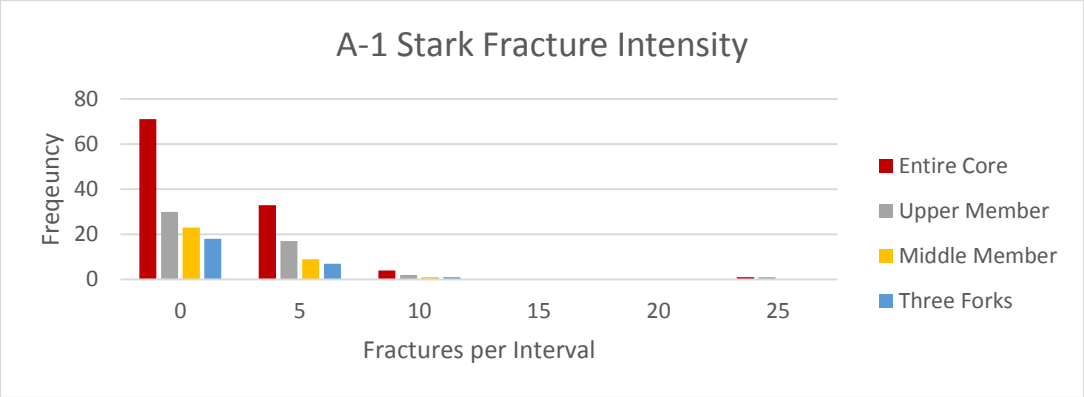
Figure 19. The combination of intensity of all fractures within the core study. Intensity is highly skewed.

their measured length most likely is limited by the width of the core, therefore being smaller. Throughout all four cores, the most frequent length was between 10 and 20 mm.

The highest frequency of aperture is between 0 and 1 mm. However, measuring fracture aperture with a metric ruler is only accurate down to 1 mm, and the majority of fractures are most likely several hundred μm wide. This inability to measure small apertures accurately on a core face causes the skew the seen in Figure 18. Fracture vein fill is composed of blocky calcite or pyrite (Figure 13A), based on the surrounding rock mineralogy.

Vein fill composition within fractures, as mention above, is a product of the composition of the surrounding rock. If these Stage 1 fractures occur within a limestone, then it is likely the fracture will be healed with calcite or dolomite. If the fractures occur within an organic rich mudrock, such as the upper member in the 44-24 Vaira core, then they will be healed with pyrite (Figure 16). Considering the early pyritization, pyrite healing likely occurred first before calcite. However, this was not determined through macroscopic observation of the cores.

Fracture intensity was calculated by summing the number of fractures that occurred within each study interval (Figure 19). Fractures that spanned two intervals were lumped into the interval that they occurred most in. Intensity is extremely skewed and is shown in Figure 18 of all fractures measured within the core analysis. The Watson Flats and Flatwillow cores do not contain the Bakken



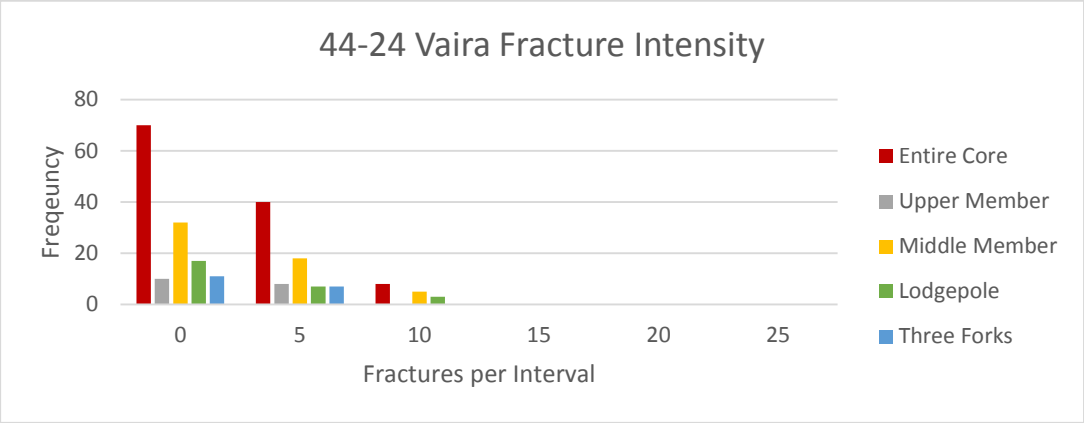


Figure 20. Fracture intensity plots of the A-1 Stark and 44-24 Vaira cores. Note the difference in fracture intensity of the upper and middle members of the Bakken Formation between the two cores.

Formation, the A-1 Stark core does not contain the Lodgepole Formation and the Watson Flats core only contains the Lodgepole Formation, so a plot showing all fractures found in the cores analyzed and split based on member reveals an extremely biased result. The fracture intensity was split by core to produce a more accurate representation of intensity (Figure 20).

Within A-1 Stark and 44-24 Vaira, the most frequent intensity is between 0 and 5 fractures. Watson Flats and Flatwillow have higher intensities, between 5

and 10 fractures. The A-1 Stark core has a higher density of fractures within the upper member than the 44-24 Vaira core. However, the upper shale member in the A-1 Stark core is much siltier than in the 44-24 Vaira core, which is the likely cause for the higher intensity of Stage 1 fractures in A-1 Stark. The middle member has a higher intensity in the 44-24 Vaira core (Figure 20), likely a result of larger amounts of organic material contained within the bounding shales.

Petrographic Analysis

Forty thin sections were examined for petrographic analysis of the A-1 Stark and 44-24 Vaira cores. Sections from the Flatwillow 1-31H and Watson Flats 1-12-23-7 cores were not examined because of the absence of the Bakken Formation. Selection was based on depth, member and fractures-present, and sections were prepared by Spectrum Petrographics Inc. Eleven thin sections from the upper shale member and twenty-one sections from the middle member were examined. The remaining eight sections were taken from the Lodgepole and Three Forks Formations.

Samples prepared by Spectrum Petrographics Inc. were epoxied and stained blue in order to make fracture, and fracture-related porosity and permeability identification easier. Sections borrowed from the USGS CRC had additional staining allowing for carbonate mineral identification. Petrographic analysis was conducted on a Leica DM 2500 P microscope.

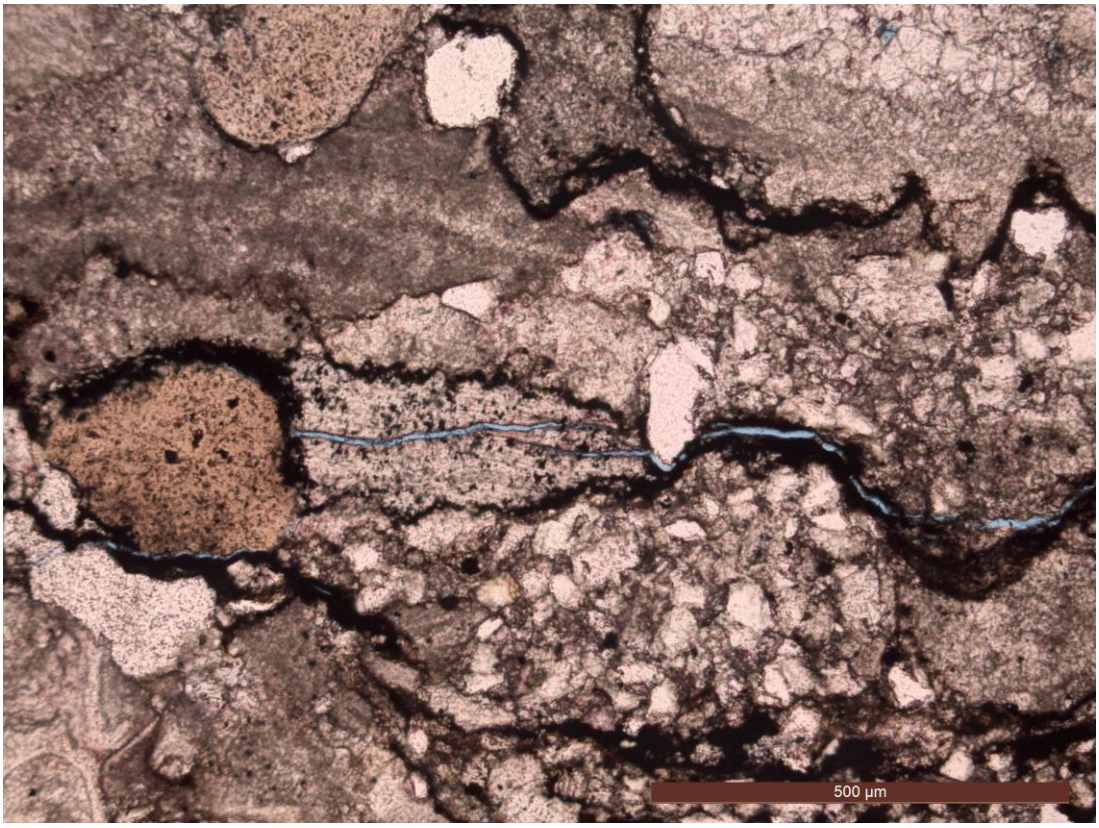


Figure 21. PPL photomicrograph of the Three Forks Formation from the A-1 Stark core displaying open fractures (blue) exploiting bedding parallel stylolites.

A-1 Stark. Within the A-1 Stark core, the Three Forks Formation lies disconformably below the middle member of the Bakken. It is a grainstone containing mollusk shell fragments, ooids, intraclasts, a micrite matrix and a sparry calcite cement. Horizons of fine, sub-angular to sub-rounded sand occur between intervals of bioclastic material. The mollusk shell fragments and ooids have been micirtized around the edges. Bedding-parallel stylolites occur usually originating in zones where large differences in grain size occur (Figure 21).

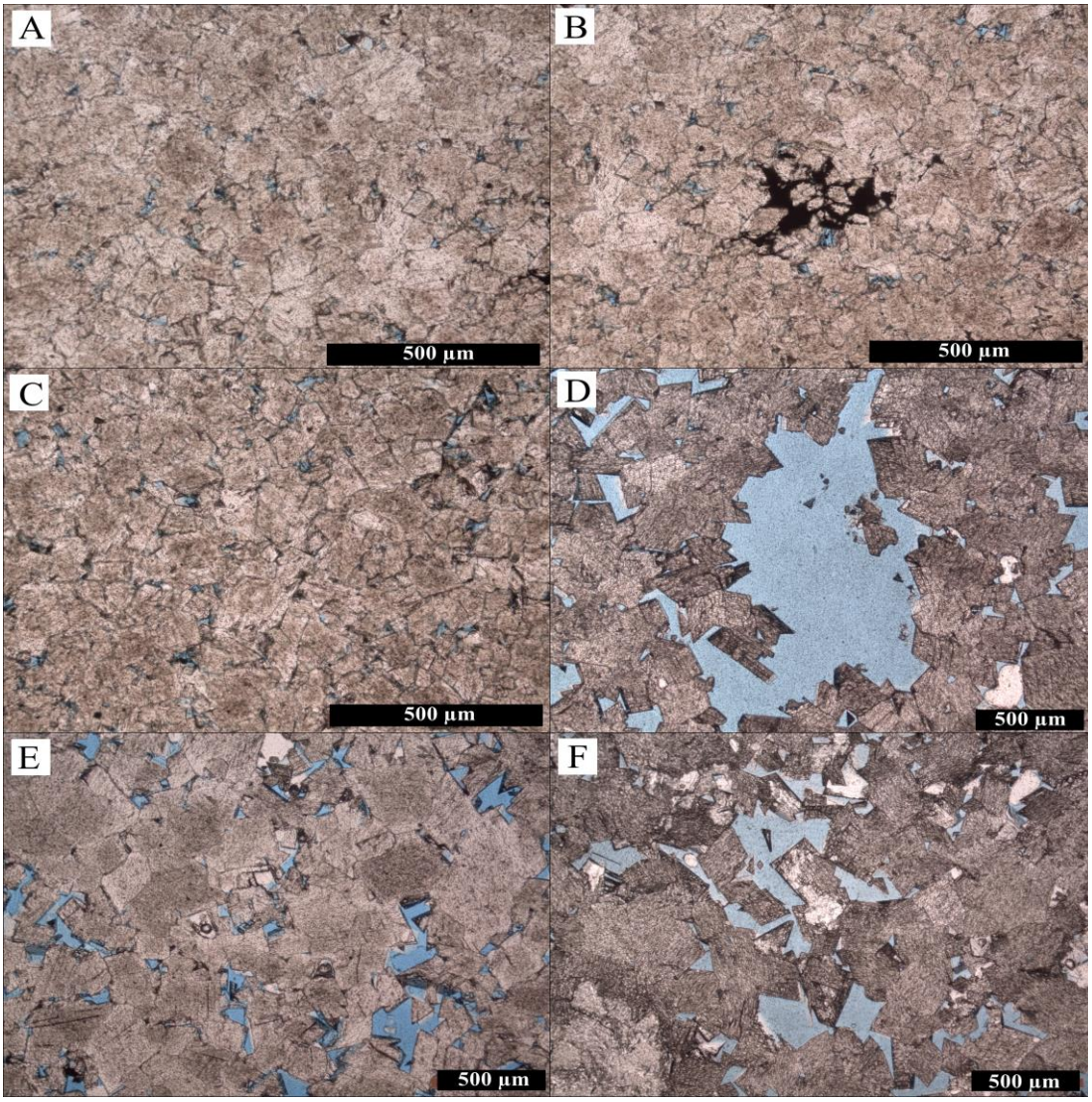


Figure 22. PPL photomicrographs taken from the middle member of the A-1 Stark core. A) Dolomite rhombs with very limited porosity. B) Insoluble material, interpreted to be bitumen, contained within the pores. C) Limited porosity within the dolomite crystals. D) A vug within the middle member caused by dissolution. E) More vugs, but with higher permeability. F) Calcite (white) being replaced by dolomite (grey).

Bedding-parallel stylolites are indicative of chemical compaction during diagenesis. As mentioned in the discussion on fractures above, these plains of weakness are exploited creating open, horizontal fractures.

The middle member of the A-1 Stark core appears to have a sandy texture when viewed in the core, but thin sections show fine- to coarse-grained euhedral dolomite crystals throughout the member with no detrital quartz visible (Figure 22). Dolomite is believed to have replaced the original framework within the middle member. Calcite is scarce within the upper extent of the middle member. In some cases it is partially replaced by dolomite. Because of the crystalline nature of the middle member, there is no matrix present.

Vugs occur throughout the middle member and most likely originated from dissolution of the original calcite framework (Figure 22E). Dolomite recrystallization is evident along fractures where smaller euhedral to subhedral crystals of dolomite form along a ~150 μm band around the fracture. Calcite is non-existent throughout the lower portion of the middle member, but it does occur within the top, closer to the upper shale member.

Microscopic fractures are scarce within the middle member due to the thermal immaturity and the organic-poor source rock. Healed, vertical fractures display halos, or zones of smaller euhedral to subhedral dolomite crystals around the fractures (Figure 23). Sub-horizontal fractures show broad zones of re-crystallized dolomite above and thin bands below the actual dilational fractures.

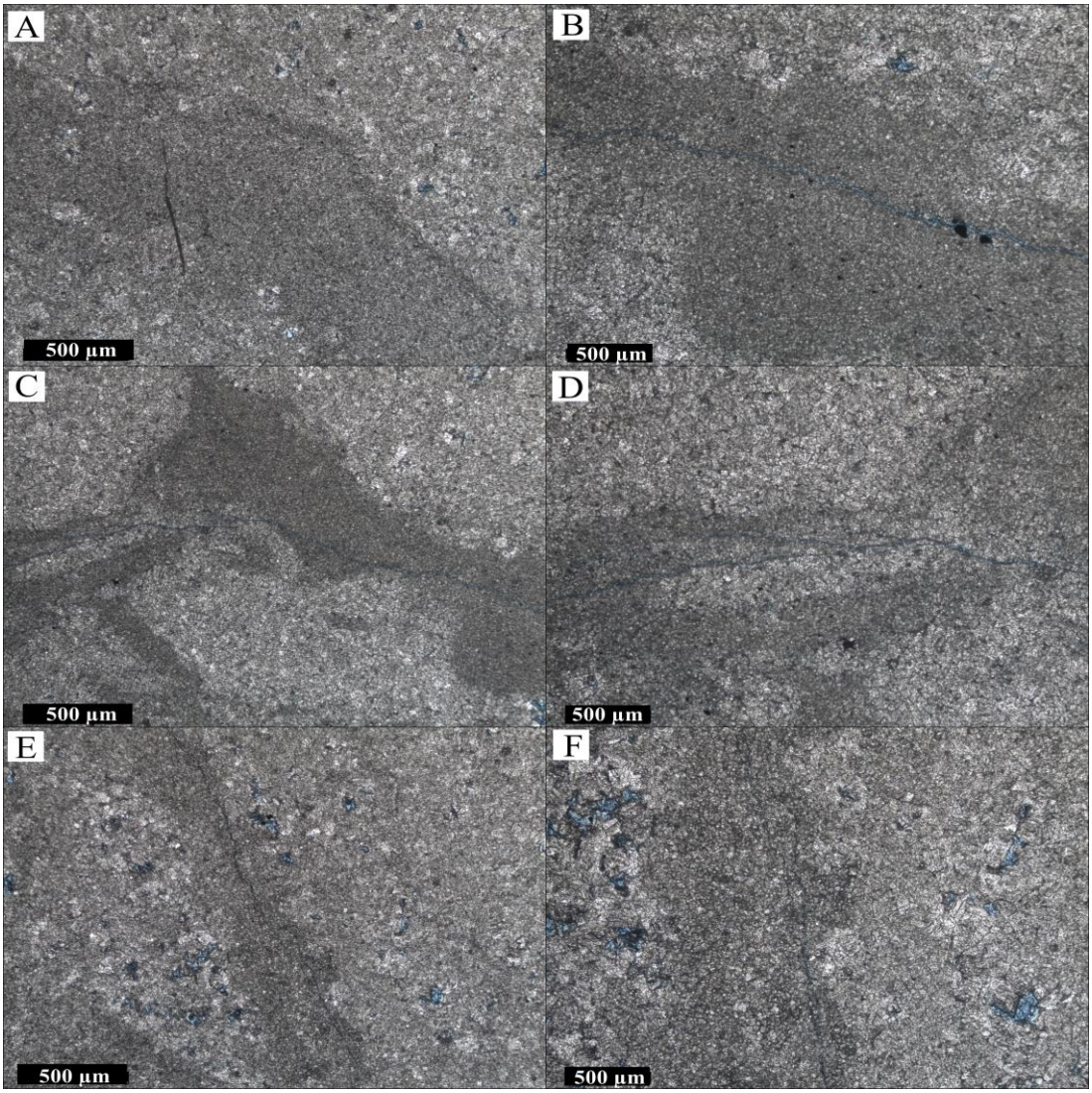


Figure 23. PPL photomicrographs of the middle member in the A-1 Stark core. Fractures with associated finer-grained dolomite forming “halos” around each fracture. The finer-grained dolomite is due to fluid flow along the fractures allowing for recrystallization of the dolomite.

Bitumen occurs within some pores in the middle member, indicating that some organic material was present during diagenesis, but not in high enough amounts to have inhibited the development of horizontal Mode I fractures.

Bedding parallel stylolites are often found within the Bakken Formation (Pitman et al., 2001), however they are absent within the Bakken Formation. The Three Forks Formation is the only member within the core that contains bedding-parallel stylolites. Chemical compaction is prevalent throughout the Three Forks Formation, but not within the Bakken.

The middle member of the Bakken Formation displays a homogenous grain size, and has not undergone dramatic diagenetic changes. Calcite was likely the original framework and was replaced by dolomite, which has preserved the sandy texture viewed in core (Figure 22F). Subsequent dissolution of dolomite has allowed for vug-style porosity to develop and reprecipitation of smaller euhedral dolomite along fractures. It appears Stage 1 fracturing was a precursor to the reprecipitation of dolomite, as evidenced by dolomite recrystallization along said fractures (Figure 23).

The upper shale member of the Bakken Formation contains large amounts of silt within various horizons. These silt grains are very fine, rounded to sub-rounded quartz, with minor amounts of calcite and dolomite, that form long-contact grain boundaries. Some pieces of crinoids are found within these coarser grain horizons. Clay makes up the matrix in these beds, and acts as the framework

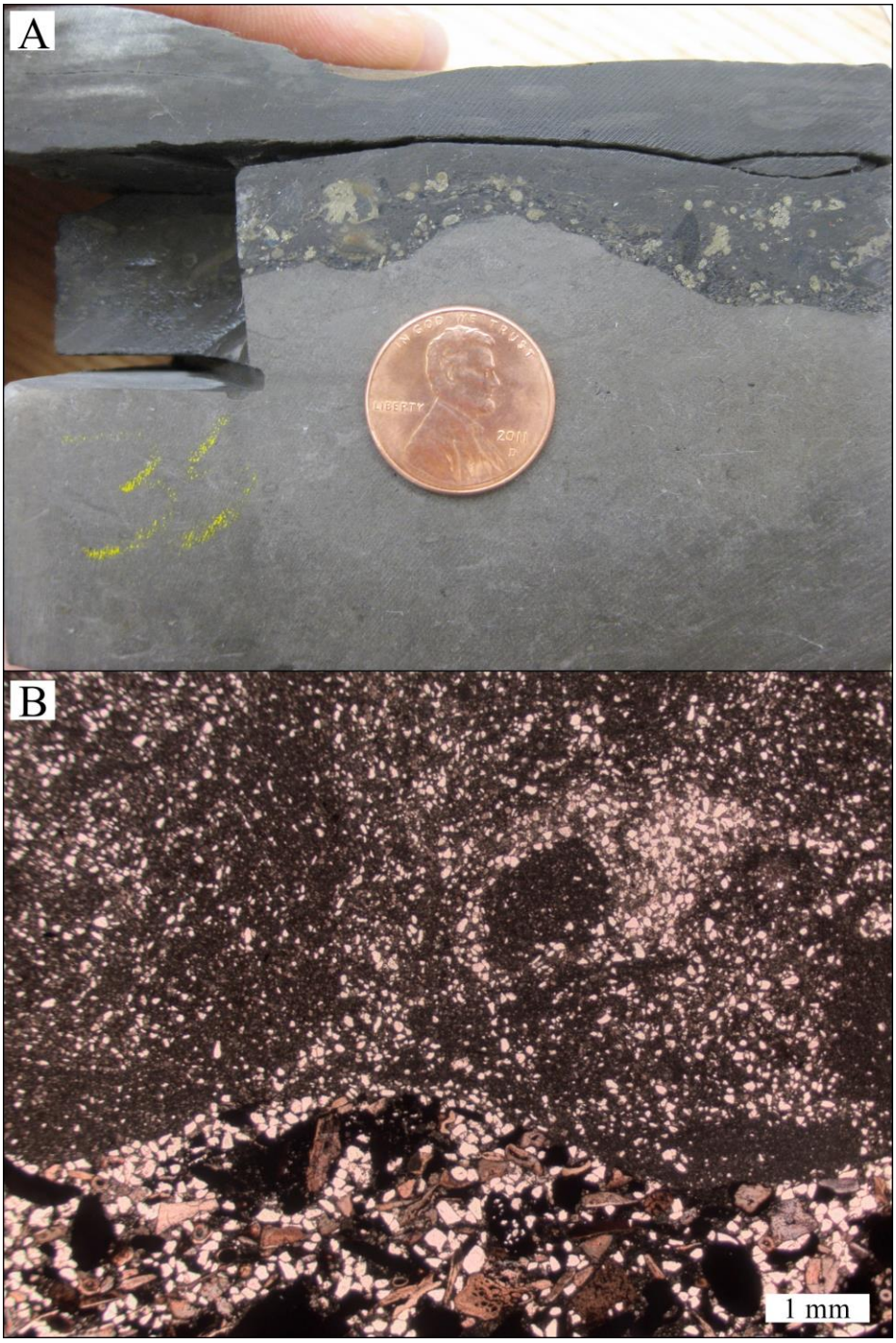


Figure 24. 44-24 Vaira in core (A) and PPL thin section (B) showing the erosional lag contact between the middle member of the Bakken and the Three Forks Formation.

in the finer, clay-sized intervals. Clay mineral identification proved very difficult to do with petrographic analysis and was left to X-ray diffraction.

44-24 Vaira. The 44-24 Vaira core contains the Three Forks Formation at the base of the cored interval. It sits disconformably below the middle Bakken member. The boundary between these two formations is abrupt, and pyritized clasts of the Three Forks Formation make up the erosional lag that is present at the boundary (Figure 24). The Three Forks is primarily a packstone, made up of ooids, echinoderms and intraclasts of calcite and dolomite with lenses of silt-sized quartz and green clayshales. Fractures occur horizontally where there is an abrupt change in grainsize (Figure 25).

The middle Bakken member within the 44-24 Vaira core coarsens upwards. A fossiliferous mudshale with fine, sub-angular to sub-rounded grains of quartz

and calcite with a micrite matrix rests disconformably above the Three Forks Formation. The middle of the member consists of silt-sized, angular to sub-angular grains of quartz with some calcite and a micrite matrix. The grains of calcite appear to be detrital from their rounded nature. Framework grain contacts are primarily long, with a clay cement (Figure 26).

In the upper portion of the middle member, the grains consist of calcite dolomite and quartz, with minor amounts of muscovite and anhydrite. The matrix is limited, but is primarily micrite and carbonate grains are rimmed by clay

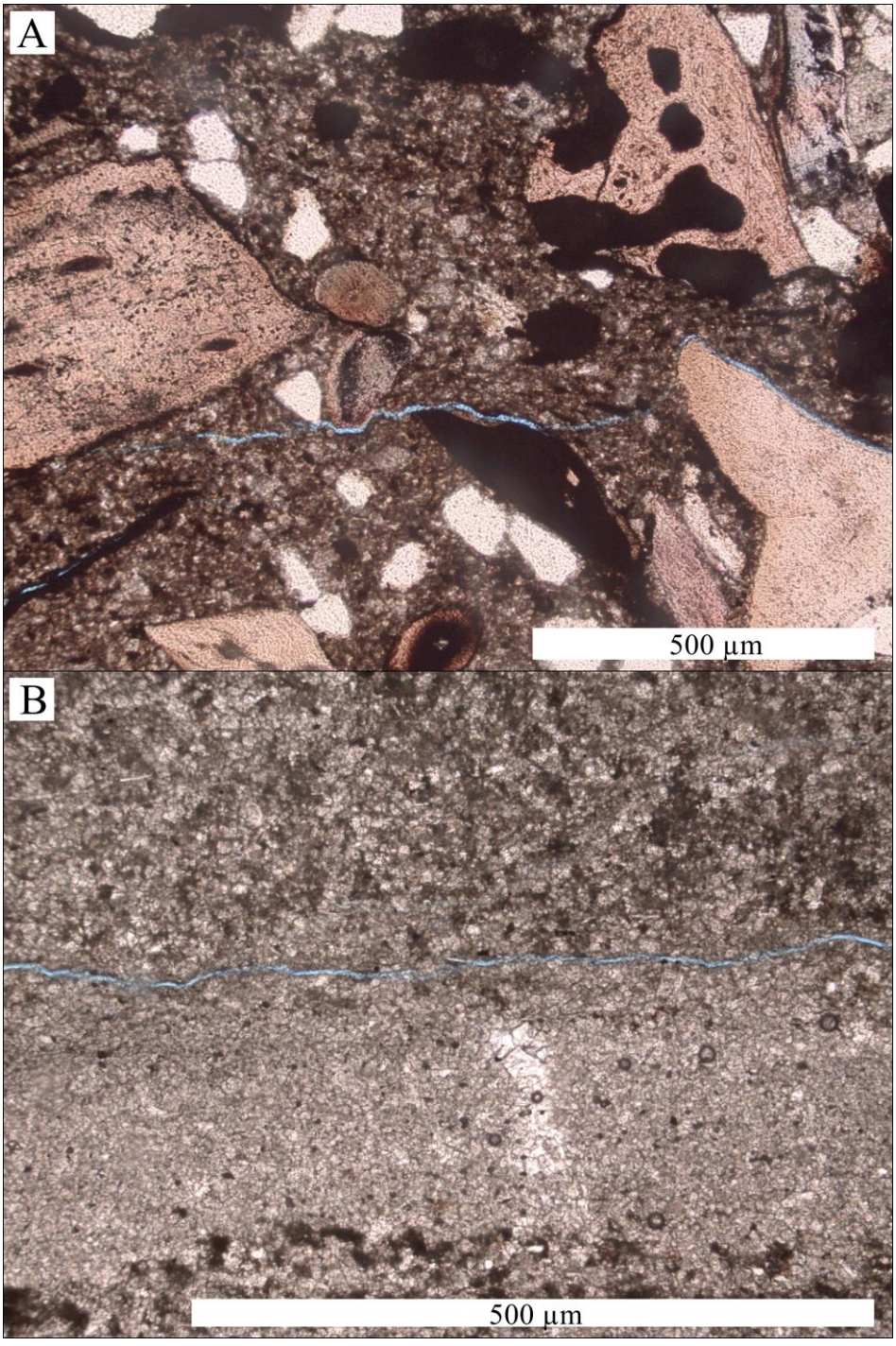


Figure 25. PPL photomicrographs of the Three Forks Formation. A) A horizontal fracture propagating around the larger clasts within the rock. B) Another horizontal fracture forming between a change in grain size.

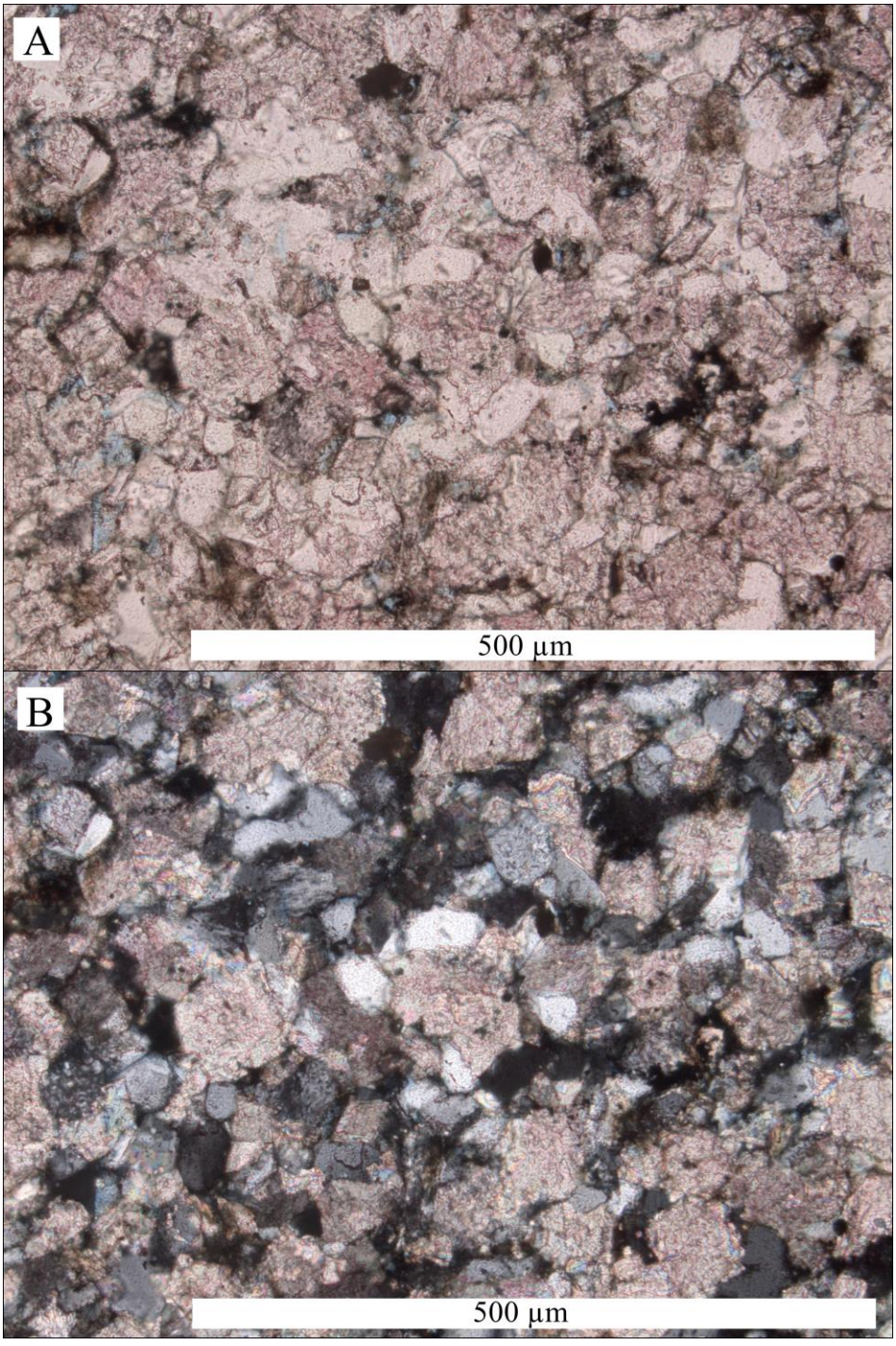


Figure 26. The framework grains of the middle member in the 44-24 Vaira core. A) PPL photomicrograph showing extremely limited porosity (blue). B) XPL of the same photomicrograph of quartz, calcite and dolomite framework grains.

cement. The quartz grains have concavo-convex grain boundaries that likely resulted from mechanical compaction. Overall the upper portion of the middle member lacks a matrix and pore space. Bitumen and pyrite occur closer to the upper shale member, rimming grains and pores.

Fractures within the middle member are relatively scarce, but are primarily Stage 2, open and horizontal. Nucleation occurs where abrupt grain-size changes occur. Fractures propagate around larger framework grains, exploiting the grain boundaries and the weaknesses bedding parallel stylolites provide. Fracture apertures ranges from 10 to 60 μm (Figure 27). Fracture-related porosity occurs within a ~100 μm band around the fracture found closer to the upper shale member. Fractures closest to the Three Forks Formation are devoid of fracture-related porosity.

The upper shale member consists of grains of calcite, pyrite and undifferentiated clay minerals, primarily clay-sized, interlayered with beds of coarser, silt-sized material (Figure 28). The top of the shale, proximal to the Lodgepole Formation, contains large pieces of crinoids and shell fragments that have been micritized on the surface. Lower portions of the shale appear much more homogenous, with coarser beds throughout.

Fractures within the upper shale member vary based on the composition of the surrounding rock. The upper extent of the shale is fossiliferous, and all the fractures that are observed are sub-vertical and fully healed with calcite or quartz.

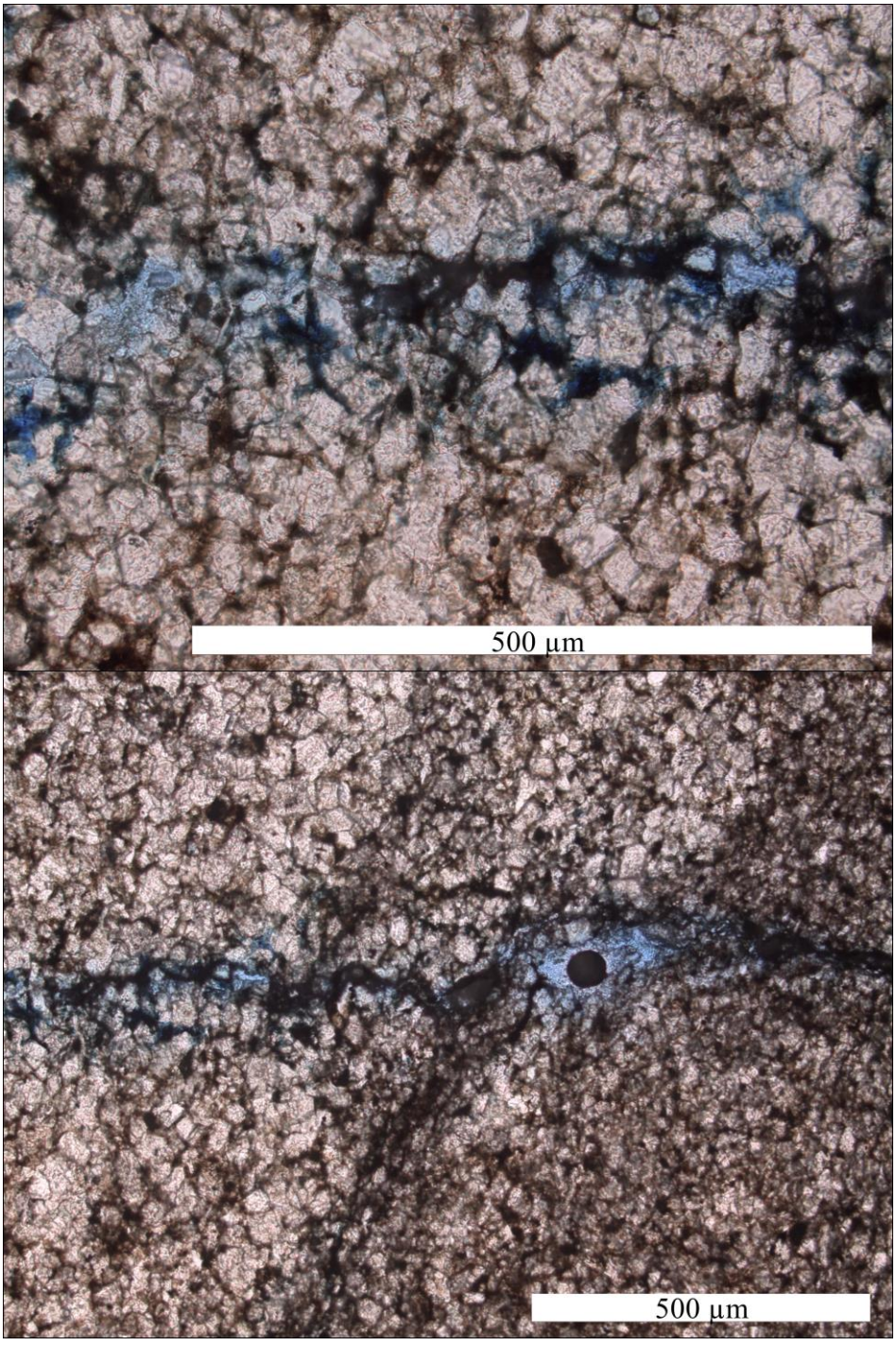


Figure 27. 44-24 Vaira core PPL photomicrographs of fractures in the middle member of the Bakken Formation. Note the porosity around the fractures (blue). Most open fractures have a ~100-150 µm band or halo around the fracture itself.

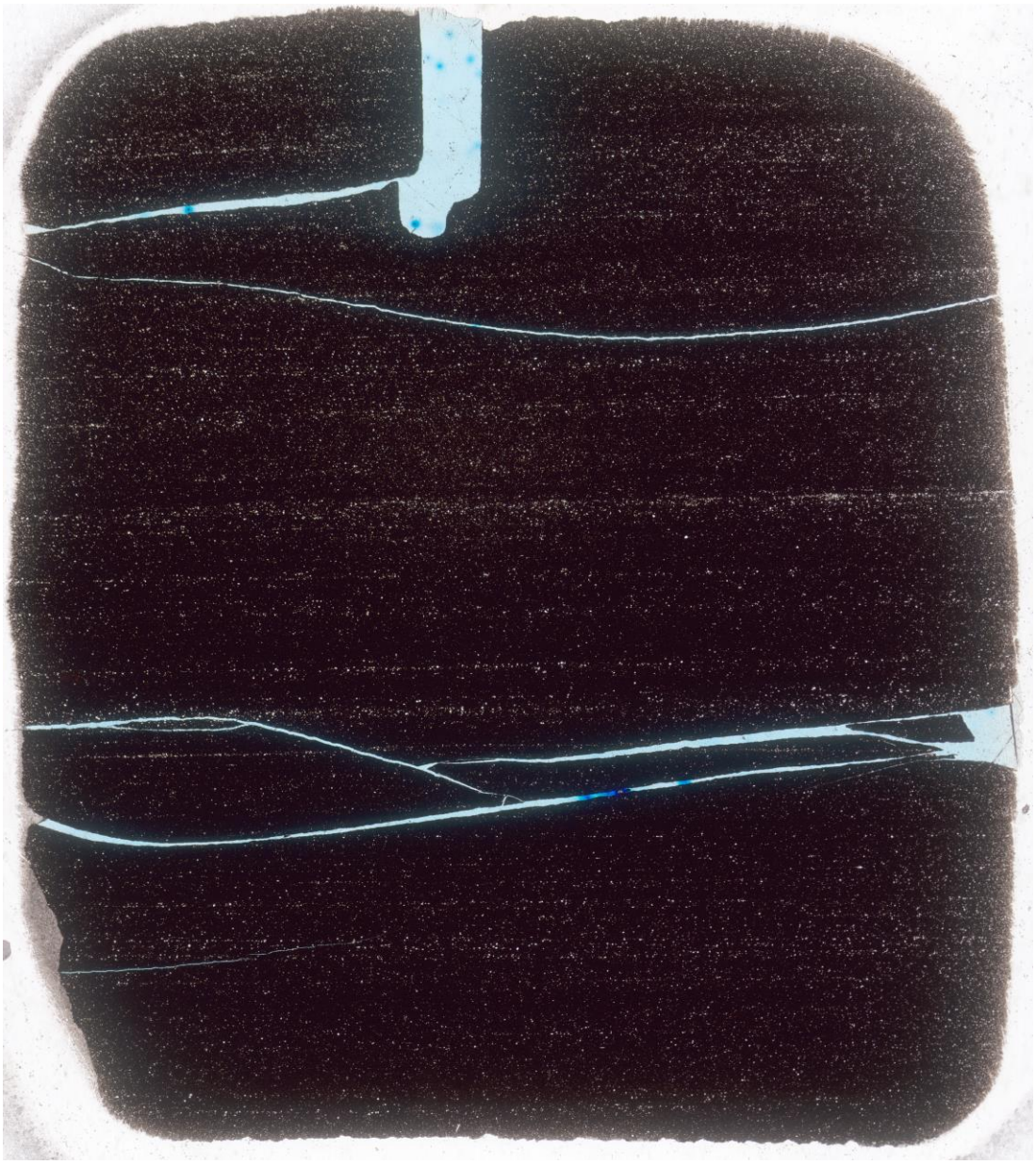


Figure 28. Thin section scan from the 44-24 Vaira core of the upper shale member. Fractures occur horizontally, most likely from clay partings in the shale. Fine laminations can be seen by the alternating grain sizes. Vertical axis 3 cm.

Within the lower extent of the shale, fractures are dominantly sub-horizontal and open. However, it is believed that these sub-horizontal fractures were formed either through core extraction or from the thin section preparation process based on the lack of fracture-related porosity viewed within the middle member of the Bakken.

The Mississippian Lodgepole Formation, at the top of the cored interval, is very similar to the upper Bakken shale member. It is primarily a wackestone with fragments of crinoids and mollusk shells. The Lodgepole in this core contains an interval known as the "False Bakken." This mudrock, the Cottonwood Creek member in the Lodgepole, shows similar signatures on gamma ray logs as the upper shale member in the Bakken. The Lodgepole limestone contains mollusk shell fragments, and crinoid stems. Fractures within the limestone are completely healed with calcite and microcrystalline quartz.

The "False Bakken" is a mudshale, similar to the upper shale member, and is composed of scarce bioclastic material, intervals of silt-sized grains, such as quartz and calcite, and a micrite matrix. Fractures within the Cottonwood Creek member are open and horizontal, and originate from the coarser-grained intervals, most likely from the fissility of the mudshale.

The 44-24 Vaira core has undergone limited diagenesis. The upper shale member of the Bakken Formation is more organic-rich than the A-1 Stark core. Because of the presence of organic material within the shale, the amount of

pyritization observed in the shale and within the upper portion of the middle member is much greater than in the A-1 Stark core. The amount of fracturing observed within the thin sections is relatively the same. Open horizontal fractures dominate the shale, however, the fractures likely formed from the core extraction process.

The middle member of the Bakken within the 44-24 Vaira core has undergone more extensive diagenesis than the A-1 Stark core. Long contacts of quartz and calcite grains indicate that mechanical compaction occurred before the dissolution of calcite and precipitation of dolomite. Chemical compaction followed mechanical compaction, resulting in stylolites, viewed in both core and thin section. Only calcite grains occur within the stylolite swarms, and dolomite occurs outside of these swarms, revealing that chemical compaction occurred before dolomite precipitation.

OUTCROP FRACTURE ANALYSIS

The Bakken Formation has outcrop analogs in Montana. The Banff and Exshaw formations are lithostratigraphically equivalent to the Bakken, outcropping in northwestern Montana. The Sappington Member of the Three Forks Formation is chronostratigraphically and lithostratigraphically equivalent to the Bakken and Banff/Exshaw Formations, however, the fracture networks are very different.

The Three Forks Formation is comprised of three members: the basal Logan Gulch Member, the middle Trident Member and the upper Sappington Member. The Logan Gulch Member is an argillaceous limestone with interbedded shale breccia and lenses of dolomite and anhydrite. It is the most extensive member within the Three Forks Formation. The Logan Gulch member represents a restricted marine environment during the upper Devonian. The middle Trident member is a slightly calcareous, fossiliferous shale and dolomite/limestone. It represents a locally restricted, open marine environment (Sandberg, 1965).

The Sappington member disconformably lies above the Trident member and disconformably underlies the basal shale unit of the Lodgepole Formation. The Sappington member consists of five lithologic units: 1) a basal, carbonaceous shale 2) a fossiliferous, nodular, silty limestone 3) a shaly siltstone 4) slightly

calcareous shale 5) and a coarse-grained, limonitic, calcareous siltstone/sandstone (Sandberg, 1965). It is interpreted to be a shallow near-shore to shelf environment.

Methods

Outcrop locations of the Three Forks Formation were selected from the Montana Bureau of Mines and Geology 1:100,000 Montana quadrangles. Locations were visited to determine the presence of the Sappington member within the Three Forks Formation. Fracture analyses were conducted at outcrops based on completeness of the units within the Sappington member (Table 2). Logan Gulch near Logan, MT, Antelope Valley near Sappington, MT, Hardscrabble Peak in the Bridger Mountain Range and Moose Creek near Big Sky, MT were selected for fracture analysis (Figure 29).

Outcrop Unit	**Logan Gulch**	**Antelope Valley**	**Hardscrabble Peak**	**Moose Creek**
Lodgepole Fm	x	x	x	x
Sandstone	x	x	x	x
Upper Shale				x
Siltstone			x	x
Limestone				
Lower Shale				

Table 2. Outcrop locations chosen for fracture analysis and units present within each outcrop location.

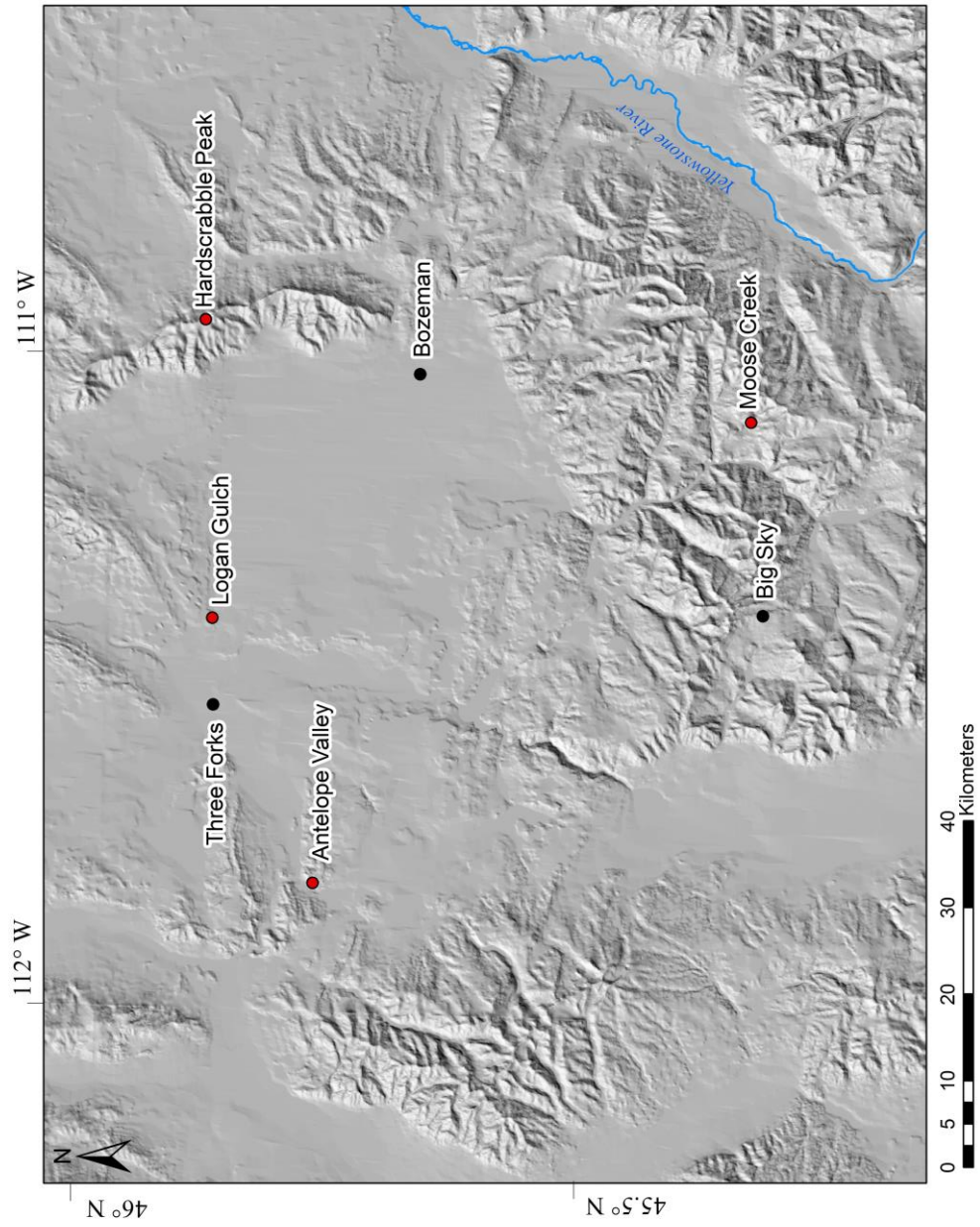


Figure 29. Map of Sappington Member outcrop locations chosen from southwestern Montana (red). Towns of Three Forks, Bozeman and Big Sky in black.

There are two major fracture analysis methods, the selection method and the inventory method. The selection method entails selecting specific fractures or fracture sets to study. The inventory method involves recording every fracture that occurs within a drawn circle or square (Davis et al., 2012). The inventory method chosen in order to measure meter-scale fractures down to centimeter-scale fractures (a scale that would be sampled within a core). A 4’ x 4’ box was drawn on the outcrop and every fracture that occurred within the outline was recorded. The bedding attitude was measured inside the inventory box before fractures were measured. Fractures of each unit were recorded separately and fracture properties such as strike, dip, length, aperture, vein-fill material and texture, arrest behavior, and relationship to surrounding fractures were measured. The complete table of fracture measurements can be found in Appendix B.

Fracture orientations were used to generate stereonets, and azimuths were used to plot rose diagrams. Fractures measured at each location were compiled into individual stereonets. Dipping beds were rotated to horizontal for each location and compared to un-rotated stereonets to attempt determination of fracture timing in relation to folding. Stereonets and rose diagrams with a stronger correlation were chosen out of the rotated and un-rotated plots. Rose diagrams were created using RockWorks 16, using a 10^{o} orientation class.

Results and Discussion

Logan Gulch, located in the Horseshoe Hills near Logan, MT, is aptly named for the type section of the Logan Member of the Three Forks Formation (Sandberg, 1965). The outcrop of the Sappington Member contains the upper sandstone. The shales can be located, but a trench must be dug in order to expose the highly weathered green mudrocks. The middle siltstone is also present, but the exceedingly weathered condition didn't allow for a fracture analysis. The Lodgepole Formation is very extensive at this location, so fractures were measured in the limestone, close to the contact with the Sappington (Figure 30).

Antelope Valley located just north of Sappington, MT, and south of Milligan Canyon contains the upper sandstone. The outcrop of the Three Forks Formation exists within an east-west trending valley. Unfortunately the other units within the Sappington are not well preserved, making it difficult to conduct a fracture analysis on the entire member. The Lodgepole Formation is also prevalent, and fractures were recorded within the limestone (Figure 31).

Hardscrabble Peak in the Bridger Mountain Range was selected for its extensive upper sandstone unit and its middle siltstone unit. The Lodgepole Formation is also prevalent and fractures were measured above the contact of the Sappington. The shales can be found by trenching, and were selected for X-ray

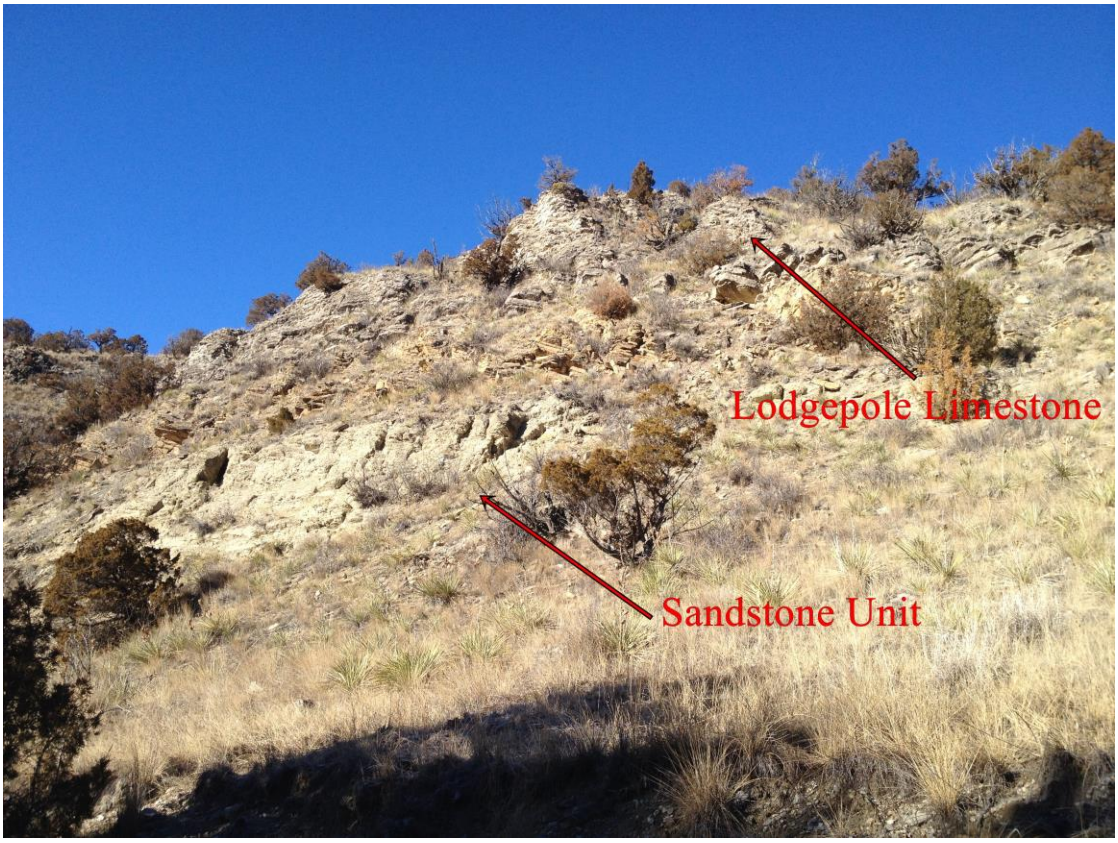


Figure 30. The Logan Gulch Outcrop of the Sappington Member. The upper mudstone can be located between the sandstone unit and the Lodgepole Formation, but a trench must be dug in order to expose it.

texture analysis at Argonne National Laboratory, however the degree of weathering did not allow for fracture measurements (Figure 32).

Moose Creek, northeast of Big Sky, MT, is the most extensive outcrop of the Sappington Member. The outcrop contains the upper mudstone, upper sandstone, middle mudstone, and middle siltstone as well as the Lodgepole Formation. The upper mudstone is inaccessible at this outcrop because of its

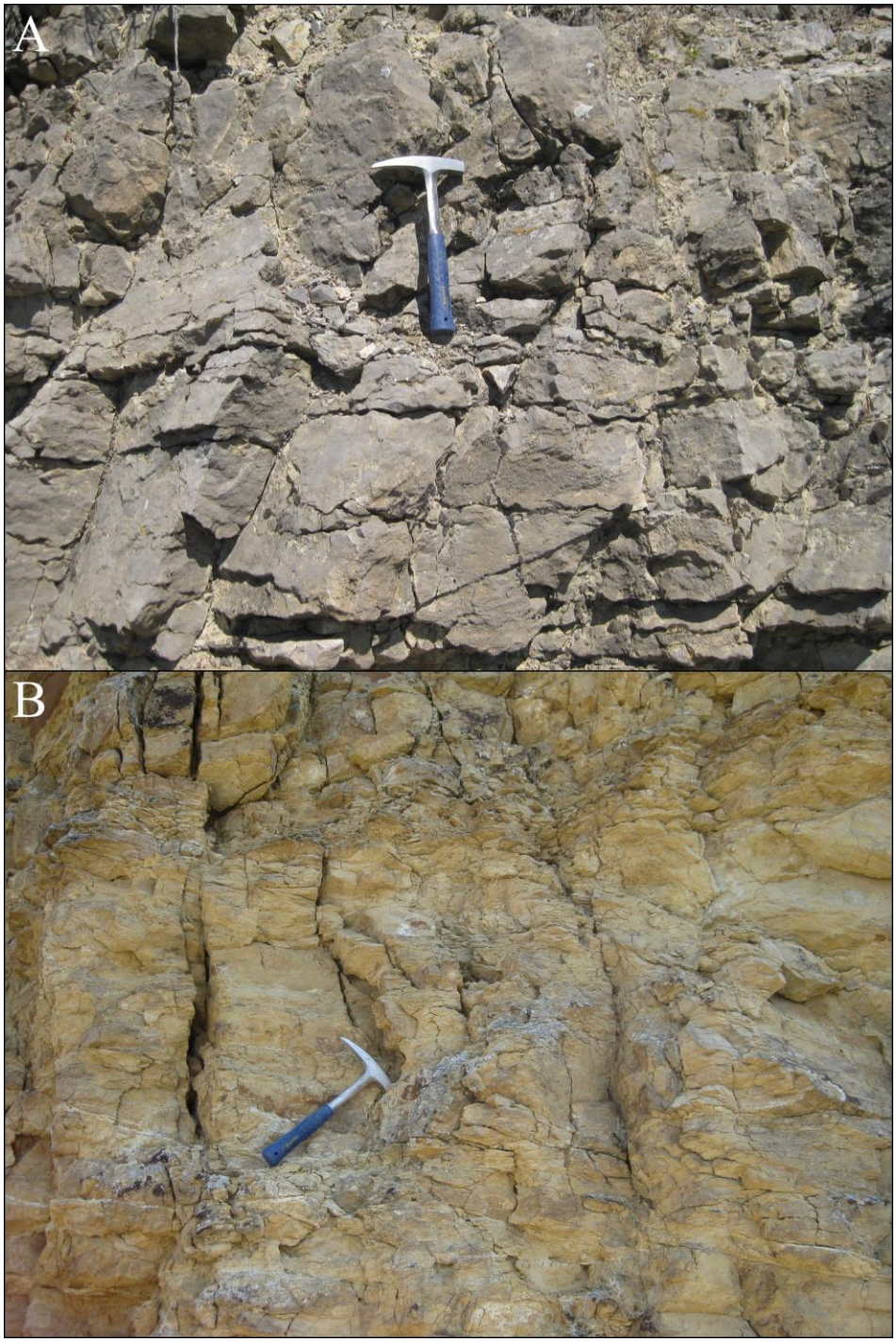


Figure 31. Antelope Valley outcrop. A). The basal unit of the Lodgepole Formation B). The Sandstone unit of the Sappington Member.

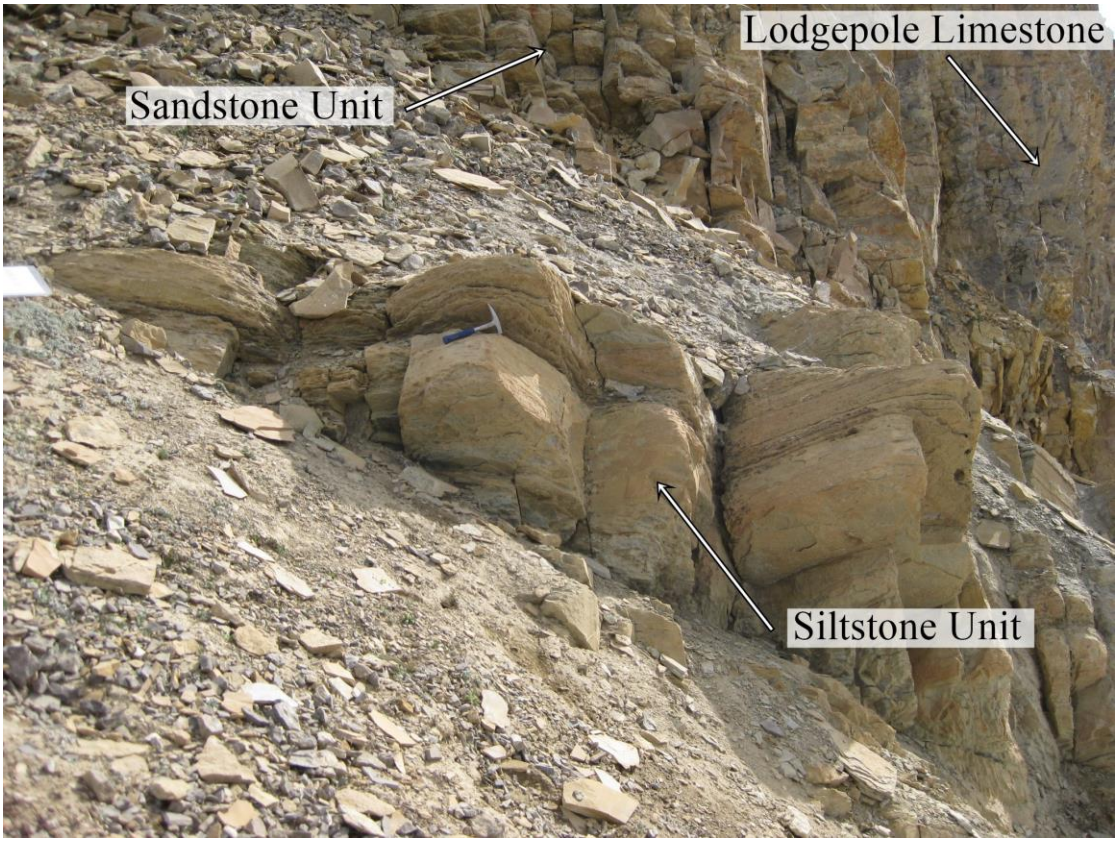


Figure 32. Hardscrabble Peak outcrop. The upper and middle mudstone members are present at this location, however a trench must be dug in order to expose them.

position on the cliff face. This outcrop location was the most fractured out of the four studied (Figure 33).

A regional fracture map compiled by Angster (2010) shows fractures measured throughout the Williston Basin and central Montana outside of the basin (Figure 34). Fractures within the Williston Basin, studied within structural features and undeformed strata, tend to have a northeast or northwest dominant trend, resulting from the wrench style deformation present within the basin. Outcrops

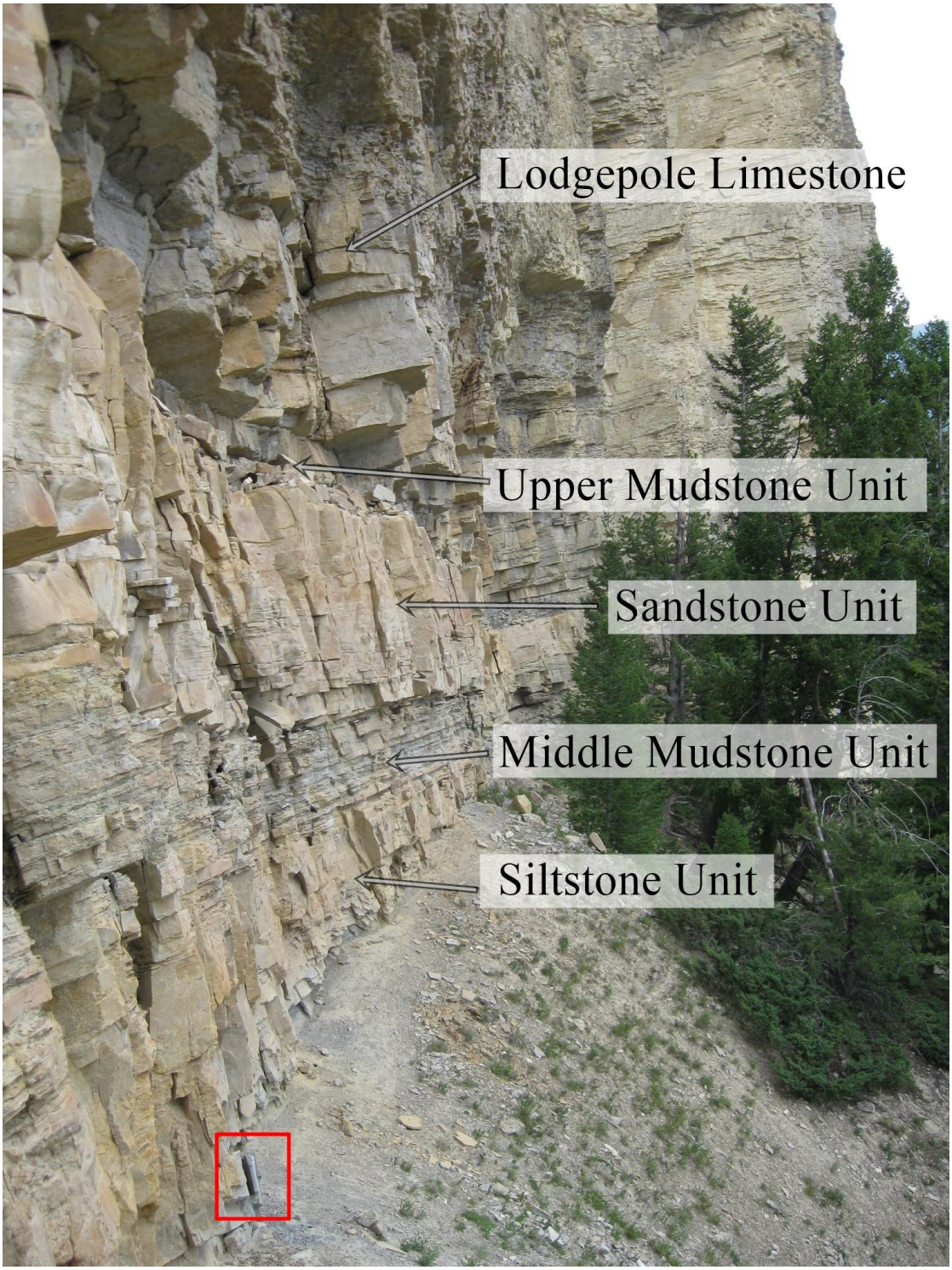


Figure 33. The Moose Creek Sappington Member outcrop with four of the seven units. Red box highlights a 12”x12” map board for scale.

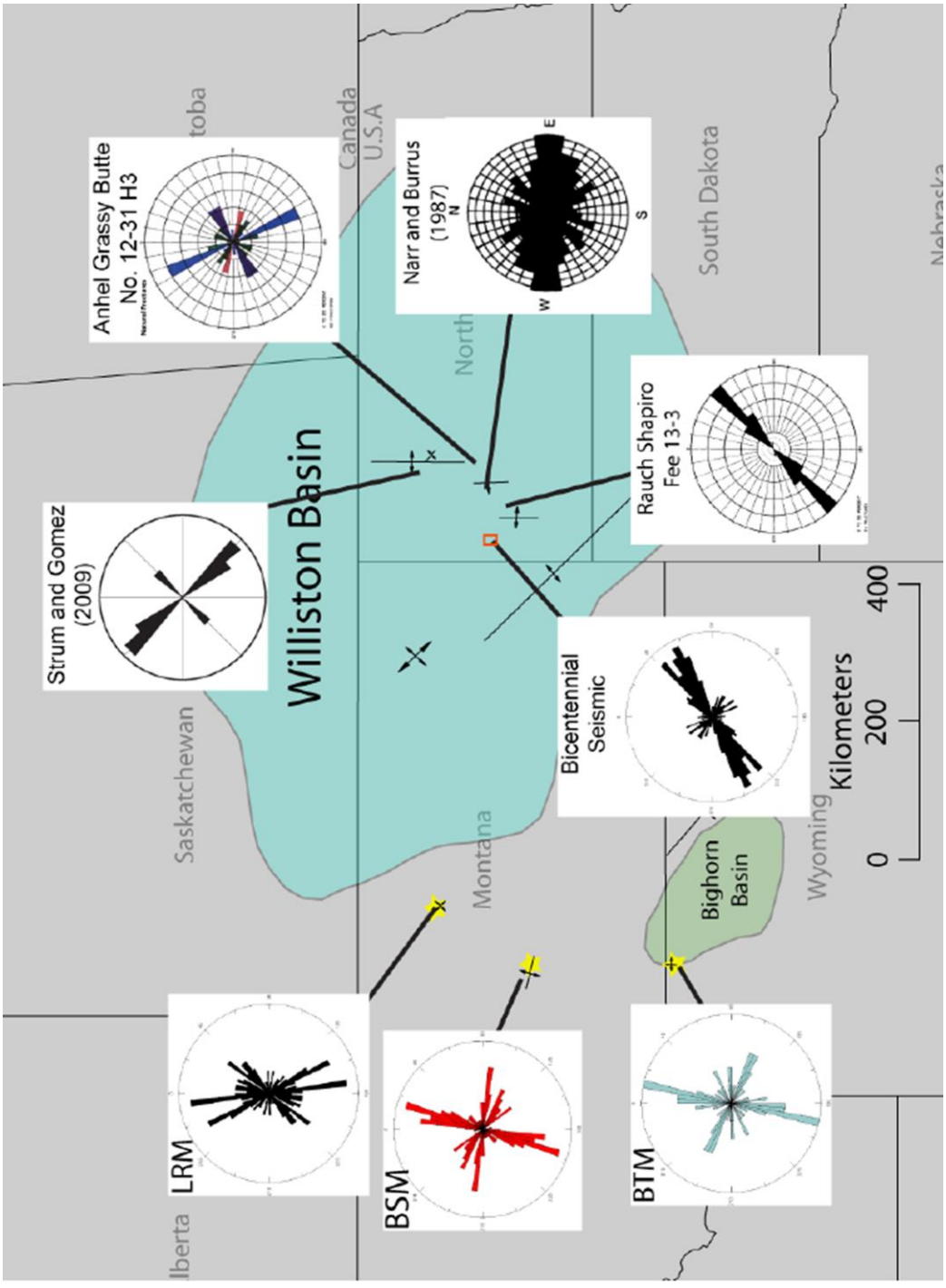


Figure 34. Map of Montana and North Dakota showing dominant fracture sets within the Williston Basin and in central Montana (Angster, 2011).

visited outside of the basin in Montana reveal a dominantly northeast strike, most likely from structure reactivation during the Laramide Orogeny (Angster, 2010).

Logan Gulch

Fractures at Logan Gulch dominantly strike 020º to 040º (200º to 220º), and are slightly bi-modal. When the dipping beds are rotated to horizontal, the dominant azimuth is 000º to 010º (180º to 190º), and no longer appears bi-modal. The outcrop is located between two northwest trending anticlines, which would affect the dominant strike of the area (Figure 35). The northeast strike of these anticlines and synclines suggest that the fractures formed during deformation.

Faults and folds within the Horseshoe Hills, which comprise the Logan Gulch outcrop, are part of the southwest Montana transverse zone of the Helena salient (Schmidt and O'Neill, 1982). This zone consists of folds and faults that trend transverse to the prevailing north/northwest trend of the overthrust belt, and separates tectonic features of the thrust belt in the north from the basement-cored uplifts of the Rocky Mountain foreland in the south. The Horseshoe Hills contains three major thrusts and many minor ones all striking between 030º-045º and dipping 40º-60º (Lageson, 1989; DeCelles, 2004).

The fractures measured at Logan Gulch strike 020º to 040º (200º to 220º), which are parallel to the strike of the large scale folds and faults within the Horseshoe Hills. Restoring the dipping beds to horizontal changes the dominant

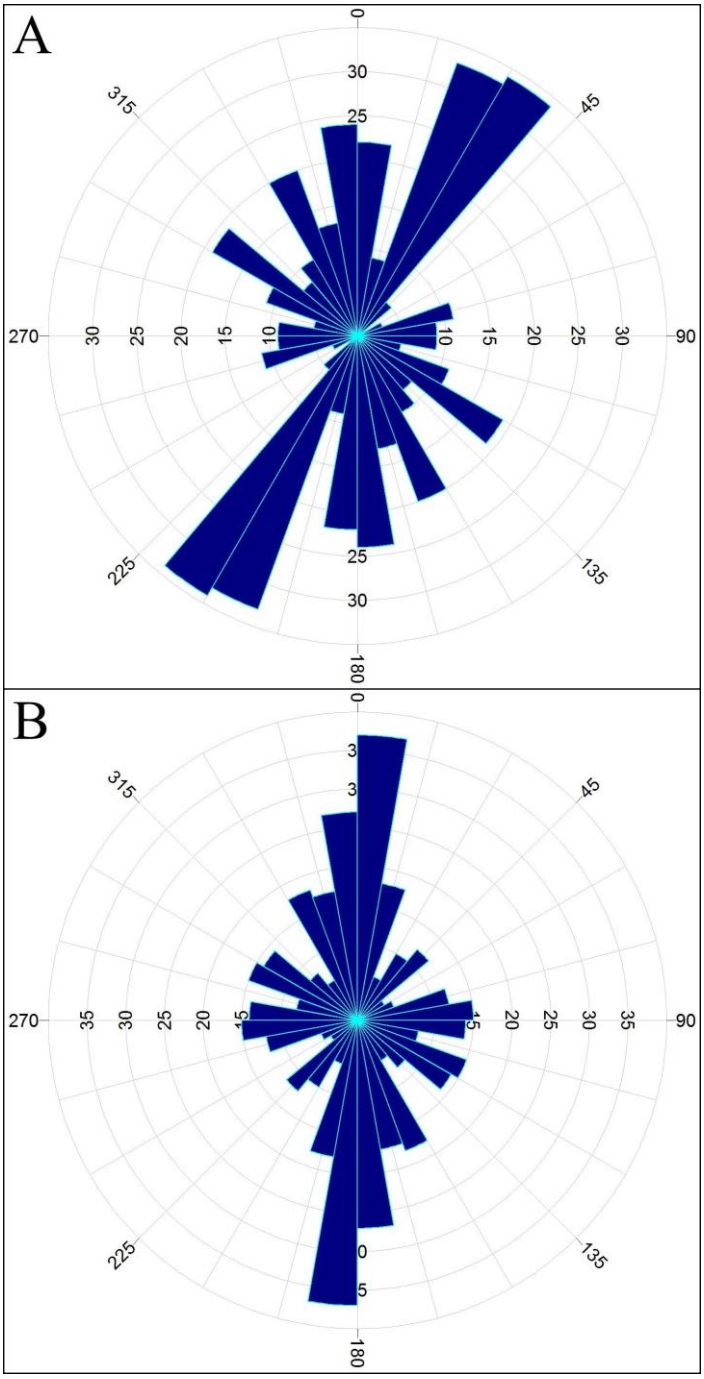


Figure 35. Rose diagrams of all fractures measured at Logan Gulch. A) Fractures before rotating dipping beds to horizontal. B) Fractures after dipping beds are restored to horizontal.

strike to 000º to 010º (180º to 190º) and the fracture set loses its bi-modal behavior. Based on the surrounding structures the fractures before dipping bed rotation reflect a more significant relationship.

Antelope Valley

Fractures at Antelope Valley are much noisier than those found at Logan Gulch (Figure 36). The dominant fracture strike is 020º to 030º (200º to 210º). When the dipping beds are rotated to horizontal, the fracture sets become more apparent with dominant sets striking 030º to 050º (210º to 230º) and 340º to 010º (160º to 190º). There are no mapped faults or folds within the study area, however, to the northwest there are a few mapped NE SW trending thrust faults.

The Antelope Valley outcrop is contained within the northern Tobacco Root-Jefferson Canyon portion of the southwest Montana transverse zone, which consists of an anastomosing array of faults. This central region is believed to be the interaction of thrust belt and foreland structures, causing faults to vary in trend and dip (Schmidt and O'Neill, 1982), which maybe the source of a chaotic spread of fractures within the outcrop location.

Hardscrabble Peak

Fractures at Hardscrabble Peak in the Bridger Mountain Range become more prominent when dipping beds are restored to horizontal (Figure 37). Before

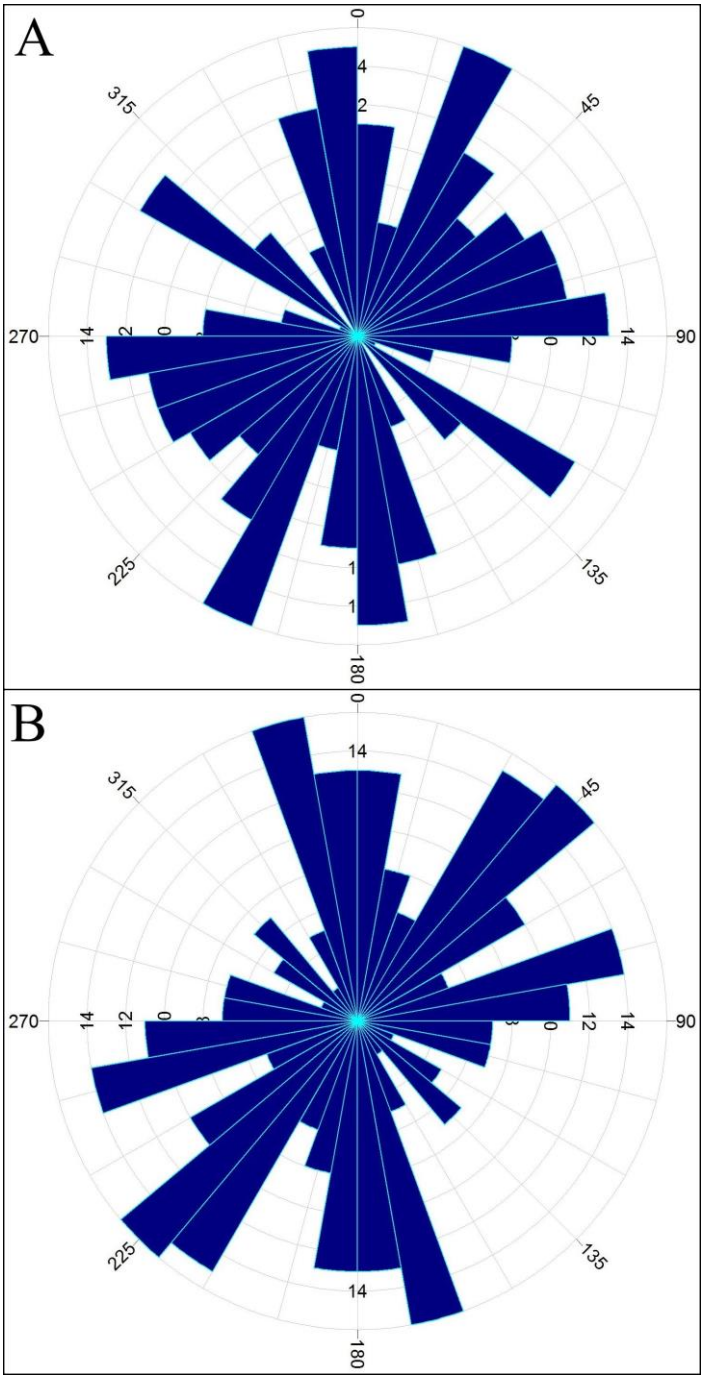


Figure 36. Rose diagrams fractures measured at the Antelope Valley outcrop. A) Fractures before rotating dipping beds to horizontal. B) Fractures after dipping beds are restored to horizontal.

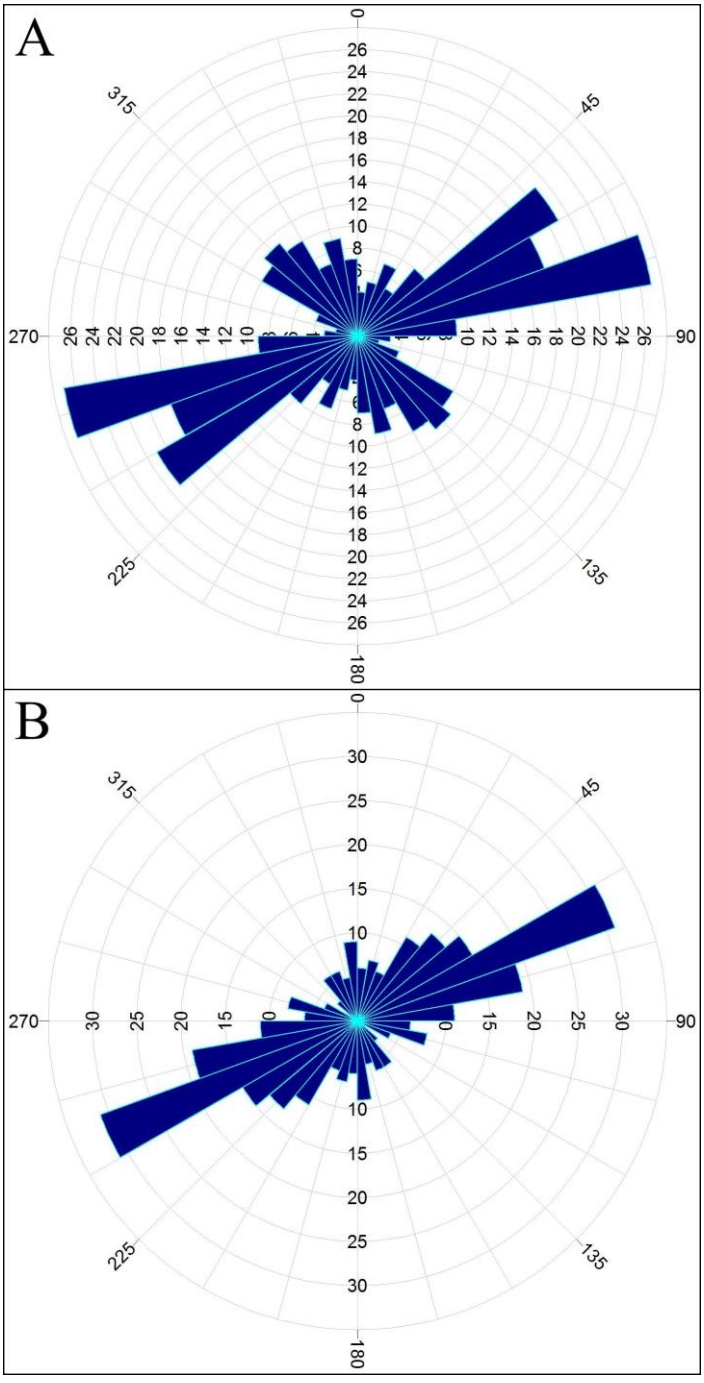


Figure 37. Rose diagram of fractures measured at Hardscrabble Peak in the Bridger Range. A) Fractures before rotating dipping beds to horizontal. B) Fractures after dipping beds are restored to horizontal.

bedding rotation, fractures are slightly bi-modal, with a dominant azimuth at 050º to 080º (230º to 260º). When rotated, the dominant strike is 060º to 070º (240º to 250º). Hardscrabble Peak is one of the many peaks that make up the ancestral Laramide Bridger Range arch.

The Bridger Range occupies a tectonically diverse region in the northern Rocky Mountains lying within an intersection of four major tectonic provinces; the two most recent events being the Laramide Orogeny and Basin and Range extension (Lageson, 1989). Erslev and Koenig (2009) estimated the maximum shortening direction that formed Laramide structures through regional minor fault and fold kinematic data, giving an average shortening direction of 066º (246º). The fractures measured at Hardscrabble Peak in the Bridger Range show a dominant strike of 060º to 070º (240º to 250º) after dipping beds were rotated to horizontal. This trend matches the average shortening direction measured by Erslev and Koenig (2009).

Moose Creek

The Moose Creek outcrop is contained within the northern portion of the Gallatin Mountain range. Fractures at Moose Creek are bi-modal with two dominant strikes. The first set strikes at 350º to 010º (170º to 190º) and the second set strikes 070º to 090º (250º to 270º). When the dipping beds are rotated to

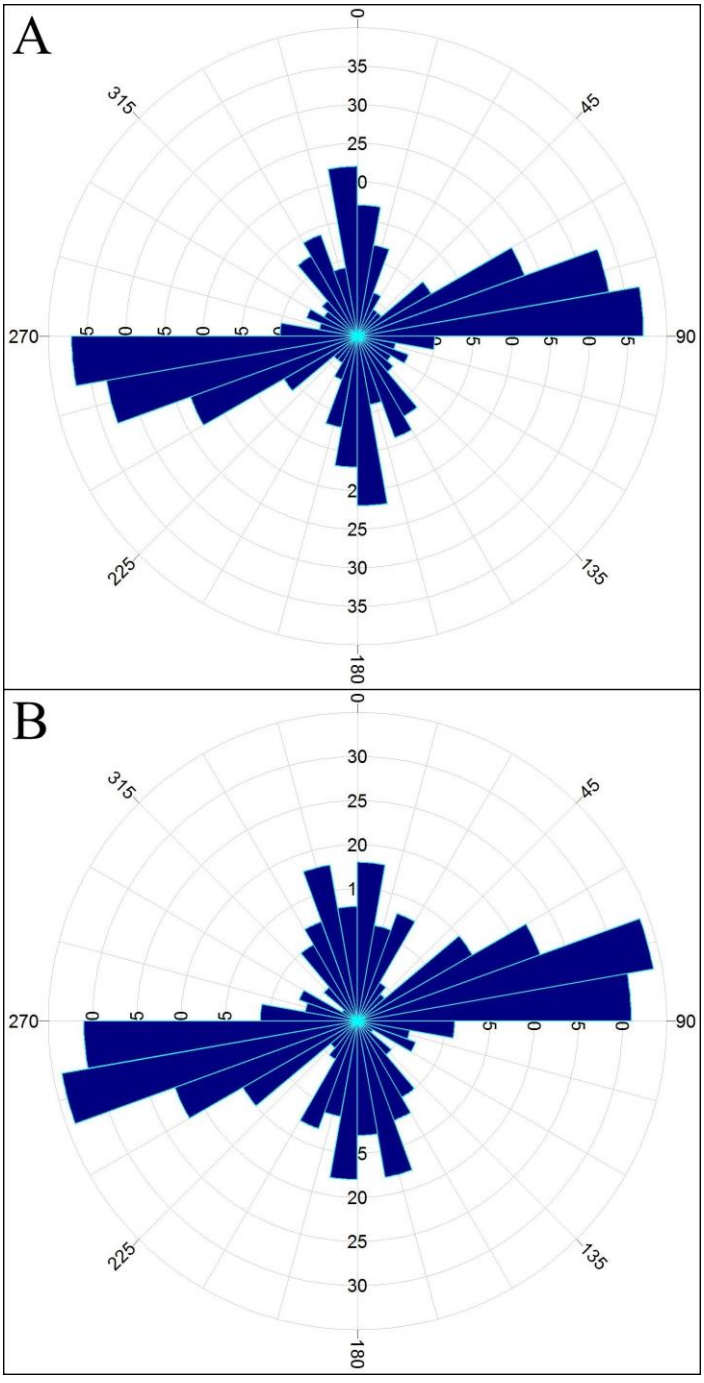


Figure 38. Rose diagram of fractures measured at Moose Creek. A) Fractures before rotating dipping beds to horizontal. B) Fractures after dipping beds are restored to horizontal.

horizontal, these sets become less apparent, losing their significance (Figure 38), indicating that fractures formed during folding and faulting.

Northwest of the Sappington outcrop, there lies a northeast trending, northwest dipping thrust fault. Southwest of the outcrop is a high-angle fault with unidentified sense of slip separating Paleoproterozoic rock from Phanerozoic rock. Given that the Gallatin Range exists within the Laramide foreland, these faults, if present before the Laramide Orogeny, could have been reactivated. Assuming that the undifferentiated southwest fault is a high angle reverse fault and the dominant fractures at the Moose Creek outcrop strike roughly N-S and E-W, then they lie oblique to the assumed maximum shortening directions (southeast and northeast) of the surrounding faults. This may be the cause of the bi-modal behavior seen within the fracture data (Figure 39).

Fracture Analysis

Fractures with vein fill were highly important for they represent fractures that initiated in the subsurface, however, fractures with vein fill were scarce, and only 13.8% of the 812 fractures measured contained vein fill. Some fractures contained a “film” of calcite along the walls (which were counted as vein fill) but the outcrops are weathered and accurate apertures could not be measured in such cases. Some fractures measured in the field only had one fracture wall (where

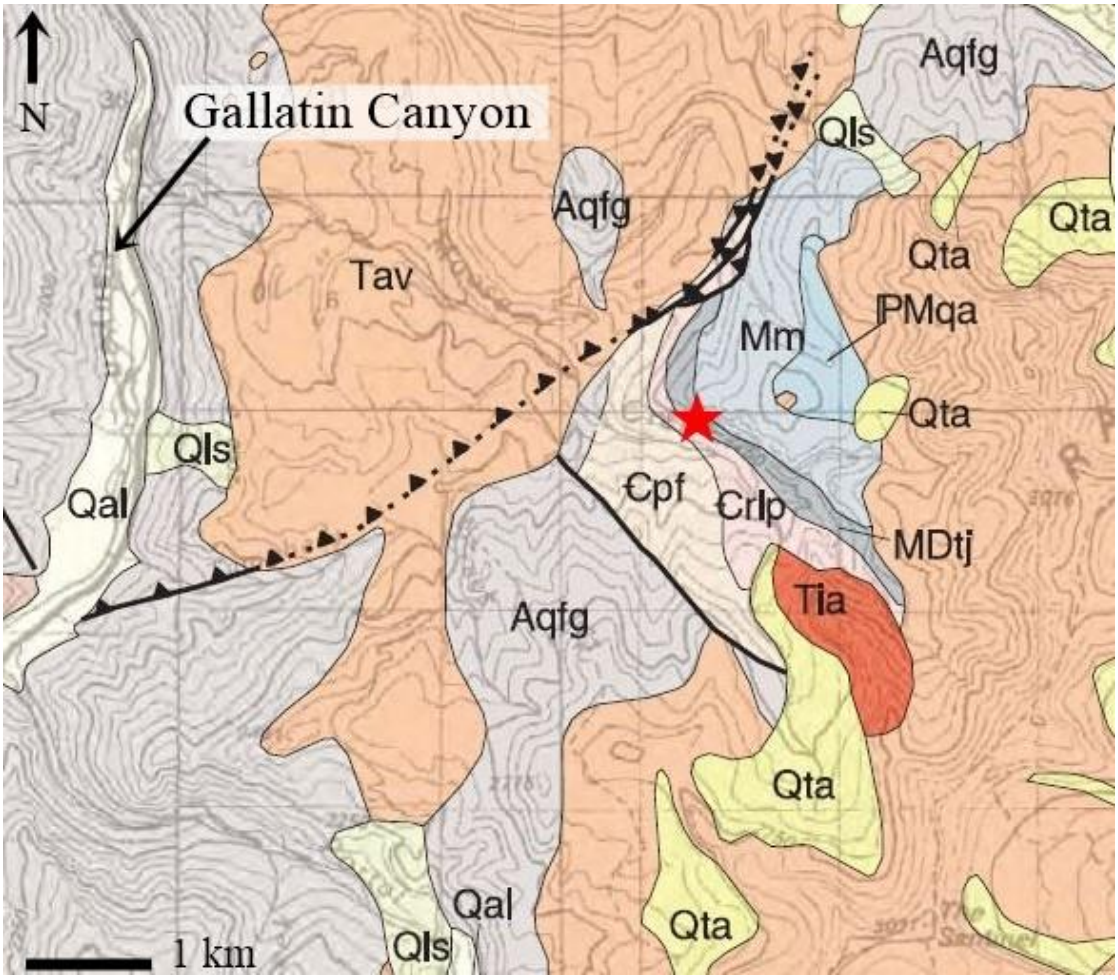


Figure 39. The surrounding geology of the Moose Creek area taken from the Montana Bureau of Mines and Geology 1:100 000 Ennis Quadrangle (Modified from Kellog and Williams, 2006). The outcrop is marked by the red star.

the other wall has been weathered away); in cases like this, the aperture was not recorded.

Fracture length throughout all outcrop locations are highly skewed. Length can only be measured as traces on exposed surfaces of the outcrops, which are

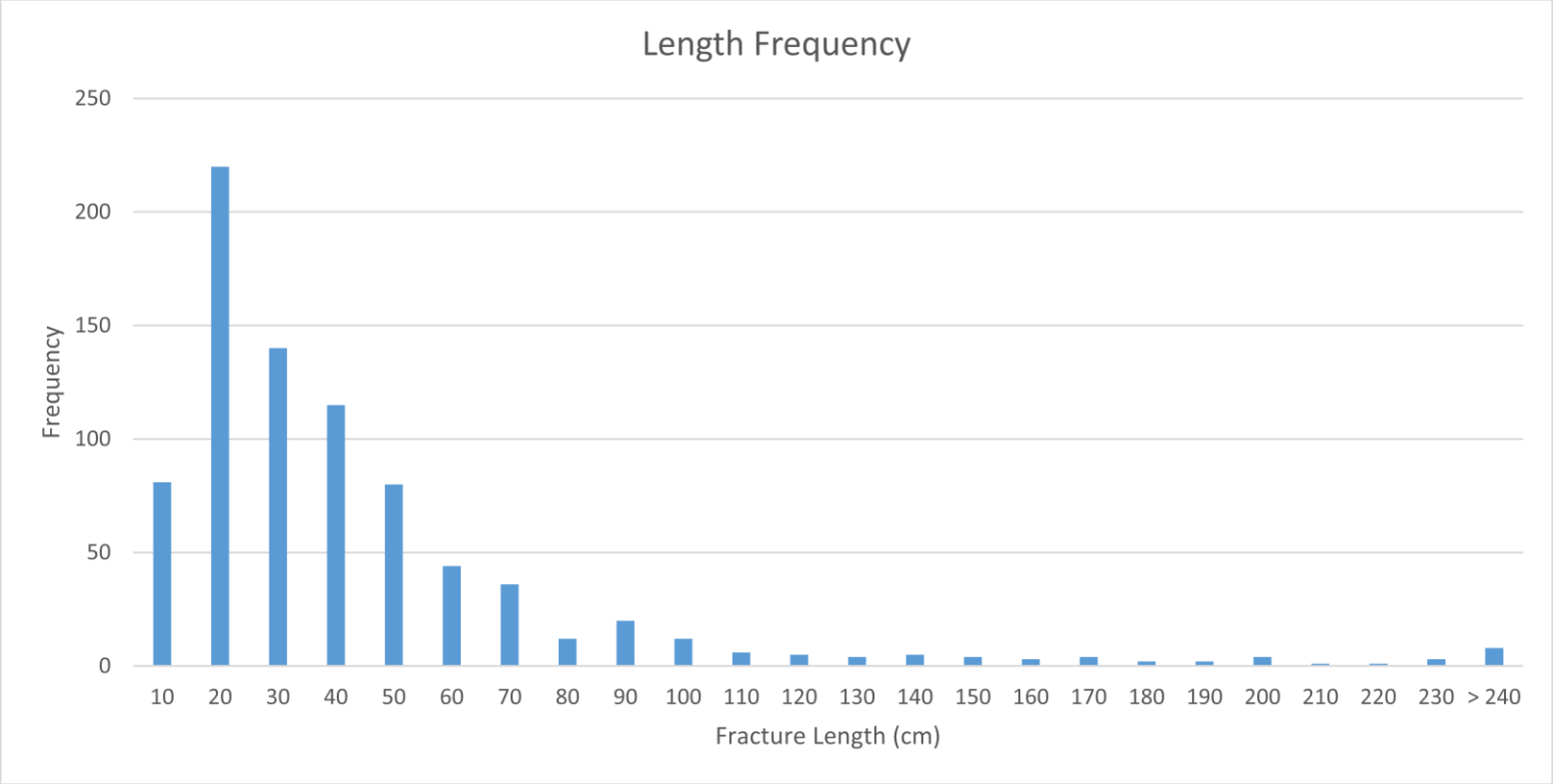


Figure 40. Bar graph of fracture trace length taken from all Sappington outcrops. Note the high skew within the smaller lengths.

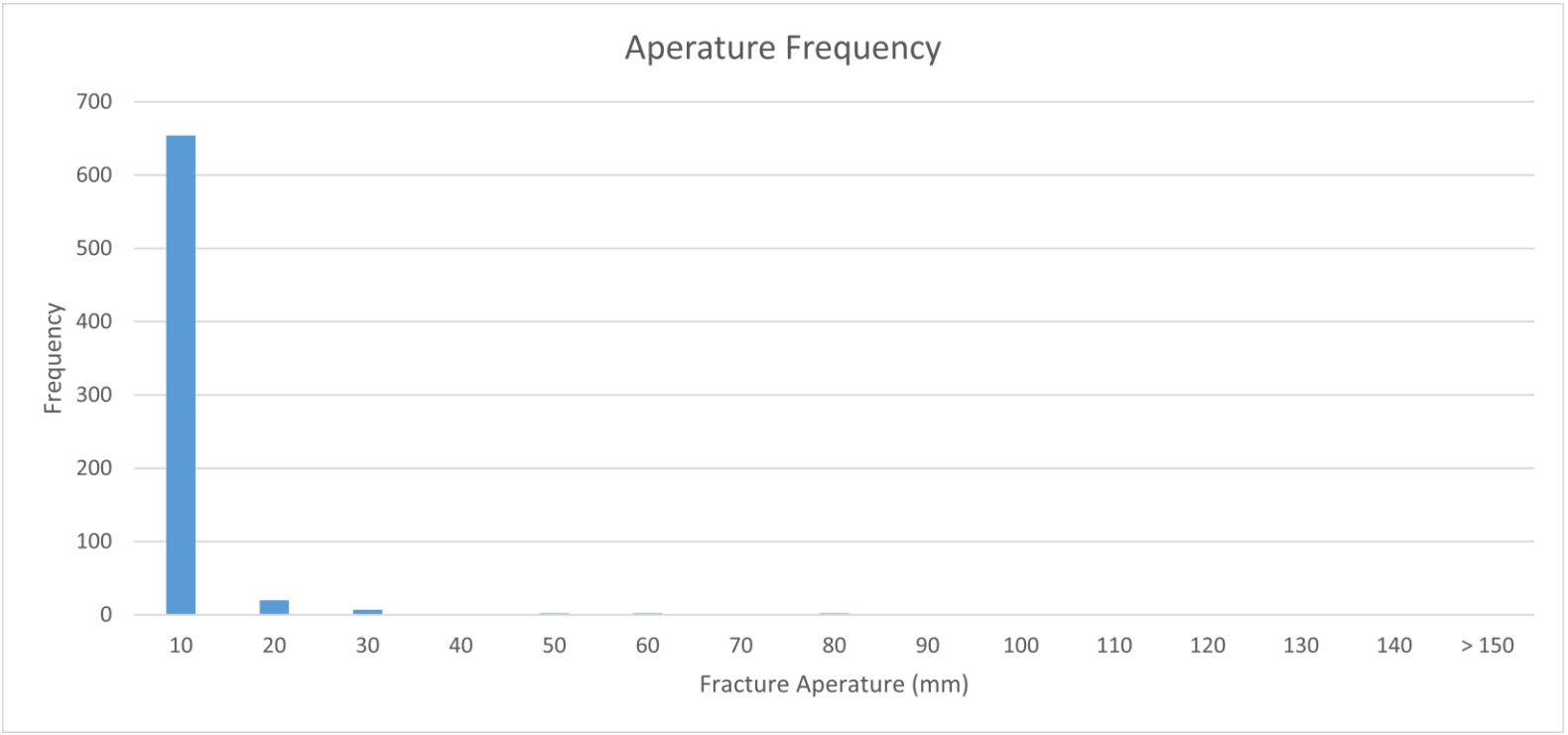


Figure 41. Bar graph showing fracture aperture of all measured fractures. The high skew can be seen between 0–10 mm.

hindered by the limited extent of an outcrop. For example fractures often extend further into covered regions past the studied outcrop. Lengths between 10 and 20 cm are the most common throughout all locations (Figure 40). This is the result of sampling bias discussed above. Fracture aperture throughout all locations is also skewed. Fractures were measured on weathered surfaces at all locations, most likely exposed by the same type and extent of mechanical and chemical weathering. This assumption allows the relative comparison of fracture aperture. Apertures between 10 and 20 mm are the most common, however some fractures measured had only one fracture wall, so aperture was omitted in this case (Figure 41).

The relationship between fracture length and aperture is not well constrained, and is a matter of debate. A hypothetical increase in energy within a rock will force the fracture wider and longer. However this relationship is not linear (Renshaw and Park, 1997; Baghbanan and Jing, 2008). Within the combined outcrops, there is a weak correlation between fracture length and aperture. Because of the high skew within both fractures measurements, a log-log plot was created to show the relationship more clearly (Figure 42). It is possible that the weak correlation is a result of the highly weathered outcrops and missing fracture walls.

Rose diagrams plotted from this study are shown in Figure 43 to compare to other regional fracture studies of the Bakken and related formations. Fractures

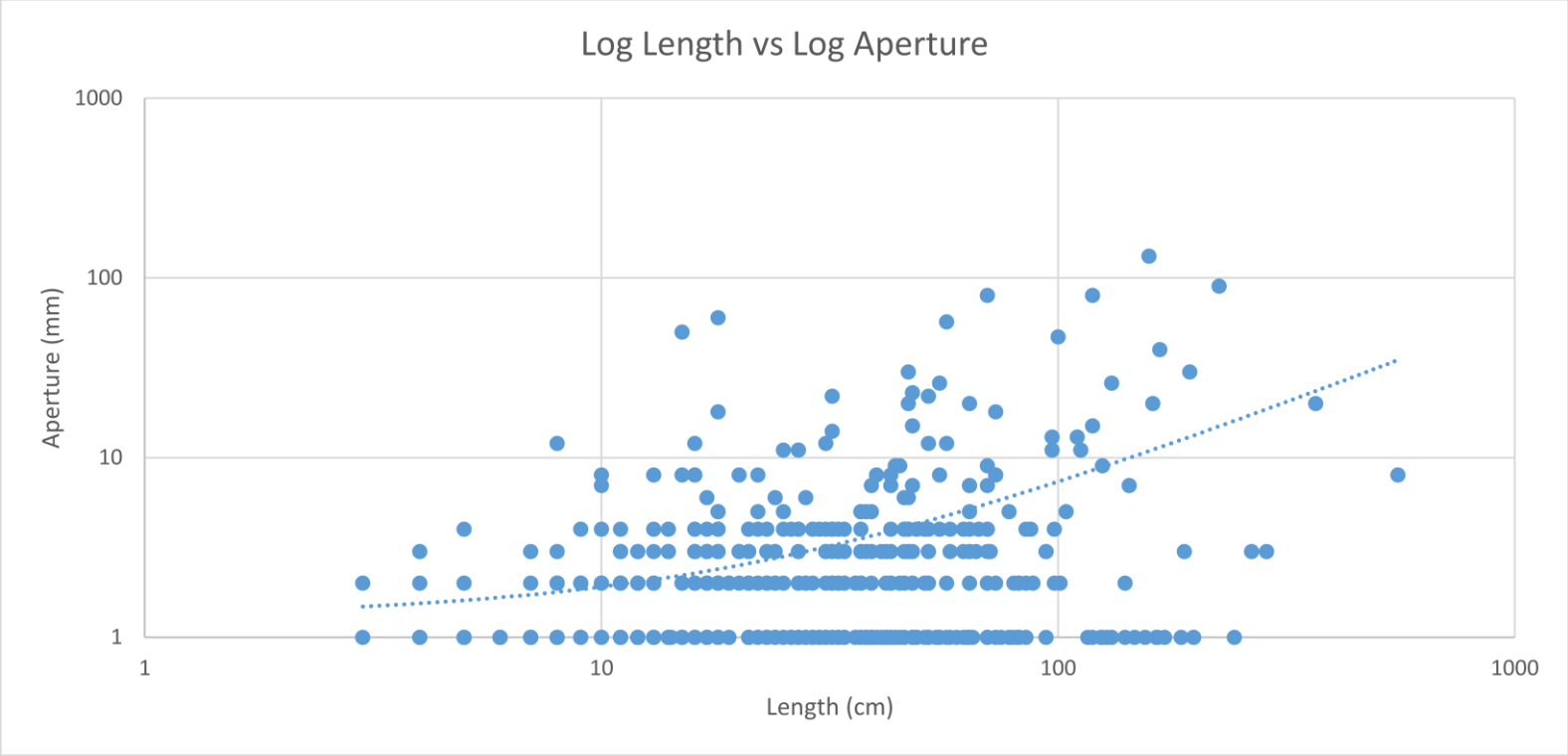


Figure 42. Log-log line graph showing the weak correlation between fracture aperture and trace length.

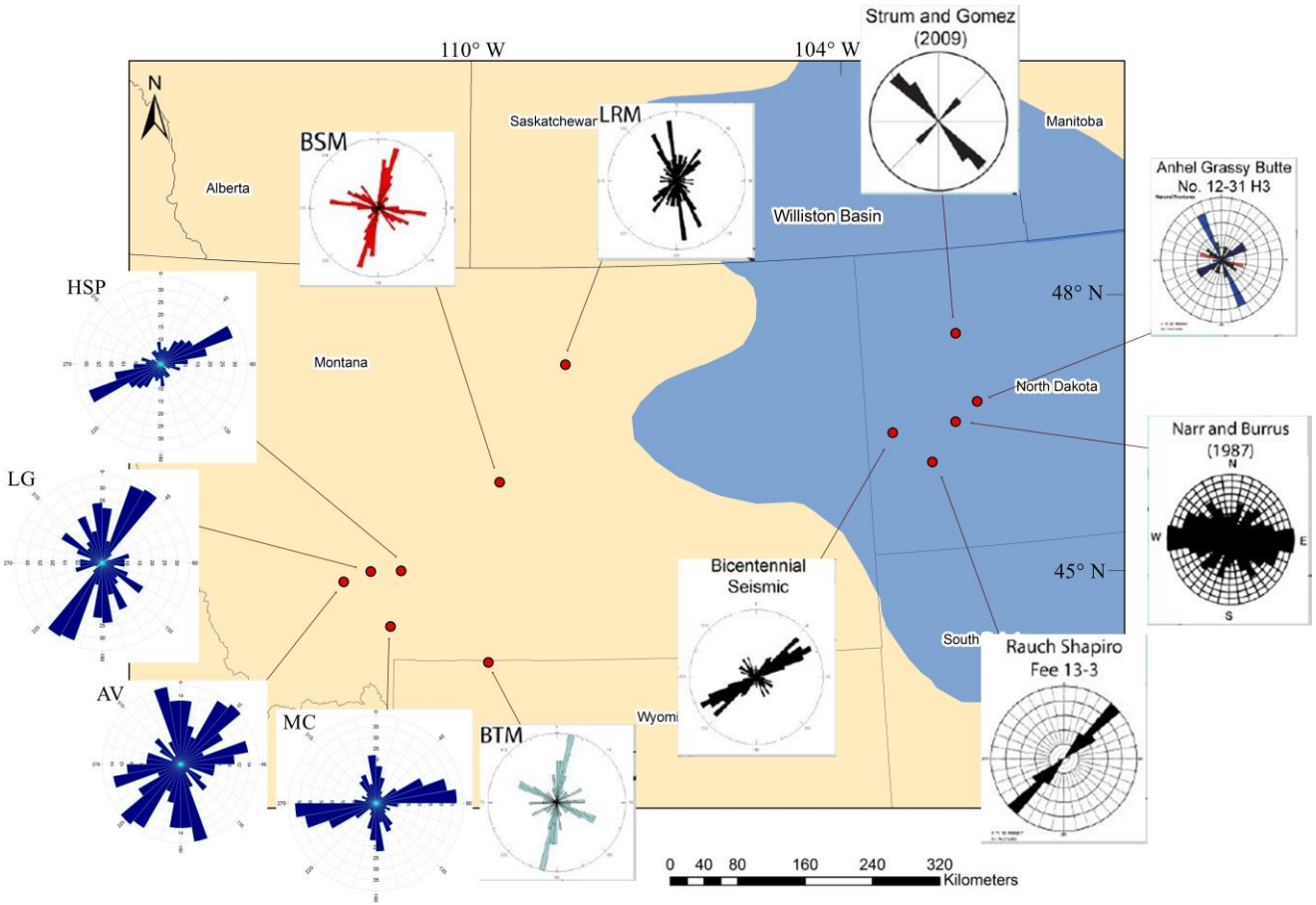


Figure 43. Map of regional fracture studies relating to the Williston Basin and the Three Forks Basin (in red) (modified from Angster, 2011). BSM = Big Snowy Mountains, LRM = Little Rocky Mountains, BTM = Beartooth Mountains, HSP = Hardscrabble Peak, LG = Logan Gulch, AV= Antelope Valley, MC = Moose Creek.

measured from Devonian and Mississippian period rocks outside of the Williston Basin in the Big Snowy Mountains and the Beartooth Mountains show a dominant NNE strike; the Little Rocky Mountains have a NW strike (Angster, 2011). Work by Narr and Burrus (1987) show a dominant east-west trend for fractures on the northern end of the Little Knife anticline in the Williston Basin. Strum and Gomez (2009) used Formation Micro Image logs within three wells drilled in "off structure" stratigraphy within the Williston Basin. Mode 1 fractures strike NW whereas induced fractures trend northeast. Fractures obtained from core also show NW and NE striking sets (Angster, 2011).

Fractures from the Sappington Member show a diverse spread of dominant strikes. Rose diagrams of fractures studied throughout Montana and North Dakota in the Bakken Formation as well as other Devonian/Mississippian period rocks highlight that fractures are controlled by local structures contained within separate basins (Figure 43). These regions may be affected by tectonic movement along the western flank of North America, however they react very differently evidenced by the range in dominant strikes.

X-RAY TEXTURE ANALYSIS

Shales make up ~50 percent of the sedimentary rock record and act as hydrocarbon sources and reservoirs around the world (Boggs, 2009). Clay-rich shales comprised of phyllosilicate minerals can acquire crystallographic preferred orientation (CPO) during deposition, burial and diagenesis. Sedimentation and compaction lead to well-defined bedding foliation, which is observed as anisotropy of texture dependent characteristics such as seismic wave propagation (Militzer et al., 2011; Kanitpanyacharoen et al., 2012). The poor crystallinity and small grain size that accompany shales such as the Bakken Formation make it difficult to quantify texture by using conventional methods such as pole figure goniometry and electron backscatter diffraction (Valcke et al., 2006).

Methods

Shales are usually composed of multiple layered silicate minerals such as phyllosilicates. During X-ray diffraction, these clay minerals display peak broadening due to small grain size, stacking disorder, polytypism, interlayering and microstrain (Wenk et al., 2008). Most shales include quartz, and carbonate minerals, as well as minor amounts of feldspars and pyrite. Because of these factors, a conventional powder X-ray diffraction pattern is too difficult to interpret. Polyphase aggregates display mineral overlaps, which makes individual

peak position identification difficult to impossible with conventional methods (Wenk et al., 2008). A method of transmission geometry that requires synchrotron X-ray diffraction has revealed the ability to successfully measure the Orientation Distribution Functions (ODF) of layered silicate minerals and was first applied to slates. This method allows for the modeling of composition, texture and microstructure of fine grain aggregates e.g. shales (Lonardelli et al., 2007; Wenk et al., 2008).

Twenty Bakken shale samples from Montana and North Dakota were prepared for hard synchrotron X-ray diffraction analysis, however, five of them were omitted due to the absence of clay minerals. The samples were carefully cut into 2 mm thin slices for synchrotron X-ray diffraction. The first set of samples (BMT and BND) were cut to thickness with a micrometer diamond saw in the MSU High Temperature Materials Laboratory; the second set of samples (R311, C605, HH and HSP) were impregnated with low-temperature hardening epoxy in a vacuum chamber, cut into cubes with a tile saw and then sanded down with sand paper to achieve the 2 mm thickness. The diffraction measurements were conducted at the Basic Energy Sciences Synchrotron Radiation Center (BESSRC) 11-ID-C Beamline of the Advanced Photon Source (APS) at Argonne National Laboratory (ANL).

Three of the samples were extracted from Levang 3-22H core (BND) operated by Helis Oil and Gas Co. in North Dakota. Eleven samples of the Bakken

Sample	Type	Formation	Member	Location	Operator
C605 A	A-1 Stark Core	Bakken	Upper Shale	Montana	Anadarko Production Company
C605 B					
C605 C					
R311 A	Vaira 44-24 Core			Montana	Balcron Oil
R311 B					
R311 C					
R311 D					
R311 E					
BND 1	Levang 3-22 H Core			North Dakota	Helis Oil and Gas Company
BND 2			Lower Shale		
BMT 2	Unknown Core		Unkown	Montana	Unknown
BMT 3					
HSP U	Hardscrabble Outcrop	Three Forks	Sappington Upper Shale		-
HSP L			Sappington Middle Shale		-
HH	Horshoe Hills Outcrop				-

Table 3. Samples used in the X-ray texture study.

shale in Montana were extracted from core; three were from an undisclosed well (BMT) within Richland County, five were extracted from the Vaira 44-24 core operated by Balcron Oil Co. (R311), and three were taken from the A-1 Stark core operated by Anadarko Production (C605). Additionally, three outcrop samples were taken from the Sappington Formation at Hardscrabble Peak (HSP) in the Bridger Range, and Logan Gulch in the Horseshoe Hills (HH) near Logan, MT. Sample information is shown in Table 3 and Figure 44.

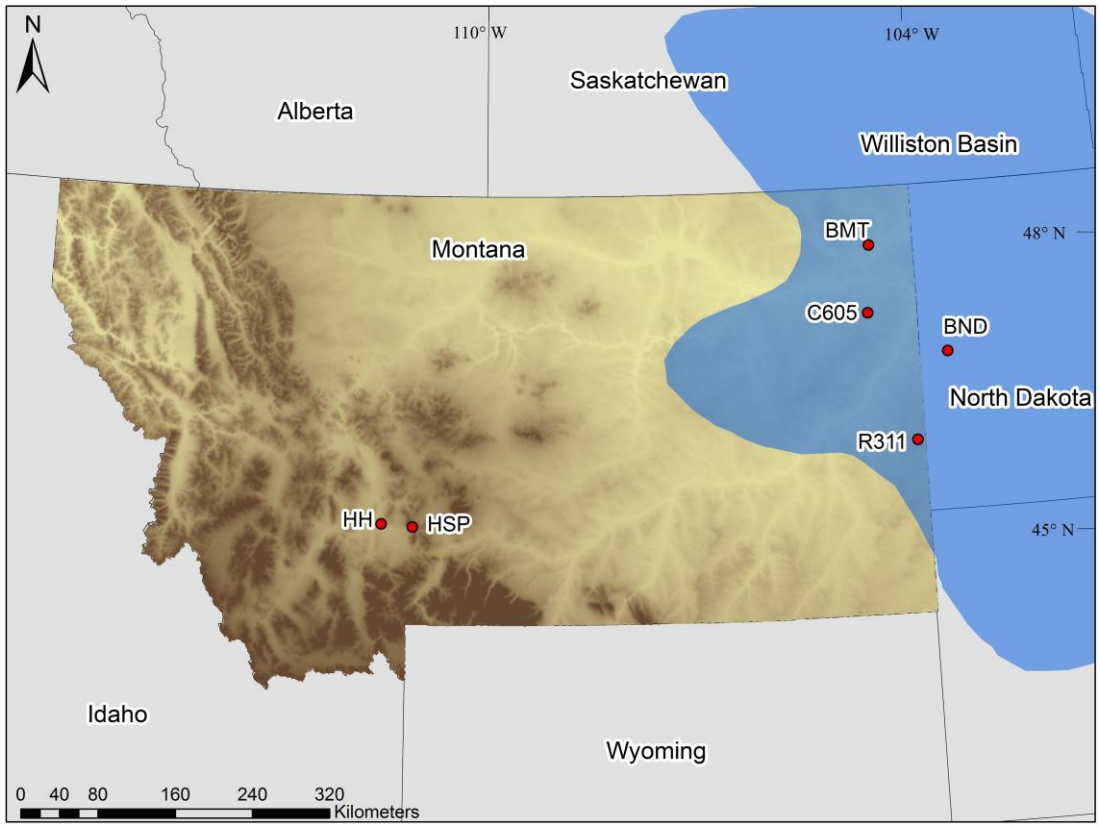


Figure 44. Map of sample locations for this study. Four cores within the Williston Basin were chosen: A-1Stark (C605), 44-24 Vaira (R311), Levang 3-22H (BND), and an undisclosed core (BMT). Two outcrop locations were chosen as well: Logan Gulch (HH), and Hardscrabble Peak (HSP).

Sector 11-ID-C at the APS uses a monochromatic X-ray beam with a wavelength set to 0.10804 Å and a diameter to 0.5 mm. Diffraction images were recorded with a Perkin-Elmer amorphous silicon image plate detector (3450 x 3450 pixels) placed ~2000 mm from the sample. High X-ray energy and thin samples are required for greater penetration and low absorption of X-rays. The shale slices were mounted on aluminum rods parallel to bedding foliation, and then connected to a single crystal goniometer that rotated around a horizontal x-axis (Omega-axis), and centered with a sighting scope (Figure 45).

During exposure of X-rays, the shale samples were rotated around Omega to average over angles (Figure 46) of a selected swath within varying increments (some samples had a -3.0 mm to 3.0 mm transect where other had a -5.0 mm to 5.0 mm transect depending on the size of the sample) to accurately capture sample orientation and grain statistics. The samples were rotated seven times at increments of 15˚, starting at -45˚ and ending at 45˚ (i.e. -45˚, -30˚, -15˚, 0˚, 15˚, 30˚, 45˚). The heterogeneity of the samples required translation and rotation during exposure to ensure averaging, eliminate statistical outliers and increase grain statistics.

Diffraction images were processed in Material Analysis Using Diffraction (MAUD). The diffraction images were integrated from 0˚ to 360˚ azimuth over 10˚ intervals to produce 36 different spectra. These spectra were calibrated with a

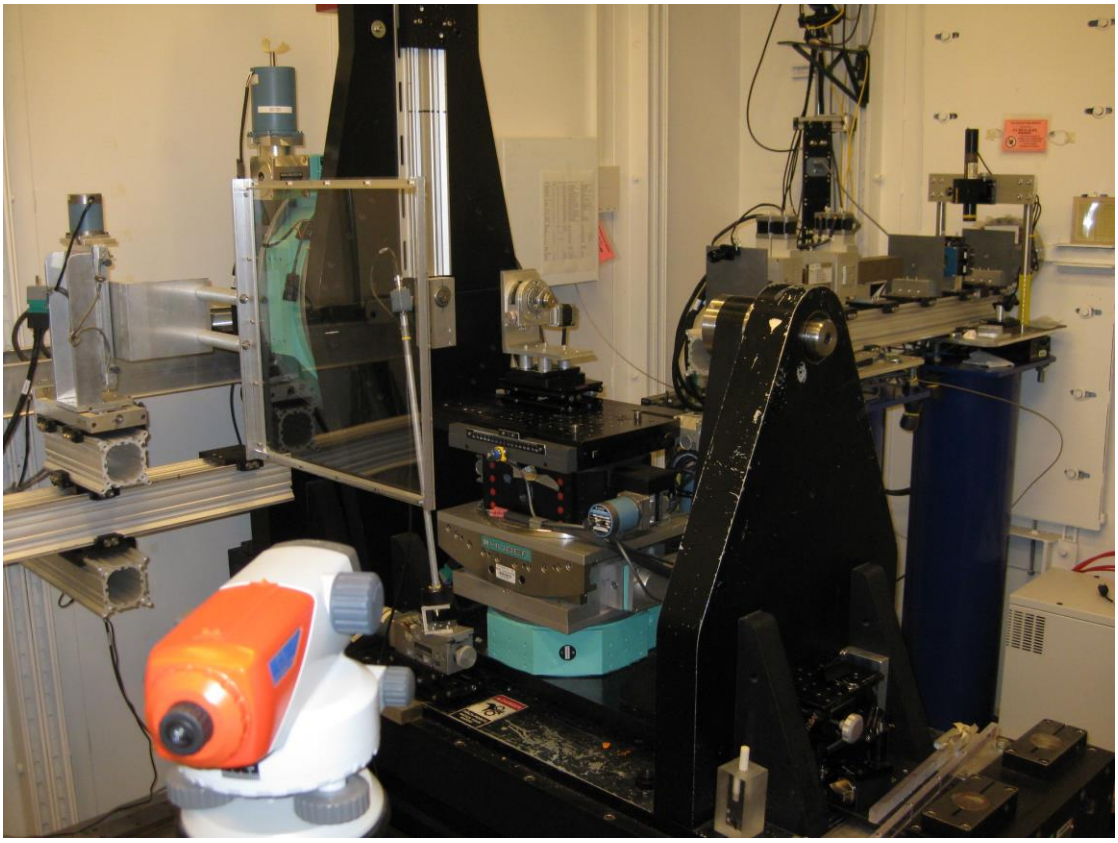


Figure 45. Sighting scope within the hutch used to orient the sample for rotation. A single crystal goniometer was used to rotate the sample.

powdered standard to refine wavelength, sample-to-detector distance, and beam center (Kanitpanyacharoen et al., 2011). A LaB_6 powder standard was used to calibrate instrument geometry for the BND and BMT samples and a CeO_2 powder standard was used to calibrate the instrument geometry for the R311, C605, HH and HSP samples. Images in Figure 47 record a 2θ angle form 0˚ -3.0˚. The 2θ angle is small because the d-spacing of clay minerals is limited. This also helps reduce computation time. Intensity variations along Debye rings indicate lattice preferred

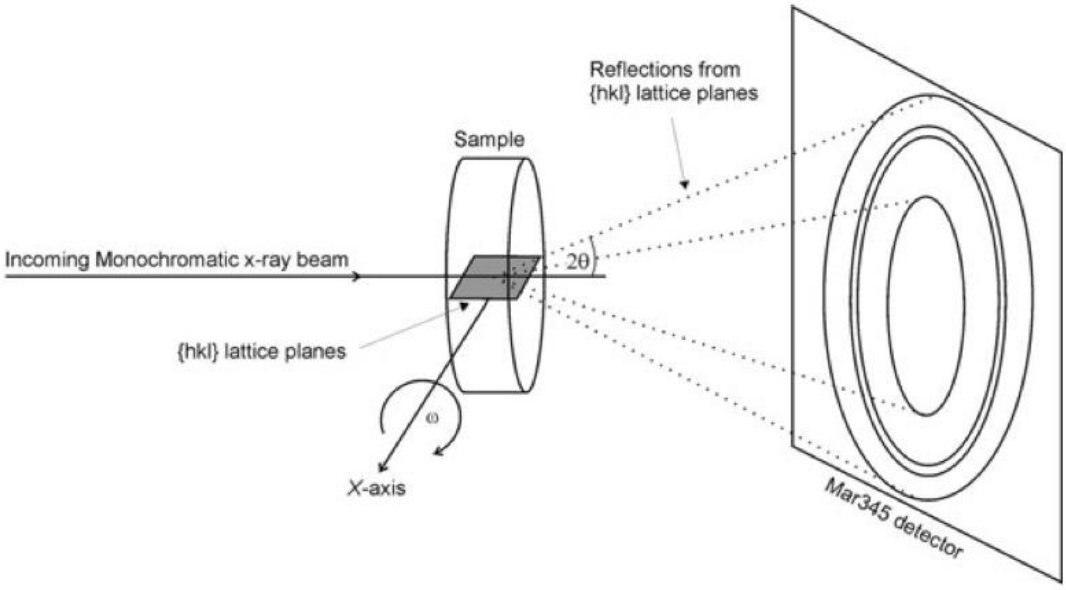


Figure 46. A sketch of the experiment set up (Kanitpanyacharoen et al., 2011). ω is the rotational axis. Note a Perkin Elmer image plate detector was used, not a Mar345 detector.

orientation (texture). Texture information can be conveniently shown using pole figures (Figures 53, 54 and 55). The seven rotations along the x-axis increase pole figure coverage, leaving less for the texture algorithm to reconstruct, resulting in a more accurate representation of the sample (Figure 49). MAUD uses a Rietveld code that allows for texture analysis. This computation uses a least-squares approach to refine a theoretical line profile until it fits the experimental profile measured. The calculated model is characterized by instrumental parameters, scattering background, crystal structure, microstructure, strain, and weight fraction of each mineral phase.

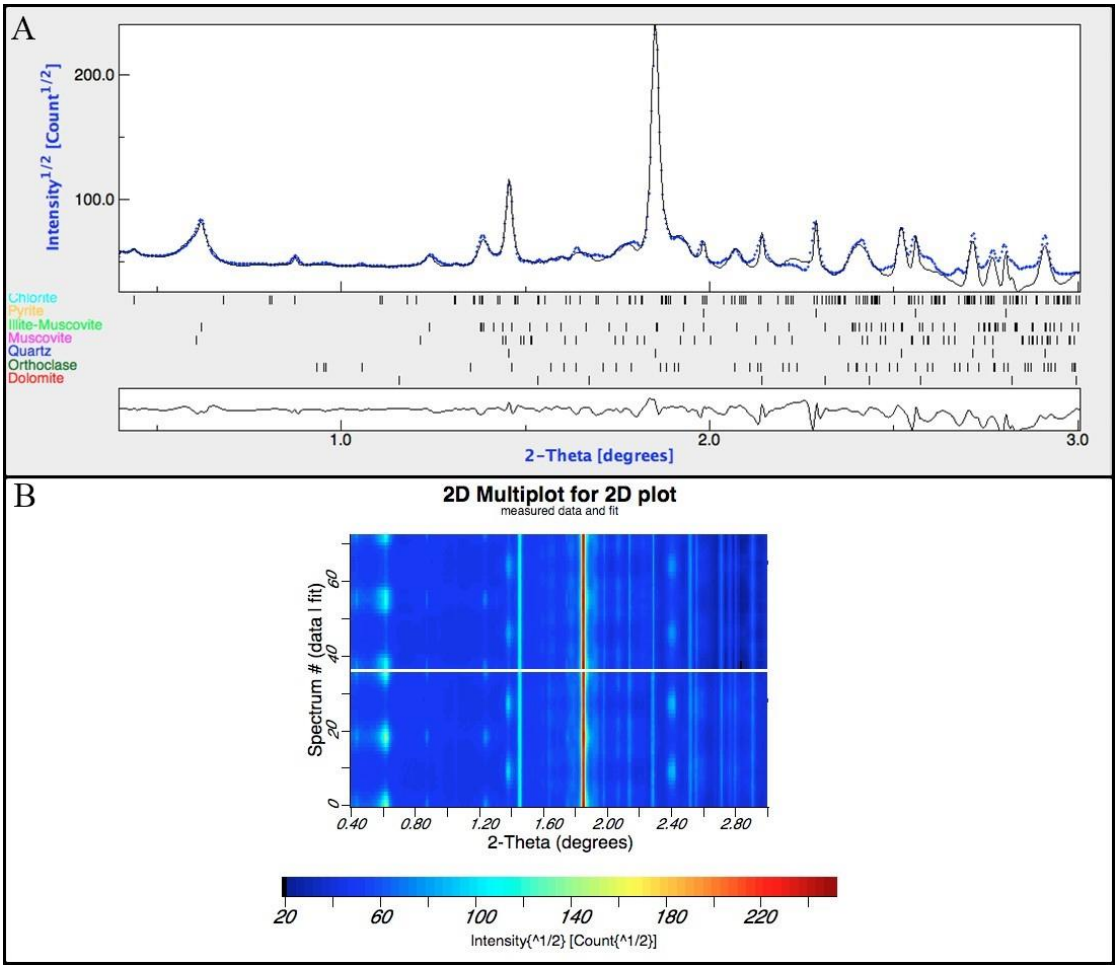


Figure 47. Sample BND1 diffraction profile from 0.0º to 3.0º 2θ. A) The blue dots are the measured profile and the black line is the calculated model. The most important information is from 0.0º to 1.0º 2θ. B) Map 2D plot of the same profile. The top is the calculated model and the bottom is the experimental diffraction spectra. The color represents intensity and the variation found within.

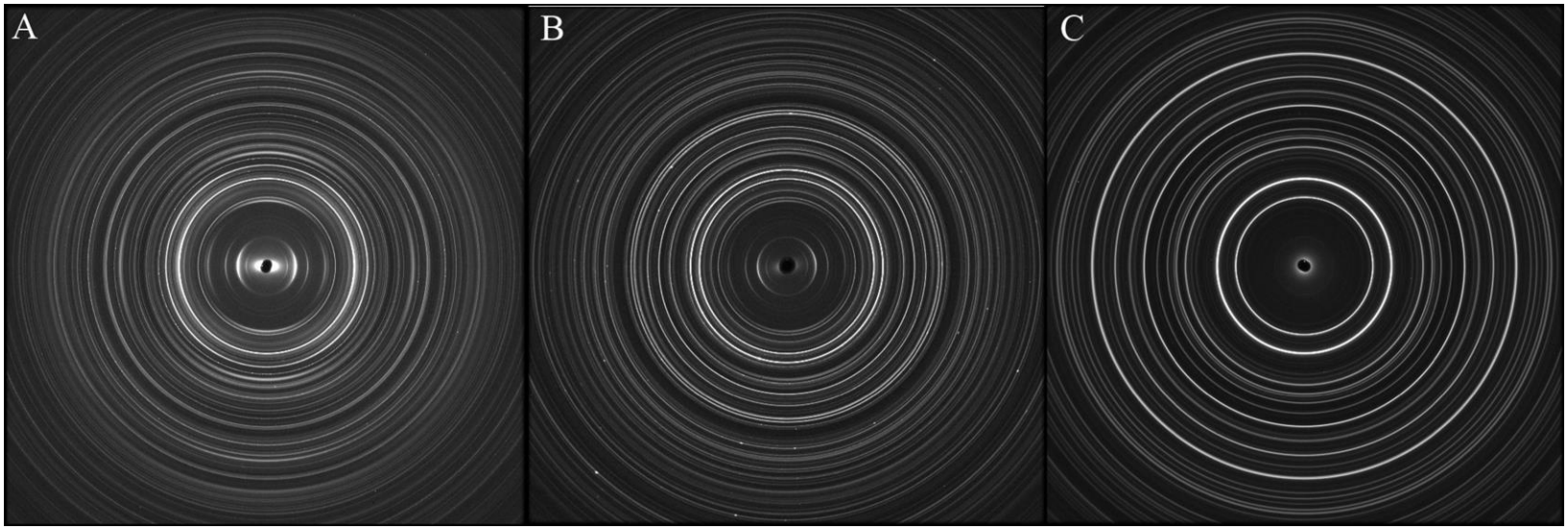


Figure 48. Debye figures from three different samples. Note the differences within the center of the figures. A) R311a Debye figure. The variation in intensity along the individual rings in the center is indicative of preferred orientation. B) Debye figure of BMT2. C) Debye figure of HSPl.

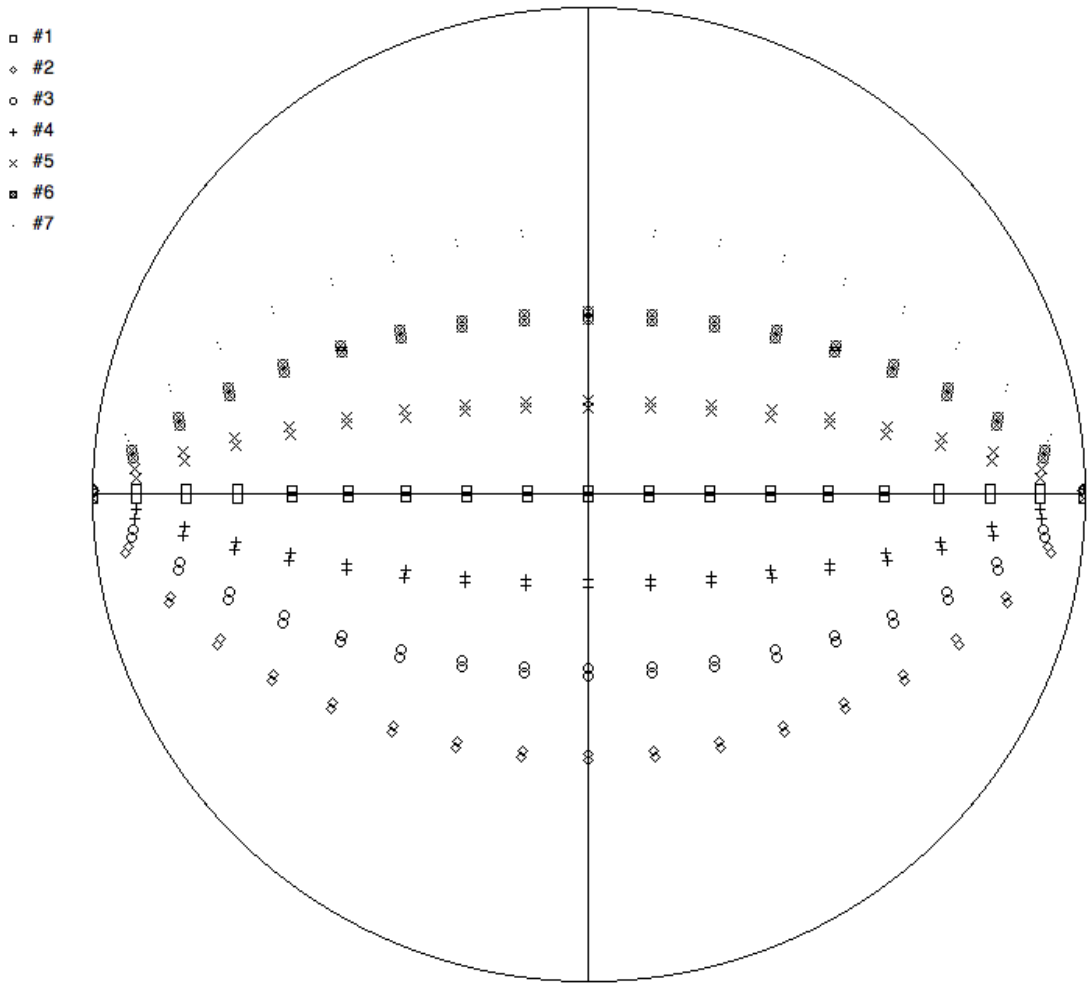


Figure 49. Pole figure coverage acquired from rotating the sample around the x-axis. Each line of symbols represents a single diffraction profile rotation of the same sample used within the Rietveld refinement. 1) ω = 0º, 2) ω = -45º, 3) ω = -30º, 4) ω = -15º, 5) ω = 15º, 6) ω = 30º, 7) ω = 45º.

This technique is useful for elucidating overlapping diffraction peaks within a multiphase sample such as a shale where diffraction peaks overlap and add.

In the Rietveld texture refinement, the parameters of the crystal structure are required. Crystallographic information files (CIFs) store information regarding

a mineral's symmetry, space group, cell parameters and microstructure. The CIFs for monoclinic illite-muscovite (Gualtierie, 2000), monoclinic illite-smectite (Plançon, 1985), monoclinic illite (Drits et al., 2010) and triclinic chlorite/penninite (Joswig et al., 1980) were imported from the American Mineralogist and Crystallographic Open Databases; the illite-muscovite structure was assembled by combining one layer of illite with one layer of muscovite, and the illite-smectite structure was built by combining one layer of illite with one layer of pyrophyllite. These mixed layered clay CIFs were chosen because they best fit the synchrotron X-ray data.

The quartz, pyrite, orthoclase, calcite, and dolomite CIFs were taken from the mineral structures database contained within MAUD. Monoclinic phyllosilicate phases are usually described in the "second setting" where b = [010] as the unique axis and (001) as the cleavage plane. For texture calculations MAUD requires the "first setting" to be used, where c = [001] as the unique axis and (100) as the cleavage plane (Matthies and Wenk, 2009).

The beamline's instrumental parameters were entered into MAUD and calibrated with either a CeO_2 or a LaB_6 standard, and each diffraction image was imported into MAUD. Lattice parameters, phase parameters and volume fractions were refined. The diffraction peak geometries are controlled by microstructural parameters, which were modeled by refining an isotropic crystallite size and microstrain. The EWIMV tomographic algorithm was used for texture analysis. A

15˚ resolution was used for the orientation distribution function, and cylindrical symmetry was imposed to produce an ODF for each mineral phase. The symmetry was removed to verify the assumption that the mineral phases are symmetric.

An ODF is a function that defines the probability of the crystallographic axes of a specific mineral to lie within a certain range of orientations with respect to the frame of reference. ODFs contain quantitative information regarding the mineral's texture and can be used to calculate physical properties of textured polyphase materials. (Cholach and Schmitt, 2003). 3D orientation distributions and single crystal elastic properties are essential for the calculation of bulk elastic properties in an anisotropic polyphase aggregate.

Each ODF was exported from MAUD into the University of California, Berkley Texture software package BEARTEX. The ODFs were smoothed with a 7.5° Gaussian filter to generate a clearer image and reduce the amount of artifacts. Equal area projection pole figures were produced from each mineral phase. Because the samples were not mounted perfectly to the aluminum rod and centered precisely, some of the ODFs had to be rotated so the bedding plane lied within the equatorial plane. The smoothed ODFs were then used to calculate the elastic properties for each mineral phase. To accomplish this, the single crystal elastic tensor coefficients (experimental elastic stiffness moduli; C_{ij}) for each mineral phase must be known. Coefficients for chlorite, illite-smectite and illite-muscovite were taken from Militzer et al. (2011), and coefficients for calcite,

dolomite, pyrite and orthoclase were taken from Bass (1995). The elastic tensor for each contributing phase was calculated by averaging the single crystal elastic properties over the mineral ODF.

To determine the elastic properties for each shale sample, each mineral tensor was weighted by volume percent of the sample and then averaged. Multiple averaging methods were used to calculate the anisotropic properties of the shales. The Voigt-Reuss-Hill (VHR) approximation was used. The Voigt approximation is an average of elastic constants (C_{ij}) and assumes constant strain, whereas the Reuss approximation is an average of elastic compliances (S_{ij}) and assumes constant stress. These provide upper and lower limits for each calculation.

A physical average of the moduli should lie between the Reuss and Voigt values. The Hill averaging scheme is an arithmetic mean of the Voigt and Reuss techniques, and provides an intermediate value for the single crystal tensors. In addition to the VRH average, a geometric mean average was used, and usually provides a value close to the Hill approximation (Chung and Buessem, 1986; Mainprice, 2007; Wenk et al., 2008). A velocity algorithm that determines the P- and S-Wave velocities from stiffness tensors were used to create a velocity model for each shale using each averaging technique (Table 4). Density of the shale is required to calculate a velocity; 2.8 g/cm^3 was used as an average density for each sample. This value was acquired from the logs that accompanied the Levang 3-22H (BND) core.

Sample	Clay (vol %)	Averaging Model	V_s min (km/s)	V_p max (km/s)	V_p min (km/s)	Anisotropy (%)
C605 A	8.72	Voigt	4.08	7.04	6.76	4.06
		Reuss	3.89	6.70	6.47	3.49
		Hill	3.99	6.87	6.62	3.71
		Geometric	3.97	6.90	6.63	3.99
C605 B	9.87	Voigt	4.03	7.01	6.75	3.78
		Reuss	3.82	6.65	6.39	3.99
		Hill	3.93	6.83	6.57	3.88
		Geometric	3.91	6.86	6.59	4.01
C605 C	4.92	Voigt	4.07	6.39	6.30	1.42
		Reuss	3.93	6.16	6.09	1.14
		Hill	4.00	6.28	6.20	1.28
		Geometric	3.99	6.29	6.20	1.44
R311 A	23.22	Voigt	3.81	6.97	6.49	7.13
		Reuss	3.50	6.39	6.12	4.32
		Hill	3.66	6.69	6.31	5.85
		Geometric	3.63	6.74	6.32	6.43
R311 B	47.19	Voigt	4.11	6.92	6.46	6.88
		Reuss	3.83	6.39	6.02	5.96
		Hill	3.97	6.66	6.25	6.35
		Geometric	3.95	6.69	6.24	6.96
R311 C	54.96	Voigt	3.91	7.35	6.19	17.13
		Reuss	3.55	6.66	5.82	13.46
		Hill	3.73	7.01	6.01	15.36
		Geometric	3.69	7.08	6.00	16.51
R311 D	15.92	Voigt	3.90	6.70	6.41	4.42
		Reuss	3.60	6.21	6.01	3.27
		Hill	3.75	6.46	6.21	3.95
		Geometric	3.73	6.49	6.21	4.41
R311 E	37.29	Voigt	4.00	7.12	6.34	11.59
		Reuss	3.71	6.55	5.99	8.93
		Hill	3.86	6.84	6.17	10.30
		Geometric	3.82	6.89	6.16	11.19
BND 1	53.55	Voigt	3.89	6.89	5.93	14.98
		Reuss	3.50	6.01	5.42	10.32
		Hill	3.70	6.61	5.68	15.13
		Geometric	3.65	6.64	5.65	16.11

Sample	Clay (vol %)	Averaging Model	V_s min (km/s)	V_p max (km/s)	V_p min (km/s)	Anisotropy (%)
BND 2	31.68	Voigt	3.66	6.82	6.16	4.06
		Reuss	3.22	6.09	5.58	3.49
		Hill	3.44	6.47	5.88	3.71
		Geometric	3.40	6.53	5.88	3.99
BMT 2	24.54	Voigt	3.75	6.73	6.04	3.78
		Reuss	3.55	6.33	5.91	3.99
		Hill	3.61	6.60	5.94	3.88
		Geometric	3.64	6.57	5.98	4.01
BMT 3	25.30	Voigt	4.04	6.91	6.67	1.42
		Reuss	3.75	6.43	6.23	1.14
		Hill	3.90	6.67	6.46	1.28
		Geometric	3.87	6.70	6.46	1.44
HSP U	28.61	Voigt	3.97	6.59	6.40	7.13
		Reuss	3.69	6.11	5.97	4.32
		Hill	3.83	6.36	6.19	5.85
		Geometric	3.81	6.38	6.19	6.43
HSP L	16.50	Voigt	4.17	6.38	6.36	6.88
		Reuss	4.01	6.12	6.10	5.96
		Hill	4.09	6.25	6.23	6.35
		Geometric	4.08	6.26	6.24	6.96
HH	6.05	Voigt	4.06	7.04	7.04	17.13
		Reuss	3.87	6.73	6.66	13.46
		Hill	3.96	6.89	6.85	15.36
		Geometric	3.96	6.92	6.89	16.51
		Reuss	3.55	6.33	5.91	6.86
		Hill	3.61	6.60	5.94	10.53
		Geometric	3.64	6.57	5.98	9.40

Table 4. Velocity calculations using the averaging models discussed above for each sample.

Results and Discussion

Preferred Orientation

Texture is assumed to be the main source of anisotropy in the Bakken Formation because clay-poor shales don't display anisotropy (Figure 50). Preferred orientation is plotted using upper hemisphere equal area projection pole figures and pole densities are normalized so that the integral over the pole figure is 1.0. These densities are given in multiples of random distribution (m.r.d.). Pole maxima between 0 and 2.0 m.r.d. represent an isotropic material (i.e. no preferred orientation) and anything higher indicates anisotropy (i.e. some degree of preferred orientation). Maxima within the clay mineral phases tested lie between 1.14 and 13.35 m.r.d. Quartz, calcite, dolomite, pyrite and orthoclase are random, with pole figure maxima between 0 and 2 m.r.d. (Figure 51). Thus phyllosilicates are the main source of preferred orientation in shales (Figure 52).

Pole figures of illite-muscovite, illite-smectite, chlorite, illite and muscovite show maxima in the (001) cleavage plane, which is high angle to the c-axis (c = [001] = unique axis) indicating that the clay platelets are approximately parallel to bedding (Figure 53). The (001) plane is within the cleavage plane. The edges of the figure are parallel with bedding, whereas the center of the figure is perpendicular. Each clay phase maxima appears within the (001) plane, which is a result of sedimentation and diagenesis. Samples taken from the outcrop of the

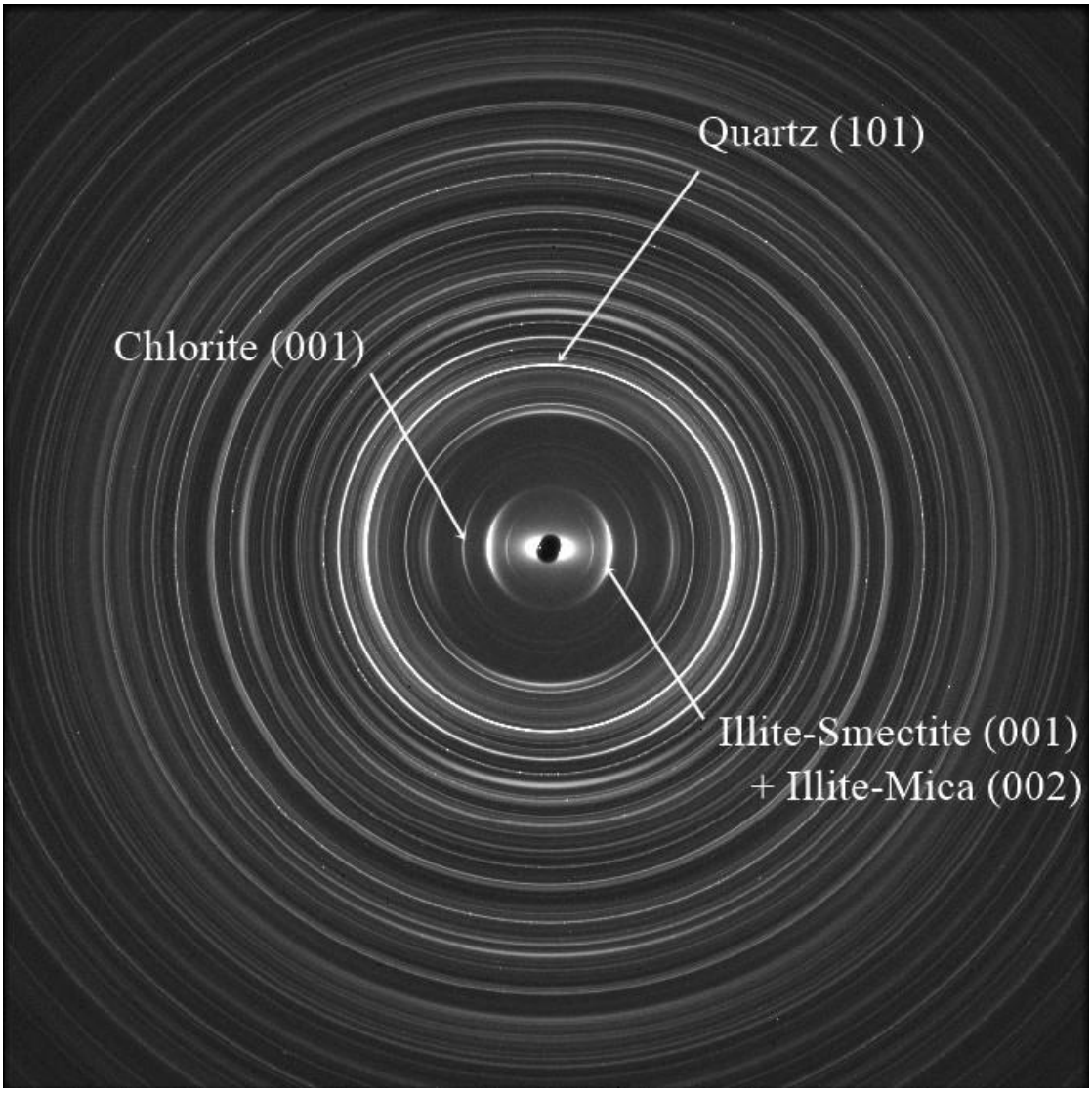


Figure 50. Diffraction image showing variation in intensity along clay Debye rings, which is indicative of preferred orientation (texture). Chlorite (001) occurs in all core samples, and usually bounds the Illite-Smectite (001) ring.

Sappington Member of the Three Forks Formation show negligible preferred orientation within the clay phases (Figure 54). Texture analyses have not been conducted on mudstones taken from outcrop. The Bakken Formation is

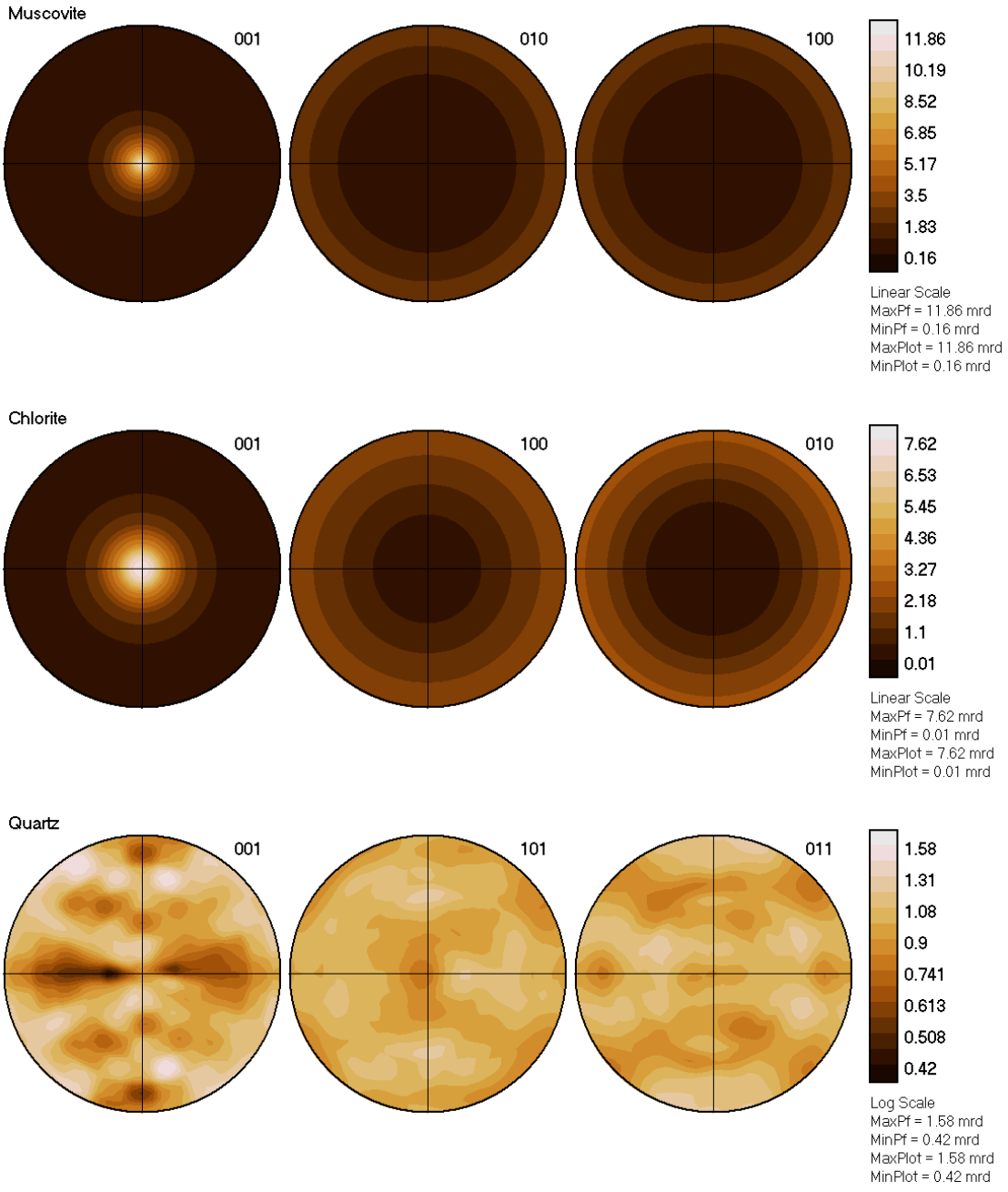


Figure 51. Pole figures of muscovite, chlorite and quartz from R311c. Scale is in multiples of random distribution (m.r.d.). Note that muscovite and chlorite have high m.r.d. and quartz has a low m.r.d. The preferred orientation is coming from the clay minerals and not quartz. Clay mineral pole density occurs in the (001) basal plane, meaning the clay platelets are parallel with bedding foliation.

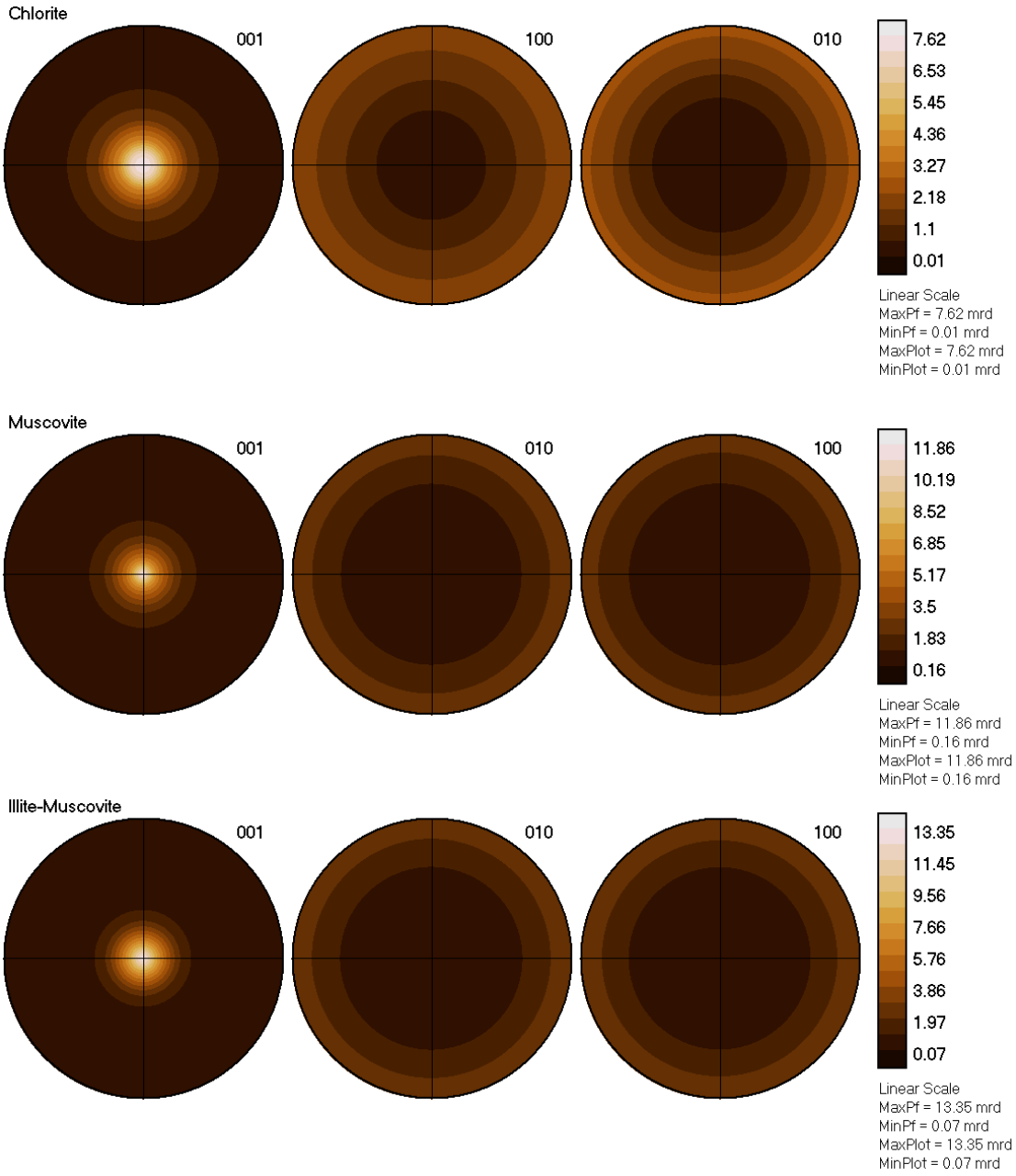


Figure 52. R311a pole figures of clay phases. Cylindrical symmetry was applied to the pole figures. High m.r.d. are seen throughout all clay minerals measured in core.

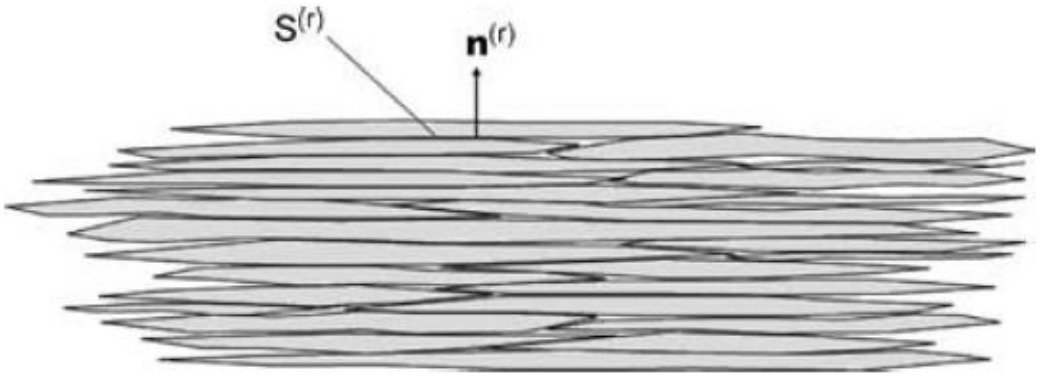


Figure 53. A sketch of a region within a shale where clay platelets locally align (Sayer et al., 2005).

lithostratigraphically and chronostratigraphically equivalent to the Sappington Member in southwestern Montana. A comparative analysis has not been conducted of rocks both in the subsurface and in outcrop using this high energy method.

The proportions of quartz to clay material in the outcrop samples are higher than the shales taken from core. Samples extracted from the outcrops of the Sappington Member are closer to mudshales rather than a true clayshale like the upper and lower Bakken members. A greater amount of silt-sized material in the rocks implies a greater amount of quartz. Non-clay minerals in larger concentrations dilute the CPO present in the sample. In the case of the Sappington mudshales, less clay material and weathering processes have reduced the degree of texture, assuming that the Sappington mudshales were similar to the Bakken clayshales. The lack of preferred orientation within these samples suggests that

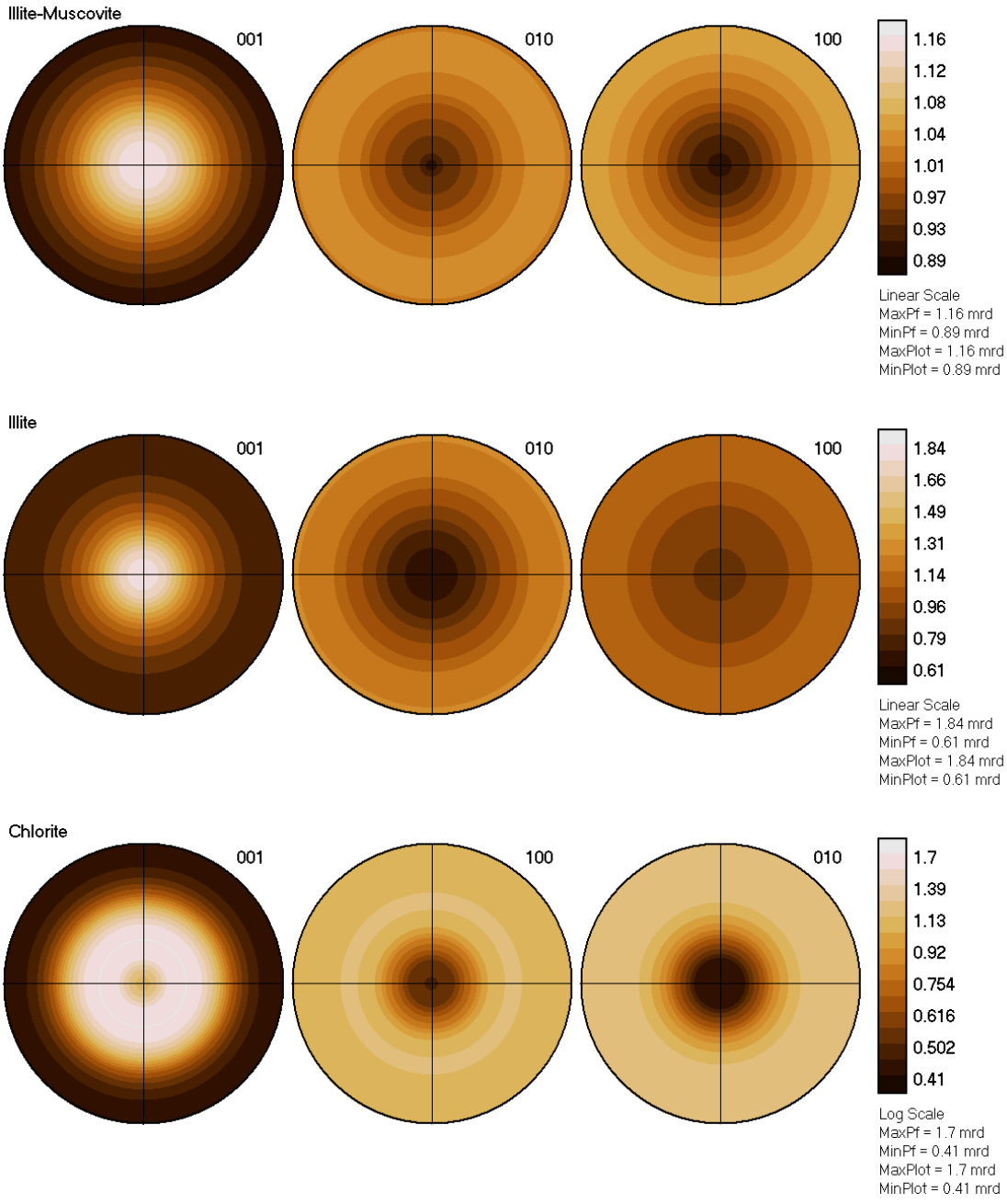


Figure 54. Pole figures of illite-muscovite (HSPl), illite (HSPu) and chlorite (HH). These clay phases show a wide ring in the (001) plane with only 1.7 m.r.d. indicating no preferred orientation. This is likely caused by exposure to surface processes, mostly chemical weathering.

surface processes, such as exhumation and chemical weathering, may have effectively destroyed the crystallographic texture within these phyllosilicate minerals.

Within the upper Bakken shale the degree of preferred orientation is highly variable due to the relative amount of clay within each sample (Figure 55). Lower clay content results in a weakly textured aggregate regardless of how strong the preferred orientation is. The upper shale in the Bakken tends to vary in composition, where some samples selected from core have higher quartz compositions due to a higher proportion of silt-sized grains. This dilutes the texture strength of the clay minerals in the aggregate. The samples from the Levang 3-22 H core in North Dakota contain higher clay volume percent and have higher anisotropy than the samples from the unknown Montana core (16.11% and 10.48% vs. 9.40% and 3.65%).

The mixed layered clays illite-muscovite and illite-smectite show greater preferred orientation than chlorite, illite, or muscovite. The presence of mixed layered illite indicates that illitization occurred during diagenesis. This could further contribute to preferred orientation after burial and compaction. Ho et al. (1999) studied the effects of the smectite-illite transition on preferred orientation within Gulf of Mexico mudstones. They found that pre-transition samples had weak, but continuous preferred orientation, whereas post-transition samples had strong preferred orientation. Depth is the main contributor to smectite-illite

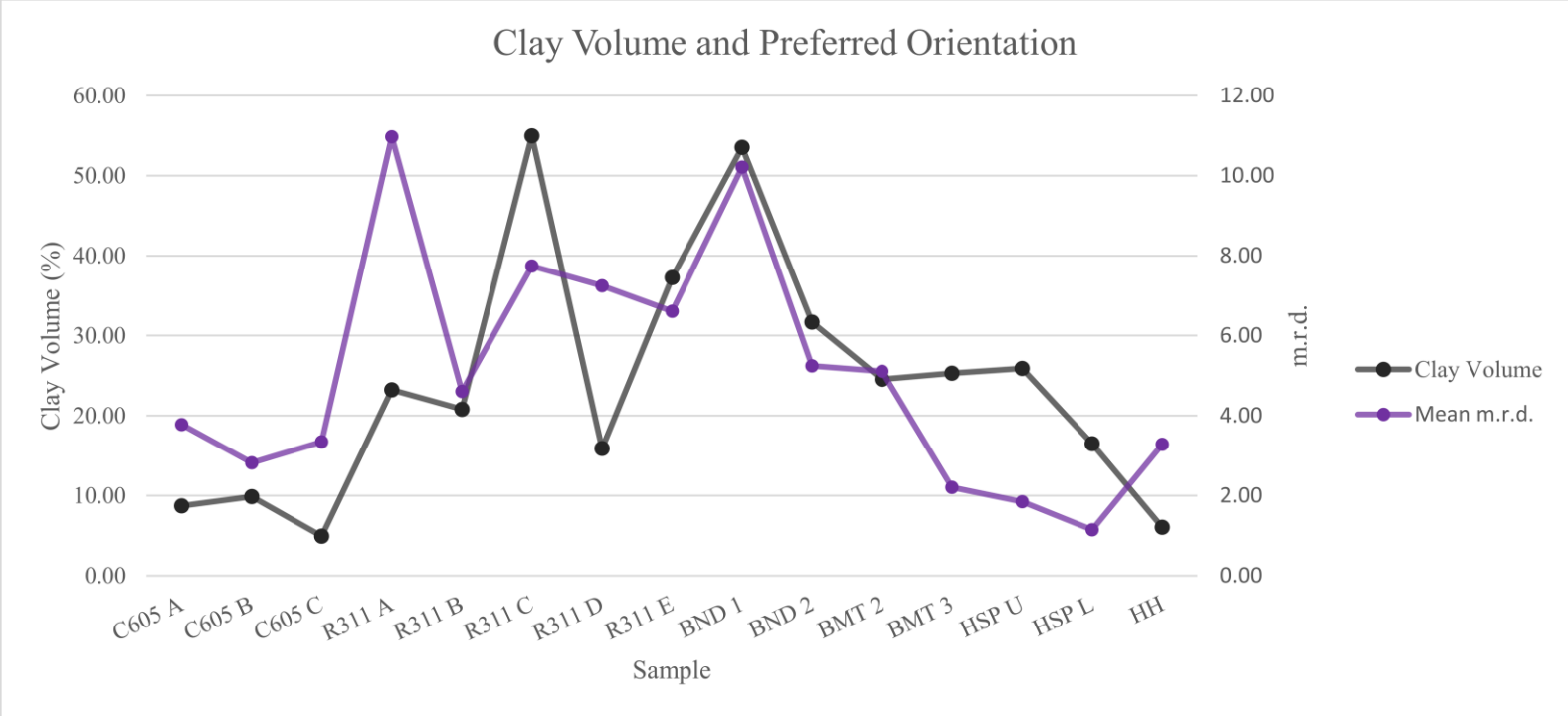


Figure 55. Percent clay volume and mean clay pole density maximum. Pole density maximum is increased when there is a higher volume of clay minerals in the sample.

transitions, the deeper the sample the greater the preferred orientation (Ho et al., 1999).

Kaolinite has been identified in oil-bearing shales around the world (Lonardelli et al., 2007; Wenk et al., 2008; Kanitpanyacharoen et al., 2012) however, kaolinite is not present within the Bakken shales. The absence of kaolinite likely indicates that these shales were far away from a sediment source, and the components of the shales were derived from aerial transport and fallout from the water column. This is the accepted view of the Bakken paleo-environment (Smith and Bustin, 2002).

Seismic Anisotropy

Seismic anisotropy can be produced by several factors including alternation of fluid filled collinear cracks with clay platelets, fine laminations, microfracturing, fluid-filled pores, stress-induced anisotropy, and clay preferred orientation (i.e. texture) as summarized by Cholach and Schmitt (2003). The methods described above only account for clay preferred orientation, so it is assumed that clay CPO is the only source of anisotropy within the Bakken shales. Anisotropy was only determined in the horizontal and vertical directions because 1) the phyllosilicates orient themselves parallel with bedding foliation, 2) cylindrical symmetry was imposed making CPO symmetric about the bedding plane normal (CPO will always be symmetric in the horizontal) and 3) every core

used in this project was un-oriented, so determining change in anisotropy within the horizontal plane is not necessary.

After the velocity was calculated from the polycrystal elasticity, anisotropy was calculated based on the modeled P-wave velocities using:

$$(\text{Anisotropy } (\%) = 200(V_p \text{ max} - V_p \text{ min})/ (V_p \text{ max} + V_p \text{ min}))$$

Anisotropy in the Bakken shale ranges from 3.65% to 16.51% and correlates with the amount of clay in each sample. Figure 56 illustrates the relationship between clay volume and anisotropy %. However, BND1, BMT2, BMT3 and R311b have high amounts of clay but show anomalously low anisotropy.

The degree of preferred orientation dictates the amount of anisotropy. Figure 56 illustrates the sum of the max pole densities of clay minerals in each sample with the anisotropy. Sample R311a is slightly anisotropic (6.43%), but its clay minerals display some of the highest preferred orientation (67.12 pole density sum). This discrepancy is a factor of the clay volume (only 23.22% by volume); a shale with high CPO but low clay content only adopts slight anisotropy because there is only a limited amount of clay to orient. Figure 58 and 59 compare quartz and carbonate (calcite and dolomite) volume to anisotropy. In general, quartz and carbonate minerals will inversely correlate with anisotropy; high quartz and carbonate mineral volumes dilute the clay minerals and lessen the degree of anisotropy. Figure 58 and 59 reveal that quartz and carbonate minerals inversely

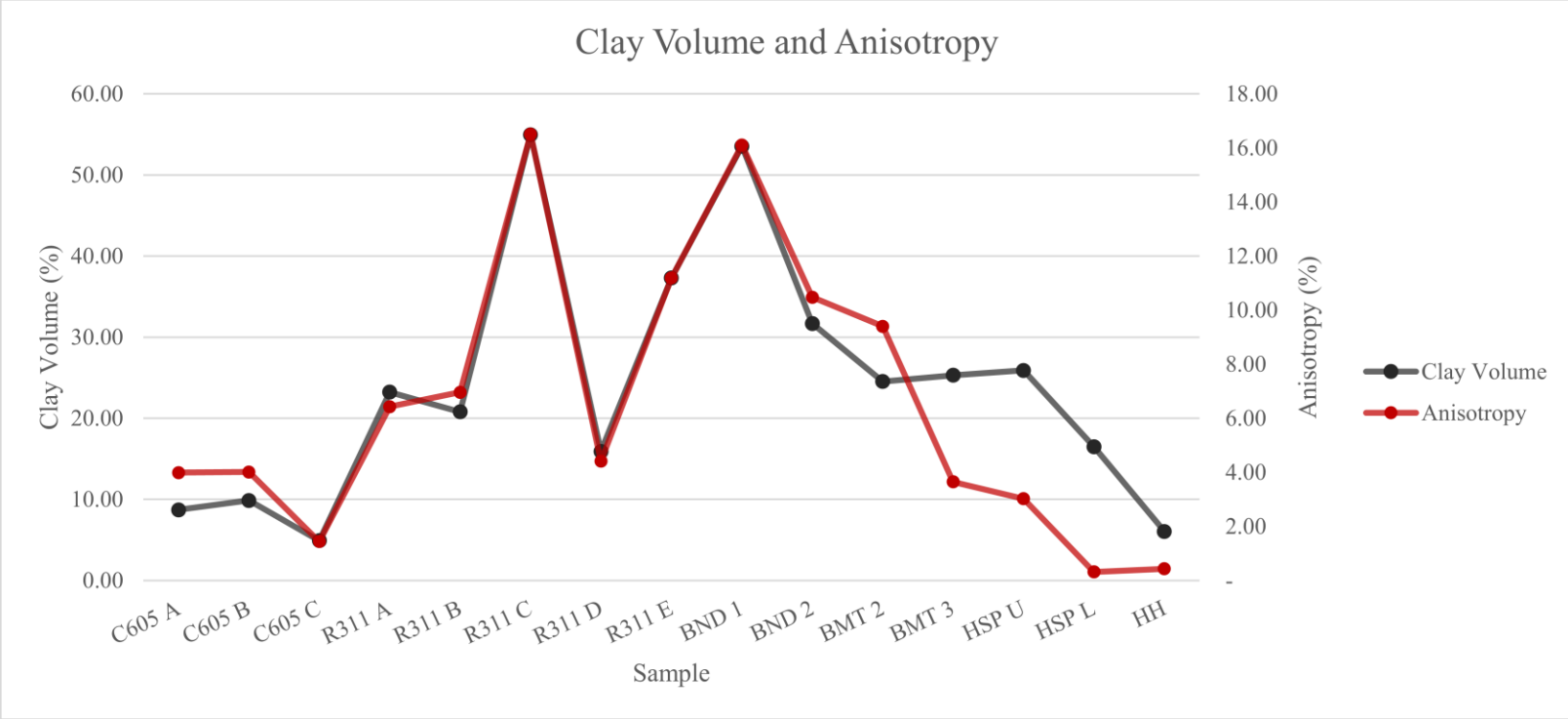


Figure 56. Line plot of percent clay volume and percent anisotropy. There is a direct relationship between anisotropy and clay volume; the more clay in each sample, the higher the anisotropy will be. The last three samples on the chart (HSP U, HSP U, and HH were taken from the Three Forks Formation and show negligible anisotropy.

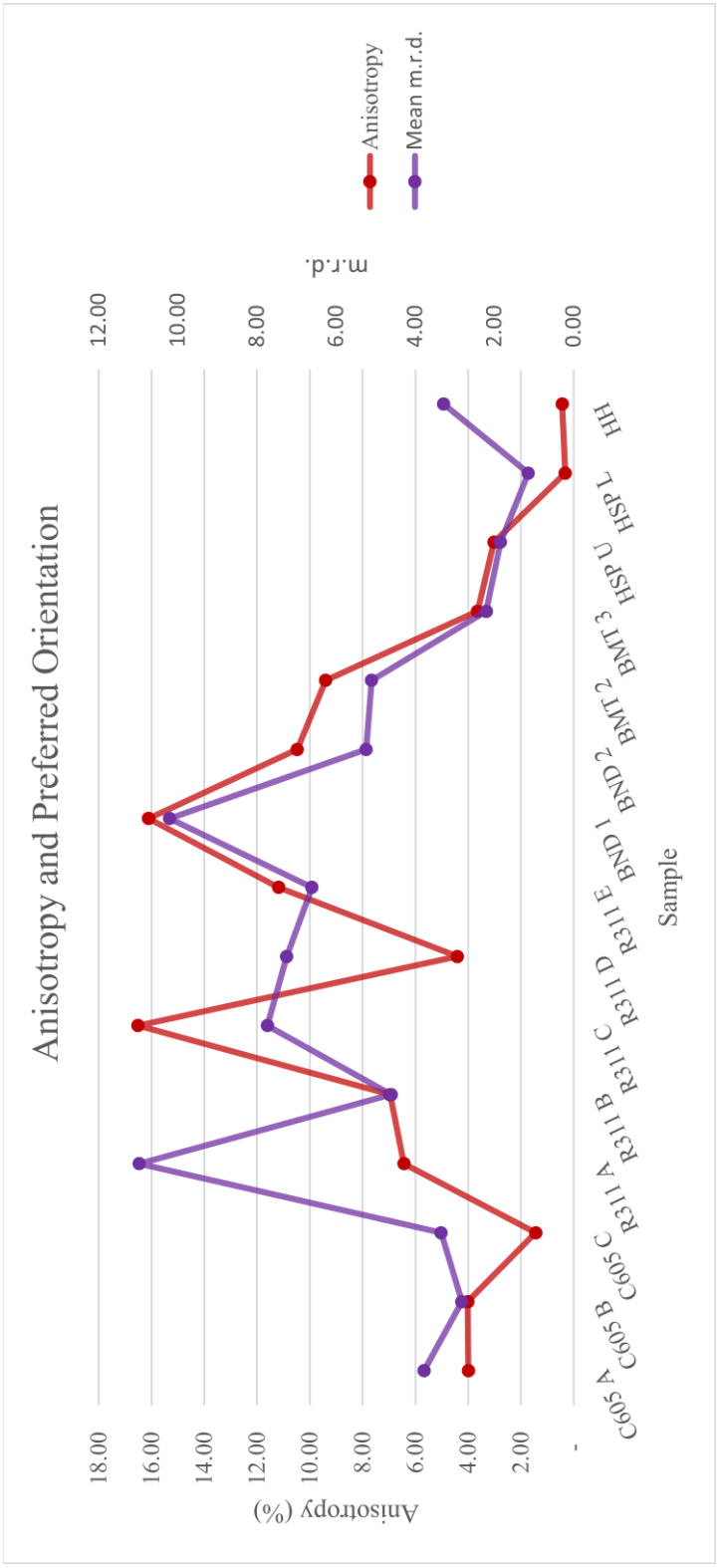


Figure 57. Line plot of percent anisotropy and mean m.r.d. slightly correlate.

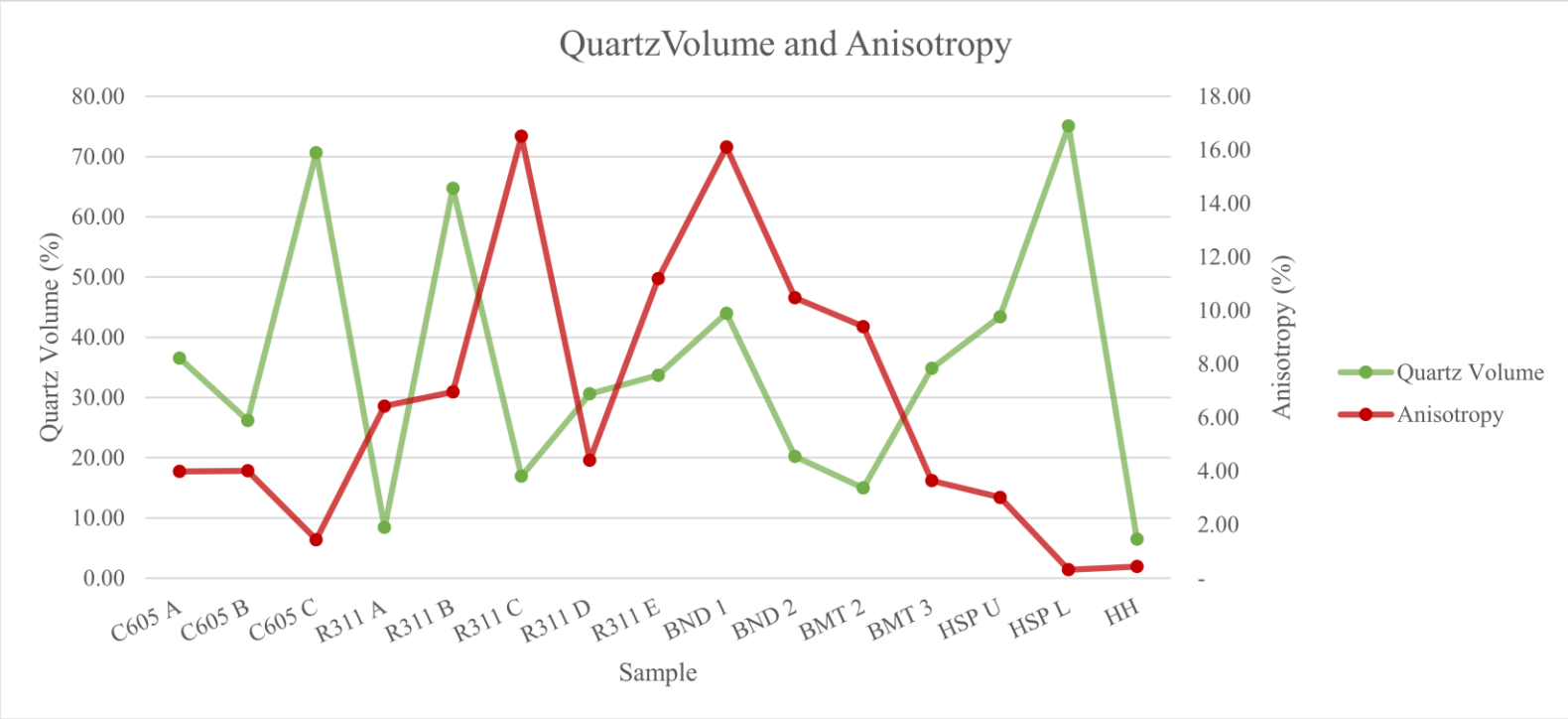


Figure 58. Line plot of quartz volume and anisotropy. There is an inverse relationship between quartz volume and anisotropy. The samples collected from outcrops of the Three Forks Formation show high quartz volumes, which is caused by the removal of other minerals through weathering processes.

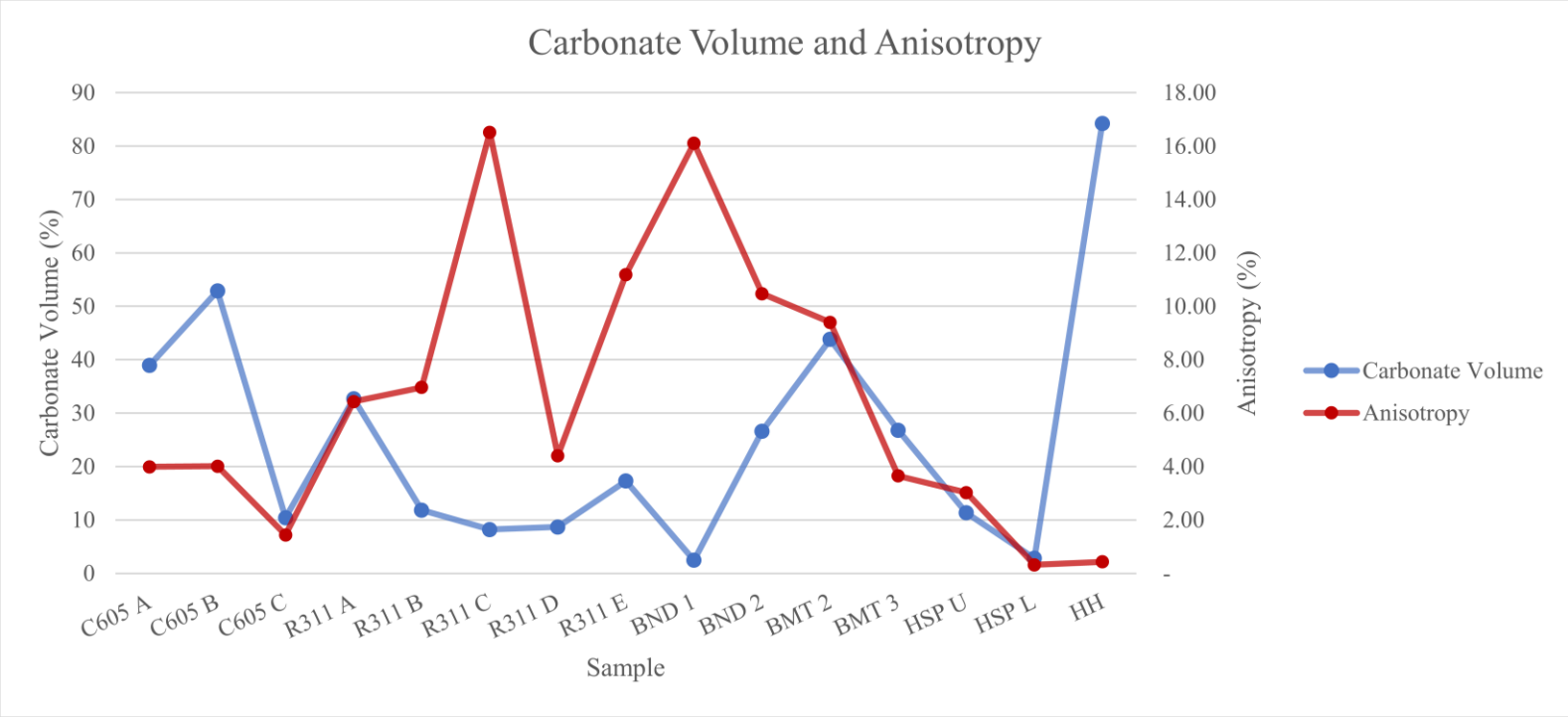


Figure 59. Line plot of carbonate mineral volume and anisotropy. There is an inverse correlation here, however it is not as strong as quartz.

correlate with anisotropy.

The samples taken from the A-1 Stark core (C605) display a small degree of anisotropy (4.01%, 3.99% and 1.44%). The A-1 Stark core, in Fallon County, MT, is located in the western extent of the Williston Basin where the Bakken Formation onlaps onto the western basin edge, resulting in a missing lower shale member. The high quartz and carbonate content (52.86% carbonate in C605b and 70.68% quartz in C605c) and the low clay content (less than 10%) are causing the limited degree of anisotropy. The average anisotropy (Table 6) calculated from the three samples is 3.15%. This is fairly small, and could probably be ignored when conducting a seismic survey.

Samples taken from the 44-24 Vaira core (R311) show a variable degree of anisotropy. The Elm Coulee field in Richland County, MT, containg the 44-24 Vaira core, has been the biggest producer of oil in the Montana portion of the Williston Basin. Like the A-1 Stark core, it is within the western-most portion of the basin and lacks the lower shale. R311 clay mineral CPO (Figure 57) correlates well with the anisotropy and explains why there is such a variation in anisotropy within the Vaira core. R311c displays the highest anisotropy out of all 15 samples analyzed (16.51%). This is due to the clay mineral volume (54.96%) and high CPO. The average anisotropy between the five samples is 9.10% (Table 5).

Sample	Clay (vol %)	V_s min (km/s)	V_p max (km/s)	V_p min (km/s)	Anisotropy (%)	Anisotropy Average
C605 A	8.72	3.97	6.90	6.63	3.99	
C605 B	9.87	3.91	6.86	6.59	4.01	3.15
C605 C	4.92	3.99	6.29	6.20	1.44	
R311 A	23.22	3.63	6.74	6.32	6.43	
R311 B	20.80	3.95	6.69	6.24	6.96	
R311 C	54.96	3.69	7.08	6.00	16.51	9.10
R311 D	15.92	3.73	6.49	6.21	4.41	
R311 E	37.29	3.82	6.89	6.16	11.19	
BND 1	53.55	3.65	6.64	5.65	16.11	13.29
BND 2	31.68	3.40	6.53	5.88	10.48	
BMT 2	24.54	3.64	6.57	5.98	9.40	6.52
BMT 3	25.30	3.87	6.70	6.46	3.65	
HSP U	25.90	3.81	6.38	6.19	3.02	
HSP L	16.50	4.08	6.26	6.24	0.32	
HH	6.05	3.96	6.92	6.89	0.43	

Table 5. Clay volume, P- and S-wave velocities, anisotropy and average anisotropy of the samples studied in this project.

Samples from the Levang 3-22H core (BND) exhibit high degree of anisotropy. The Levang core is from the North Dakota portion of the Williston Basin in McKenzie County. Sampling was limited, so the upper shale was chosen for synchrotron diffraction. Both samples from the Levang core display similar degrees of anisotropy (Figure 56), with the average between the two samples being 10.99% (Table 6).

The samples from the unknown Montana core (BMT) display a variation in anisotropy. Based on the depth of the core, the quartz content, and the generalized onlapping relationship with the Williston Basin, it is believed that these samples are from the upper shale member of the Bakken. The lower shale tends to have lower quartz content and higher clay content.

Figure 60 was created by plotting the P-wave velocity against the degree from bedding normal. Samples show a lower P-wave velocity perpendicular to the bedding plane (0°) than parallel. No shear wave splitting is observed when perpendicular to the bedding plane, but gradually increases when closer to the bedding angle. This just demonstrates the difference in seismic wave propagation based on the angle from bedding.

R311, BMT and BND samples yield anisotropies similar to values (Figure 61) reported in other studies: 11% in the Qusaiba Shale in Saudi Arabia (Kanitpanyacharoen et al., 2012), 12% in North Sea shale (Valcke et al., 2006),

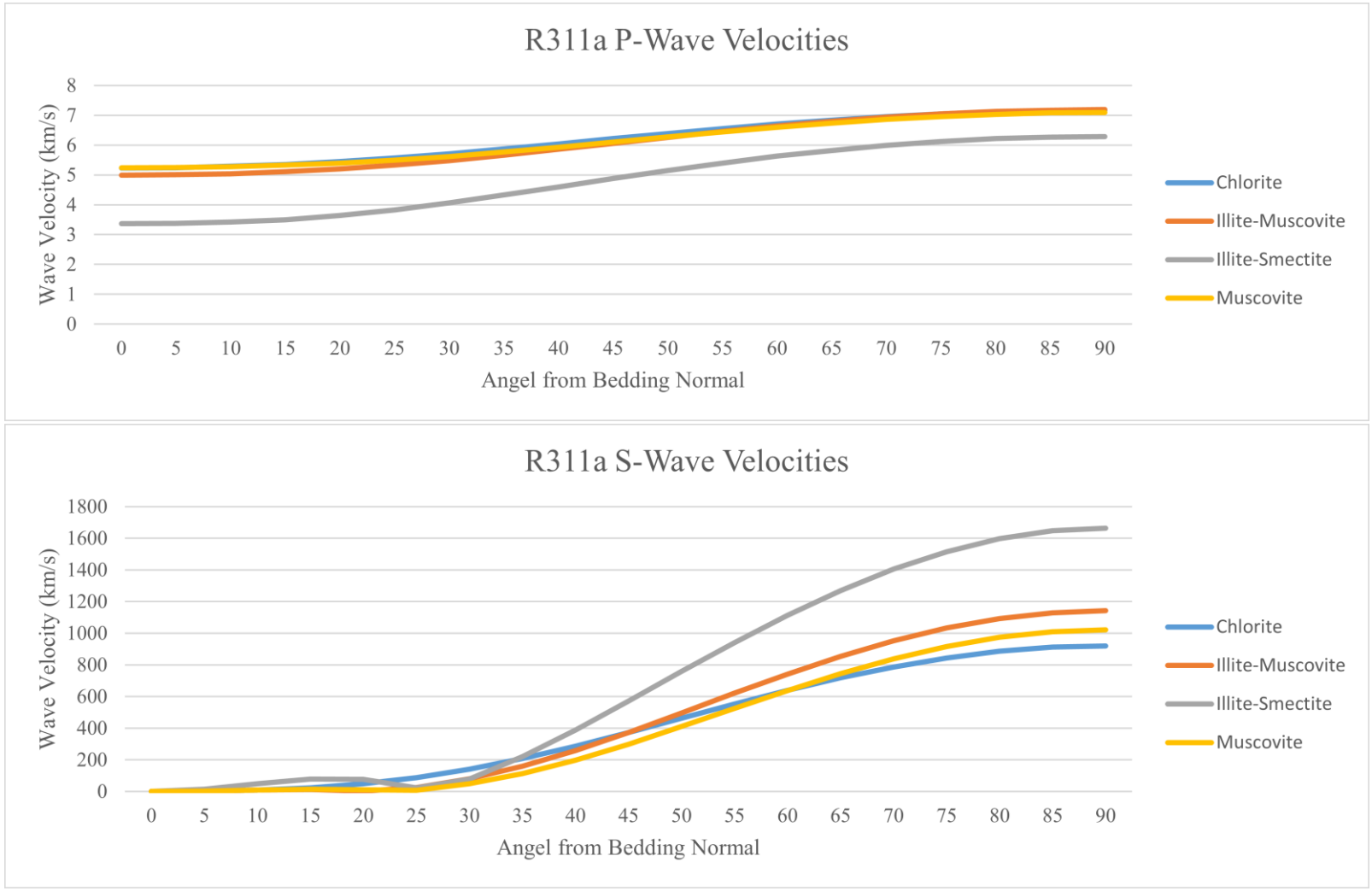


Figure 60. P- and S-wave velocities of each clay mineral found within the R311a sample.

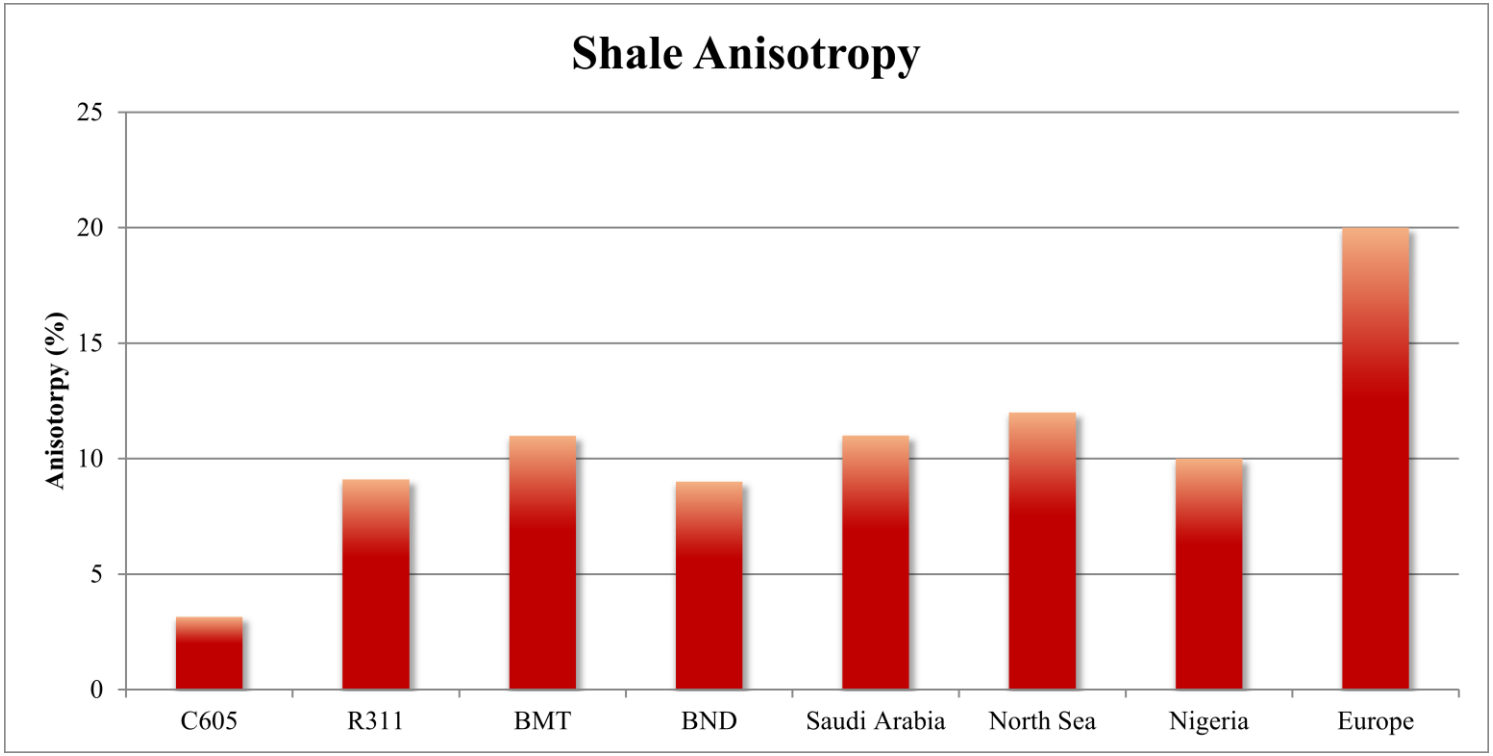


Figure 61. Samples from this study compared with those of similar studies on oil-bearing shales around the world. Saudi Arabia (Kanitpanyacharoen et al., 2011); North Sea (Valcke et al., 2006); Nigeria Lonardelli et al., 2007); Europe (Wenk et al., 2001).

10% in an offshore Nigerian shale (Lonardelli et al., 2007), and 20% in the Mont Teri Shale in France and Switzerland (Wenk et al., 2008). Kanitpanaycharoen et al. (2012) found kaolinite, illite-smectite, illite-mica and chlorite in their samples from Saudi Arabia; Valcke et al. (2006) identified chlorite, kaolinite, illite and mica in the North Sea shale; Londardelli et al. (2007) discovered kaolinite and illite-smectite in a shale from Nigeria; Wenk et al. (2008) found kaolinite, illite, and chlorite in their samples from Europe. For the exception of kaolinite, these oil-bearing shales contain the same clay minerals that cause anisotropy found in the Bakken Formation.

The Sappington member samples display extremely low anisotropies (between 0.32% and 3.02%). This is to be expected considering 1) the low volume of clay minerals and high volume of quartz and calcite within these samples and 2) the destruction of clay-mineral texture from being exposed at the surface. It is surprising to see that the upper Sappington mudstone (HSPu), taken from Hardscrabble Peak, has relatively high anisotropy for outcrop samples. This may be due to the larger portion of clay volume present within the sample. HSPl and HH show extremely high volumes of quartz and carbonate minerals respectively. Clay minerals were likely removed from the mudstone through either chemical weathering at the surface or telogenetic processes. Regardless of the mechanisms of removal, texture will be negligible from the lack of clay minerals in the mudstone.

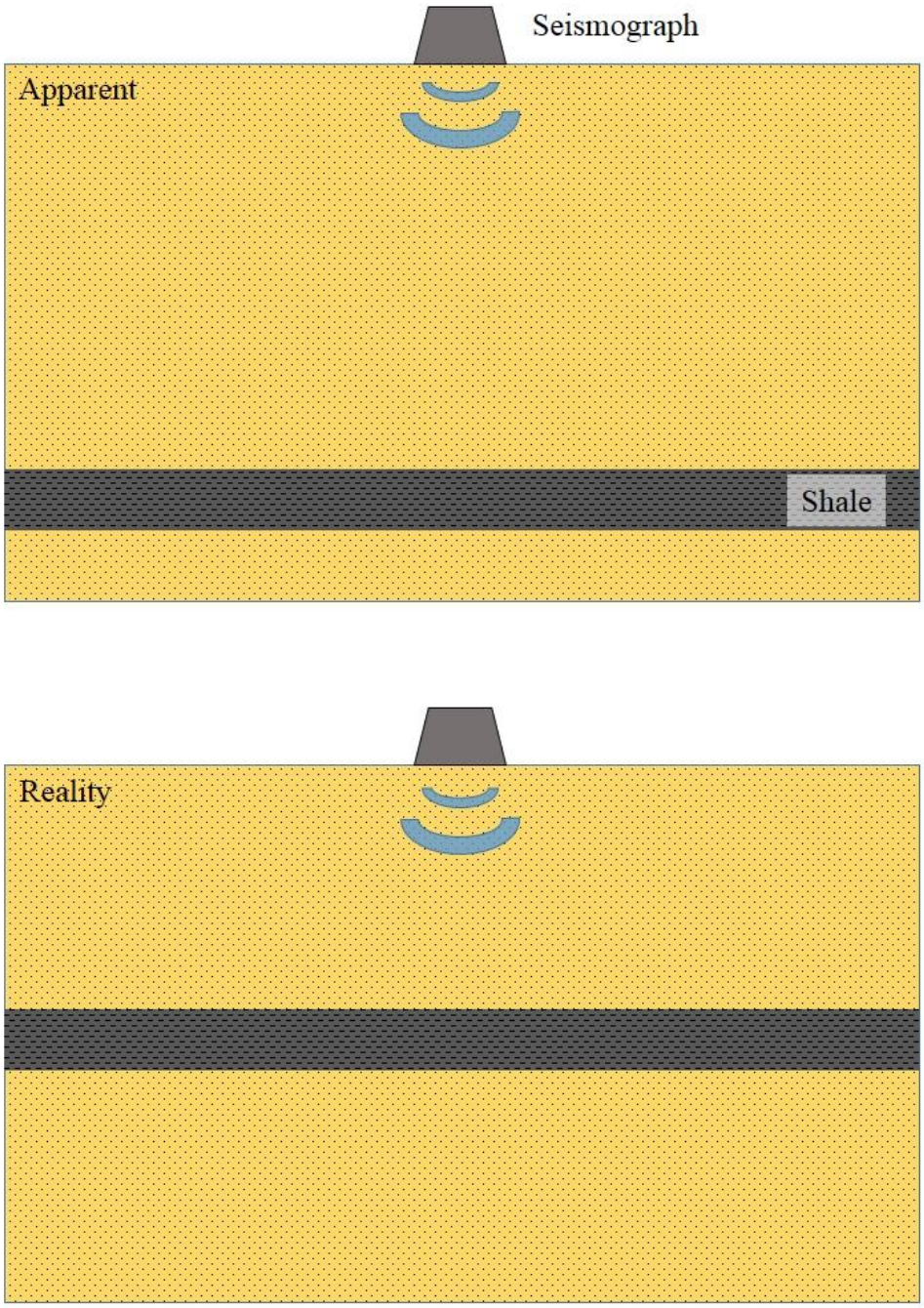


Figure 62. A simplified diagram of a seismic survey. Note the clay-rich shale differing in position due to anisotropy. A seismically slower reflection will appear lower within the survey if anisotropy is not known or corrected for.

Seismic anisotropy can greatly affect the analysis and interpretation of seismic surveys when conducted on unconventional oil and gas shale reservoirs. The Bakken Formation within Montana displays roughly a 1 km/s difference in horizontal and vertical P- and S-wave velocities. This discrepancy, if slower perpendicular to bedding, as seen in shale oil reservoirs around the world, will effect seismic waves as they propagate through the shale. This will result in the shale appearing deeper than in reality leading to misinterpretation of seismic surveys if no other data is available. Figure 62 illustrates the difference between raw and corrected seismic data. However, it shows extreme vertical exaggeration, and the Bakken Formation itself would not contribute to a large error due to the thickness of the shales. With the growth in production of unconventional shale reservoirs, knowledge of how shale anisotropy affects seismic prospecting can be helpful when determining target depth.

CONCLUSIONS

The Bakken Formation is considered one of the largest and most important, domestic, conventional and unconventional reservoirs (Pitman et al., 2005; LeFever 2005; Sonnenberg et al, 2011). Understanding reservoir characteristics and the relationship between fractures and production is well confined. However, the spatial diversity of stratigraphy, lithology, structure, and seismic anisotropy makes producing from the Bakken Formation a new challenge (Mark Sonnenfeld, personal communication).

The middle member of the Bakken Formation acts as a conventional reservoir and is exploited when part of a structural high. Fractures within the upper and lower shale members allow for oil migration into the conventional middle member (Pitman et al., 2005; Sonnenberg et al, 2011). Fracturing occurs within two stages. The first stage takes place during and after mechanical compaction, creating vertical, mode-1 fractures, which are often partially to fully healed with calcite, dolomite or pyrite through dissolution and precipitation. The second stage of fracturing occurs late in diagenesis and is a product of kerogen generation where water reacts with kerogen, absorbing the hydrogen molecules and releasing oxygen in the form of CO_2. This expulsion of CO_2 causes overpressurization within the reservoir required to initiate in-situ horizontal fractures (Pitman et al., 2001).

Stage 2 fractures likely give the Bakken Formation its permeability, porosity and ability to produce from the shales. However, the extent of Stage 2 fracturing is directly linked to thermal maturity, thickness and distance from source rock, and total organic carbon (TOC). The cores observed in this study had low TOC and fractures that were measured were primarily Stage 1. Within thin section, open fractures that did occur displayed halos of porosity surrounding the fracture, and fractures that were healed exhibited halos of fine-grained, reprecipitated dolomite.

The Sappington Member of the Three Forks Formation is often regarded as the southwestern Montana Bakken equivalent, however, there are major differences between the two. The Bakken Formation is considered a purely subsurface formation contained within the bounds of the Williston Basin (USGS, 2008). It represents a deep marine environment within an epicontinental sea and records a major sea-level transgression within its strata. The Sappington Member of the Three Forks Formation, present in southwestern Montana, represents a near shore marine environment, which records the same sea-level transgression within a different basin (Sandberg, 1965).

Regional fracture studies reveal a local control on structure. Fractures measured in Devonian/Mississippian period rocks within the Big Snowy, Little Rocky and Beartooth Mountains reveal dominantly northwest trending fractures (Angster, 2011). The Williston Basin reveals a diverse spread of orientations,

which all relate to large scale structures such as the Little Knife Anticline. Sappington outcrops, encapsulated by the Three Forks Basin, display dissimilar fracture trends, which are locally controlled by large scale lineaments.

The shales within the Bakken Formation are highly anisotropic, which is caused by the preferred orientation of phyllosilicate minerals such as chlorite, muscovite, smectite and mixed layered clays like illite-smectite. In large amounts, these clay minerals preferentially align with bedding direction during sedimentation, burial and diagenesis, causing the observed anisotropy. Shales with high amounts of quartz, calcite and dolomite display low amounts of anisotropy. There is a direct correlation between clay volume and degree of anisotropy. Differences in P-wave anisotropy within a single sample reach to 1 km/s in direction and S-wave velocity to 0.5 km/s.

The Montana portion of the Bakken Formation shows the same degree of anisotropy as oil-bearing shales from Nigeria, the North Sea and Saudi Arabia (Kanitpanyacharoen et al., 2011; Lonardelli et al., 2007; Valcke et al., 2006; Wenk et al., 2001). Degree of anisotropy within the Sappington Member is extremely low. This is likely a result of exhumation and surface weathering processes have removed and re-aligned the clay minerals from the mudrocks, destroying the texture.

REFERENCES CITED

Ahern, J.L., and Mrkvicka, S.R., 1984, A mechanical and thermal model for the evolution of the Williston Basin: Tectonics, v. 3, p. 79–102.

Angster, S., 2010, Fracture analysis of the Bakken Formation, Williston Basin; field studies in the Little Rocky Mountains and Big Snowy Mountains, MT, and Beartooth Mountains, WY, and 3D seismic data, Williston Basin [Master's Thesis]: Colorado School of Mines, 67 p.

Angulo, S., and Buatois, L.A., 2012, Ichnology of a Late Devonian–Early Carboniferous low-energy seaway: The Bakken Formation of subsurface Saskatchewan, Canada: Assessing paleoenvironmental controls and biotic responses: Palaeogeography, Palaeoclimatology, Palaeoecology, v. 315-316, p. 46–60.

Anna, L.O., Pollastro, R.M., and Gaswirth, S.B., 2010, Williston Basin Province—Stratigraphic and Structural Framework to a Geologic Assessment of Undiscovered Oil and Gas Resources, *in* Assessment of Undiscovered Oil and Gas Resources of the Williston Basin Province of North Dakota, Montana, and South Dakota, 2010, U.S. Geological Survey Digital Data Series DDS–69–W, p. 1–17.

Baghbanan, A., and Jing, L., 2008, Hydraulic properties of fractured rock masses with correlated fracture length and aperture: International Journal of Rock Mechanics and Mining Sciences, v. 44, p. 704–719.

Baird, D.J., Knapp, J.H., Steer, D.N., Brown, L.D., and Nelson, K.D., 1995, Upper-mantle reflectivity beneath the Williston basin, phase-change Moho, and the origin of intracratonic basins: Geology, v. 23, p. 431–434.

Bass, J.D., 1995, Elasticity of Minerals, Glasses and Melts, *in* Mineral Physics and Crystallography: A Handbook of Physical Constants, AGU, p. 45–63.

Bensen, G.D., Ritzwoller, M.H., and Yang, Y., 2009, A 3-D shear velocity model of the crust and uppermost mantle beneath the United States from ambient seismic noise: Geophysical Journal International, v. 177, p. 1177–1196.

Boggs, S.J., 2009, Petrology of Sedimentary Rocks: Cambridge University Press, 600 p.

Carlisle, W.J., Dryuff, L., Fryt, M.S., Artindale, J.S., and Von Der Dick, H., 1992, The Bakken Formation-An Integrated Geologic Approach to Horizontal Drilling, *in* Geological Studies Relevant to Horizontal Drilling: Examples from Western North America, The Rocky Mountain Association of Geologists.

Chen, Z., Osadetz, K.G., Jiang, C., and Li, M., 2009, Spatial variation of Bakken or Lodgepole oils in the Canadian Williston Basin: American Association of Petroleum Geologists Bulletin, v. 93, p. 829–851.

Cholach, P., and Schmitt, D., 2003, Seismic anisotropy of shales: CSEG Recorder, v. 28, p. 39–42.

Chung, D.H., and Buessem, W.R., 1968, The Voigt-Reuss-Hill (VRH) Approximation and the Elastic Moduli of Polycrystalline ZnO, TiO2 (Rutile), and α-Al2O3: Journal of Applied Physics, v. 39, p. 2777–2782.

Crowley, K.D., Ahern, J.L., and Naeser, C.W., 1985, Origin and epeirogenic history of the Williston Basin: Evidence from fission-track analysis of apatite: Geology, v. 13, p. 620–623.

Davis, G.H., Reynolds, S.J., and Kluth, C.F., 2012, Carrying Out Joint Analysis, *in* Structural Geology of Rocks and Regions, p. 769–779.

DeCelles, P.G., 2004, Late Jurassic to Eocene Evolution of the Cordilleran thrust belt and foreland basin system, Western U.S.A.: American Journal of Science, v. 3044, p. 105–168.

Drits, V.A., Zviagina, B.B., McCarty, D.K., and Salyn, A.L., 2010, Factors responsible for crystal-chemical variations in the solid solutions from illite to aluminoceladonite and from glauconite to celadonite: American Mineralogist,, p. 348–361.

Erslev, E.A., and Koenig, N.B., 2009, 3D Kinematics of Laramide, basement-involved Rocky Mountain deformation, U.S.A.: Insights from minor faults and GIS-enhanced maps, *in* Kay, S., Ramos, V., and Dickinson, W.R. eds., Backbone of the Americas: Shallow subduction, plateau uplift and ridge and terrane collision, GSA Memoir, p. 125–150.

Fowler, C., and Nisbet, E., 1985, Subsidence of the Williston Basin: Canadian Journal of Earth Sciences, v. 22, p. 408–415.

Gerhard, L.C., Anderson, S.B., and LeFever, J.A., 1987, Structural history of the Nesson anticline, North Dakota: Rocky Mountain Association of Geologists Symposium, p. 337–353.

Gualtieri, A.F., 2000, Accuracy of XRPD QPA using the combined Rietveld-RIR method: Journal of Applied Crystallography, v. 47, p. 267–278.

Gudmunsson, A., 2011, Rock Fractures in Geological Processes: Cambridge University Press, 578 p.

Hill, R., 2012, Bitumen filled fractures in the Bakken Formation and implications for gas shale systems: Abstracts with Programs - Geological Society of America, v. 42, p. 11–12.

Hlava, K., Campion, K., and Bayer, S., 2012, Sequence-Stratigraphic and Depositional Framework of the Middle Bakken Formation, Williston Basin, North Dakota.

Ho, N.-C., Peacor, D.R., and van der Pluijm, B.A., 1999, Preferred Orientation of Phyllosilicates in Gulf Coast Mudstones and Relation to the Smectite-Illite Transition: Clays and Clay Minerals, v. 47, p. 495–504.

Joswig, W., Fuess, H., Rothbauer, R., Takeuchi, Y., and Mason, S.A., 1980, A neutron diffraction study of a one-layer triclinic chlorite (penninite): American Mineralogist, v. 68, p. 349–352.

Kanitpanyacharoen, W., Wenk, H.-R., Kets, F., Lehr, C., and Wirth, R., 2011, Texture and anisotropy analysis of Qusaiba shales: Geophysical Prospecting, v. 59, p. 536–556.

Karma, R., 1991, Geology and geochemistry of the Bakken Formation (Devonian-Mississippian) in Saskatchewan [Master's]: University of Regina, Regina, SK, Canada (CAN), 308 p.

Kreis, K., and Costa, A., 2005, Hydrocarbon Potential of the Bakken and Torquay Formations, Southeastern Saskatchewan: Saskatchewan Geological Survey: Summary of Investigations, v. 1, p. 1–10.

Kreis, K., Costa, A., and Osadetz, K., 2006, Hydrocarbon Potential of Bakken and Torquay Formations, Southeastern Saskatchewan: Saskatchewan Geological Society Special Publication, v. 19, p. 118–137.

Kuhn, P.P., Primio, R. di, Hill, R., Lawrence, J.R., and Horsfield, B., 2012, Three-dimensional modeling study of the low-permeability petroleum system of the Bakken Formation: American Association of Petroleum Geologists Bulletin, v. 96, p. 1867–1897.

Lageson, D.R., 1989, Reactivation of a Proterozoic Continental Margin, Bridger Range, Southwestern Montana, *in* French, D.E. and Grabb, R.F. eds., Geologic resources of Montana: Montana Geological Society Field Conference Guidebook-Montana Centennial Edition, p. 279–298.

LeFever, J.A., Martiniuk, C.D., Dancsok, E.F.R., and Mahnic, P.A., 1991, Petroleum potential of the middle member, Bakken Formation, Williston Basin, *in* Proceedings of the Sixth International Williston Basin Symposium, Special Publication 11, p. 76–94.

LeFever, J., 2005, Oil Production from the Bakken Formation: A short History: North Dakota Geological Survey Newsletter, v. 32.

Lonardelli, I., Wenk, H.-R., and Ren, Y., 2007, Preferred orientation and elastic anisotropy in shales: Geophysics, v. 72, p. D33.

Lundegard, P.D., and Samuels, N.D., 1980, Field classification of fine-grained sedimentary rocks: Journal of Sedimentary Petrology, v. 50, p. 781–786.

Magoon, L.B., and Schmoker, J.W., 2000, The Total Petroleum System - The Natural Fluid Network that Constrains the Assesment Unit, *in* U.S. Geological Survey Digital Data Series 60.

Mainprice, D., 2007, Seismic Anisotropy of the Deep Earth from a Mineral and Rock Physics Perspective, *in* Treatise on Geophysics, p. 437–491.

Matthies, S., and Wenk, H.-R., 2009, Transformations for monoclinic crystal symmetry in texture analysis: Journal of Applied Crystallography, v. 42, p. 564–571.

Meissner, F., 1984, Petroleum geology of the Bakken Formation Williston Basin, North Dakota and Montana: American Association of Petroleum Geologists Special Publication,, p. 159–179.

Militzer, B., Wenk, H.-R., Stackhouse, S., and Stixrude, L., 2010, First-principles calculation of the elastic moduli of sheet silicates and their application to shale anisotropy: American Mineralogist, v. 96, p. 125–137.

Narr, W., and Burruss, R.C., 1984, Origin of Reservoir Fractures in Little Knife Field, North Dakota: American Association of Petroleum Geologists Bulletin, v. 68, p. 1087–1100.

Nelson, K.D., Baird, D.J., Walters, J.J., Hauck, M., Brown, L.D., Oliver, J.E., Ahern, J.L., Hajnal, Z., Jones, A.G., and Sloss, L.L., 1993, Trans-Hudson orogen and Williston basin in Montana and North Dakota: New COCORP deep-profiling results: Geology, v. 21, p. 447–450.

Pitman, J., Price, L., and LeFever, J., 2001, Diagenesis and Fracture Development in the Bakken Formation, Williston Basin: Implications for Reservoir Quality in the Middle Member: U.S. Geological Survey Professional Paper 1653.

Plançon, A., Tsipurski, S.I., and Drits, V.A., 1985, Calculation of intensity distribution in the case of oblique texture electron diffusion: Journal of Applied Crystallography, v. 18, p. 191–196.

Pollastro, R.M., Roberts, L.M.R., and Cook, T.A. Geologic Model for the Assessment of Technically Recoverable Oil in the Devonian–Mississippian Bakken Formation, Williston Basin, *in* Shale reservoirs — Giant resources for the 21st century, American Association of Petroleum Geologists Memoir 97, American Association of Petroleum Geologists, p. 205–257.

Porter, J.W., Price, R.A., and McCrossan, R.G., 1982, The Western Canada Sedimentary Basin: Philosophical Transactions of the Royal Society of London. Series A, Mathematical and Physical Sciences, v. 305, p. 169–192.

Price, L.C., 2000, Origins and Characteristics of the Basin-Centered Continuous Reservoir Unconventional Oil-Resource Base of the Bakken Source System, Williston Basin.

Price, L.C., and LeFever, J.A. Does Bakken Horizontal Drilling Imply a Huge Oil-Resource Base in Fractured Shales?, *in* Geological Studies Relevant to Horizontal Drilling: Examples from Western North America, Rocky Mountain Association of Geologists.

Price, L., and Stolper, K., 2000, Evidence and Causes of Super-Lithostatic Fracturing.

Renshaw, C.E., and Park, J.C., 1997, Effect of mechanical interactions on the scaling of fracture length and aperture: Nature, v. 386, p. 482–484.

Robinson, G.D., 1961, Origin and Development of the Three Forks Basin, Montana: Geological Society of America Bulletin, v. 72, p. 1003–1013.

Sandberg, C.A., 1965, Nomenclature and Correlation of Lithologic Subdivisions of the Jefferson and Three Forks Formations of Southern Montana and Northern Wyoming: Geological Survey Bulletin, v. 1194-N.

Sarg, J.F., 2012, The Bakken – An Unconventional Petroleum and Reservoir System: United States Department of Energy National Energy Technology Laboratory DOE Award No.: DE-NT0005672, 1–64 p.

Sayers, C.M., 2005, Seismic anisotropy of shales: Geophysical Prospecting, v. 53, p. 667–676.

Schmidt, C.J., and O'Neill, J., Michael, 1982, Structural Evolution of the Southwest Montana Transverse Zone: Rocky Mountain Association of Geologists Geologic Studies of the Cordilleran Thrust Belt, v. I, p. 193–218.

Smith, T., Genaud, E., and White, H., 2005a, A-1 Stark Core Examination: KM Core Report.

Smith, T., Genaud, E., and White, H., 2005b, 44-24 Vaira Core Examination: KM Core Report.

Smith, M.G., and Bustin, R.M., 2000, Late Devonian and Early Mississippian Bakken and Exshaw black shale source rocks, Western Canada Sedimentary Basin: a sequence stratigraphic interpretation: American Association of Petroleum Geologists bulletin, v. 84, p. 940–960.

Smith, M.G., and Bustin, R.M., 1998, Production and preservation of organic matter during deposition of the Bakken Formation (Late Devonian and Early Mississippian), Williston Basin: Paleogeography, Paleoclimatology, Paleoecology, v. 142, p. 185–200.

Sonnenberg, S.A., and Pramudito, A., 2009, Petroleum geology of the giant Elm Coulee field, Williston Basin: American Association of Petroleum Geologists Bulletin, v. 93, p. 1127–1153.

Sonnenberg, S., Vickery, J., and Sarg, J.F., 2011, Middle Bakken Facies, Williston Basin, USA: A Key to Prolific Production.

Strum, S.D., and Gomez, E., 2009, Role of Natural Fracturing in Production from the Bakken Formation, Williston Basin, North Dakota, *in* Denver, Colorado.

U.S. Department of the Interior, and U.S. Geological Survey, 2013, Assessment of undiscovered oil resources in the Bakken and Three Forks Formations, Williston Basin Province, Montana, North Dakota, and South Dakota, 2013: National Assessment of Oil and Gas Fact Sheet 2013-3013, 4 p.

Valcke, S.L.A., Casey, M., Lloyd, G.E., Kendall, J.-M., and Fisher, Q.J., 2006, Lattice preferred orientation and seismic anisotropy in sedimentary rocks: Geophysical Journal International, v. 166, p. 652–666.

Warner, L.A., 1978, The Colorado Lineament: A middle Precambrian wrench fault system: Geological Society of America Bulletin, v. 89, p. 161–171.

Wenk, H.-R., Voltolini, M., Mazurek, M., Loon, L.R.V., and Vinsot, A., 2008, Preferred Orientations and Anisotropy in Shales: Callovo-Oxfordian Shale (France) and Opalinus Clay (Switzerland): Clays and Clay Minerals, v. 56, p. 285–306.

Zou, C., Zhang, G., Yang, Z., Tao, S., Hou, L., Zhu, R., Yuan, X., Ran, Q., Li, D., and Wang, Z., 2013, Concepts, characteristics, potential and technology of unconventional hydrocarbons: On unconventional petroleum geology: Petroleum Exploration and Developement, v. 40, p. 413–428.

APPENDICES

APPENDIX A

FRACTURE DATA COLLECTED IN CORE

Appendix A contains all of the fracture data collected in core. s: systematic, ns: nonsystematic, if: into fracture, icb: into core boundary.

Apparent dip	Length (mm)	Aperture (mm)	Mode	Termination Pattern	Vein fill	Depth	
91	9	<1	1	dies out	pyrite	9182.2	A-1 Stark
28	10.5	<1	1	dies out	none	9183.7	
61	23	<1	1	dies out	none	9138.8	
359	14	<1	1	if	pyrite	9183.8	
90	16	<1	1	dies out	pyrite	9190.2	
112	18	<1	1	dies out	calcite	9190.2	
87	54	<1	1	if	py/ca	9190.2	
74	39	<1		dies out		9190.2	
9	45	<1		icb	calcite	9190.2	
105	8	<1	1	icb	calcite	9190.2	
11	20	<1	1	if	calcite	9190.2	
82	17	<1	1	dies out	calcite	9190.2	
165	10	<1	1	if	calcite	9190.2	
0	18	<1	1	dies out	calcite	9190.2	
80	19	<1	1s	dies out	calcite	9190.2	
145	11	1	1	if	calcite	9190.2	
111	18	<1	1	dies out	calcite	9190.2	
19	14	<1	1	if	calcite	9190.2	
87	12	<1	1	dies out	calcite	9190.2	
0	13	<1	1	if, icb	calcite	9190.2	
19	24	<1	1	dies out	calcite	9190.4	
132	18	<1	1	dies out	calcite	9190.4	
61	41	<1	1	icb, dies out	calcite	9190.4	
79	45	<1	1	dies out	calcite	9190.4	
72	59	<1	1	dies out	calcite	9190.4	
155	33	<1	1	icb	calcite	9190.4	
62	21	<1	1	dies out	calcite	9190.4	
69	44	<1	1	dies out	calcite	9190.4	
120	25	<1	1	dies out	calcite	9190.7	
172	30	<1	1	icb, dies out	calcite	9190.7	
21	106	<1	1	dies out	calcite	9190.7	

189	15	<1	1	dies out	calcite	9192.45
91	14	<1	1	dies out	calcite	9192.45
101	26	<1	1	dies out	calcite	9192.6
76	31	<1	1	dies out	calcite	9193.7
108	19	<1	1	dies out	calcite	9193.7
103	35	<1	1	dies out	calcite	9194.25
60	12	<1	1	dies out	calcite	9196.2
137	9	<1	1	dies out	calcite	9196.2
71	27	<1	1	dies out	calcite	9197.8
91	26	<1	1	dies out	calcite	9197.8
93	12	<1	1	dies out	calcite	9197.8
30	7	<1	1	dies out	pyrite	9197.9
93	12	<1	1	dies out	calcite	9198.8
95	14	<1	1	dies out	calcite	9198.8
41	15	<1	1	dies out	calcite	9198.8
93	28	<1	1	dies out	calcite	9199.2
69	21	<1	1	dies out	calcite	9199.2
92	13	1	1	dies out	calcite	9199.2
106	14	<1	1	dies out	calcite	9199.2
73	33	<1	1	dies out	calcite	9199.2
51	9	<1	1	dies out	calcite	9199.2
71	25	<1	1	dies out	calcite	9199.9
70	26	<1	1	dies out	calcite	9199.9
74	56	<1	1	dies out	calcite	9200.7
77	114	<1	1	dies out	calcite	9201.6
81	35	<1	1	icb	calcite	9202.2
78	27	<1	1	icb	calcite	9202.2
90	11	<1	1	dies out	calcite	9202.2
0	40	<1	1	if	calcite	9202.2
0	58	<1 to 7	1	dies out	calcite	9202.2
67	11	<1	1	dies out	calcite	9202.6
94	13	<1	1	dies out	calcite	9202.6
90	24	<1	1	dies out	calcite	9202.6
81	90	<1	1	dies out	calcite	9202.6
91	19	<1	1	dies out	calcite	9203.3
94	23	<1	1	dies out	calcite	9203.3
91	17	<1	1	dies out	calcite	9204.75
155	77	<1	1s	dies out	calcite	9204.8

102	41	<1	1ns	dies out	calcite	9204.8
87	31	<1	1ns	dies out	calcite	9204.8
92	14	1-1.5	1 or 2	dies out	calcite	9205.3
89	28	<1	1 or 2	dies out	py/ca	9205.3
97	24	<1	1 or 2	dies out	calcite	9205.3
91	12	<1	1	dies out	calcite	9205.3
89	20	<1	1	dies out	pyrite	9205.3
109	26	<1	1	dies out	calcite	9205.3
29	69	<1	4	icb		9209.2
144	59	<1	1	icb	calcite	9211.7
2	82	<1	1	icb	calcite	9212.2
12	54	<1	1	icb	calcite	9212.45
151	52	<1	4	if		9212.45
67	23	<1	1	icb	calcite	9214.2
172	27	<1	1	if	calcite	9214.2
0	11	<1	1	icb	calcite	9214.2
10	31	<1	1		calcite	9214.2
18	47	0	4	icb		9214.2
0	81	0-2	4	icb	clay1	9214.6
178	21	<1	1	icb	calcite	9214.6
69	11	<1	1	dies out	calcite	9214.6
0	82	0-5	1	icb	calcite	9215.1
93	96	<1	1	icb	calcite	9219.6
123	21	<1	1	if	calcite	9219.7
23	22	<1	1	dies out	calcite	9219.8
141	21	<1	1	icb	calcite	9219.8
155	42	<1	1	icb	calcite	9219.8
75	98	<1	1	icb	calcite	9220.2
89	56	<1	1	icb	calcite	9220.2
92	96	<1	1	icb	calcite	9220.6
0	51	<1	1	icb	calcite	9221.4
59	61	<1	1	icb	calcite	9222.3
92	95	<1	1	icb	calcite	9222.3
0	82	<1	1	icb	calcite	9224.1
9	81	<1	4	icb	calcite	9224.9
8	33	<1	1	icb, dies out	calcite	9225.8
151	42	<1	1	icb, dies out	calcite	9227.1
29	45	<1	4	icb, dies out	calcite	9227.4

18	61	<1	1	dies out	calcite	9228.3	
11	74	<1	1	icb	pyrite	9228.4	
12	42	<1	1	icb, dies out	calcite	9231.75	
125	21	<1	1	icb, dies out	calcite	9233.3	
35	94	<1	4	icb	pyrite	9233.3	
128	20	<1	1	icb, dies out	calcite	9234.6	
21	41	<1	1	icb, dies out	calcite	9234.8	
8	59	<1	1	icb, dies out	calcite	9234.8	
13	44	<1	1	dies out	calcite	9234.8	
92	15	<1	1	icb, dies out	calcite	9234.8	
105	16	<1	1	dies out	calcite	9234.8	
30	12	<1	1	if	calcite	9234.8	
5	82.5	<1	1	icb	calcite	9986.4	
176	78	<1	1	icb	calcite	9987.2	
177	64	<1	1	icb, dies out	calcite	9987.4	
169	81	<1	1	icb, dies out	calcite	9987.5	
9	84	<1	1	icb	calcite	9988.1	
3	82	<1	1	icb	calcite	9988.3	
2	82	<1	1	icb	calcite	9988.3	
4	80	<1	1	icb	calcite	9988.3	
124	71	<1	1	icb	calcite	9990.3	
11	15	<1	1	icb, dies out	calcite	9990.3	
40	11	<1	1	dies out	calcite	9990.3	
29	35	<1	1	icb, dies out	calcite	9991.2	
31	73	<1	1	icb, dies out	calcite	9991.2	44-24 Vaira
2	46	<1	1	dies out	calcite	9991.2	
145	23	<1	1	icb, dies out	calcite	9991.4	
63	54	<1	1	dies out	calcite	9991.4	
164	19	<1	1	if, dies out	calcite	9991.4	
162	36	<1	1	if, dies out	calcite	9991.4	
122	18	2	1	dies out	calcite	9992.1	
138	28	1	1	dies out	calcite	9992.1	
134	15.5	<1	1	dies out	calcite	9992.1	
74	12	<1	1	if, icb	calcite	9992.1	
70	11	<1	1	dies out	calcite	9992.1	
0	95	<1	1	icb	calcite	9992.6	
30	9	<1	1	dies out	calcite	9992.6	
18	14	<1	1	dies out	calcite	9992.6	

151	27	<1	1	dies out	calcite	9992.8
161	27	<1	1	dies out	calcite	9992.8
159	15	<1	1	dies out	calcite	9992.8
9	39	<1	1	dies out	calcite	9992.8
11	57	<1	1	icb, dies out	calcite	9992.8
26	27	<1	1	dies out	calcite	9994.3
19	16	<1	1	dies out	calcite	9994.3
8	11	<1	1	dies out	calcite	9994.3
166	33	<1	1	dies out	calcite	9994.3
175	48	<1	1	dies out	calcite	9994.3
10	58	<1	1	dies out	calcite	9994.3
2	94	<1	1	icb, dies out	calcite	9994.4
171	56	<1	4	icb, dies out	calcite	9995.1
5	94	<1	4	icb, dies out	calcite	9995.2
15	89	<1	4	icb, dies out	calcite	9995.4
12	93	<1	4	icb	calcite	9995.5
8	13	<1	1	icb, dies out		9999.1
170	12	<1	1			9999.1
9	18	<1	1	icb, dies out	calcite	9999.1
9	14	<1	1	icb, dies out	calcite	9999.4
164	11	<1	1	icb, dies out	calcite	9999.4
0	12	<1	1	icb, dies out	calcite	9999.5
178	72	<1	4	icb, dies out		9999.7
11	44	<1	1	icb, dies out		9999.9
8	36	<1	1	icb, dies out		9999.9
165	9	<1	1	icb, dies out		9999.9
176	68	<1	1	icb, dies out		10000.1
7	19	<1	1	icb, dies out	nothing	10000.3
172	85	<1	1	icb	nothing	10000.3
4	23	<1	1	dies out	nothing	10002
0	61	<1	1	icb	nothing	10002.2
179	37	<1	1	icb	nothing	10002.2
174	23	<1	1	dies out	nothing	10003.8
4	68	<1	1	icb	nothing	10003.8
8	51	<1	1	icb	nothing	10003.8
70	21	<1	1	icb, dies out	nothing	10003.8
11	51	<1	1	icb	nothing	10004.1
169	19	<1	1	icb	nothing	10004.1

18	61	<1	1	icb	nothing	10005.1
16	31	<1	1	icb	nothing	10005.1
174	38	<1	1	icb	nothing	10005.3
4	52	<1	1	icb	nothing	10005.3
18	48	<1	1		nothing	10006.2
4	83	<1	1	icb	nothing	10006.7
6	81	<1	1	icb	nothing	10006.7
178	9	<1	1	icb, dies out	nothing	10006.7
14	11	<1	1	icb, dies out	nothing	10006.9
10	70	<1	4	icb		10010.8
174	71	<1	1	icb, dies out		10016.8
11	16	<1	1	dies out	pyrite	10023.6
0	19	<1	1	dies out	pyrite	10023.6
178	36	<1	1	dies out	pyrite	10023.6
0	13	<1	1	icb, dies out	pyrite	10023.8
165	58	<1	1	icb, dies out	pyrite	10023.8
3	17	<1	1	icb, dies out	pyrite	10023.8
8	21	<1	1	dies out	pyrite	10023.8
177	65	<1	1	icb, dies out	pyrite	10023.8
172	14	<1	1	icb, dies out	pyrite	10025.2
162	56	<1	1	dies out	pyrite	10025.3
0	14	<1	1	dies out	pyrite	10025.4
6	70	<1	1	dies out	pyrite	10025.4
4	8	<1	1	icb, dies out	pyrite	10025.4
153	29	<1	1	icb, dies out	calcite	10025.6
162	59	<1	1	icb, dies out	calcite	10025.8
8	55	<1	1	icb, dies out	calcite	10025.8
0	23	<1	1	dies out	calcite	10025.8
171	34	<1	1	icb, dies out	calcite	10025.8
15	76	<1	1	icb	calcite	10026
5	79	<1	1	icb, dies out	calcite	10026.2
29	58	<1	1	icb, dies out		10026.4
177	48	<1	1	icb, dies out	calcite	10026.4
179	39	<1	1	dies out	calcite	10026.4
17	26	<1	1	icb, dies out	calcite	10026.4
167	25	<1	1	icb, dies out		10026.4
2	47	<1	1	icb, dies out	calcite	10026.5
21	24	<1	1	dies out		10026.5

0	29	<1	1	icb, dies out	pyrite	10026.5
12	24	<1	1	icb, dies out	calcite	10026.7
9	66	<1	1	dies out	calcite	10026.8
2	24	<1	1	icb, dies out	calcite	10026.8
2	57	<1	1	icb, dies out	calcite	10026.8
6	24	<1	1	icb, dies out	calcite	10026.8
165	34	<1	1	icb, dies out	calcite	10026.8
0	53	<1	1	icb, dies out	calcite	10027.1
2	35	<1	1	dies out		10027.1
8	26	<1	1	dies out		10027.1
31	22	<1	1	icb, dies out		10027.3
2	21	<1	1	dies out	calcite	10027.4
174	38	<1	1	dies out		10027.4
167	86	<1	1	dies out		10027.7
165	35	<1	1	icb, dies out	calcite	10027.7
171	29	<1	1	icb, dies out		10027.8
179	10	<1	1	icb, dies out		10027.8
174	92	<1	1	icb		10027.8
168	24	<1	1	icb, dies out	calcite	10027.8
4	16	<1	1	icb, dies out		10028.3
0	93	<1	1	icb	calcite	10028.3
179	93	<1	1	icb	calcite	10028.3
24	46	<1	1	dies out		10028.6
4	33	<1	1	icb, dies out	calcite	10028.7
12	41	<1	1	dies out		10028.7
178	94	<1	1	icb	pyrite	10029.1
11	21	<1	1	dies out	pyrite	10029.4
162	62	<1	1	icb	pyrite	10029.8
170	72	<1	1	icb, dies out		10029.8
19	95	<1	1	icb		10030.1
175	69	<1	1	icb, dies out	pyrite	10030.1
0	70	<1	1	icb	pyrite	10030.7
11	94	<1	1	icb	pyrite	10031.4
16	95	<1	1	icb	pyrite	10031.4
9	35	<1	1	icb, dies out	pyrite	10031.7
17	86	<1	1	icb, dies out	pyrite	10031.7
172	33	<1	1	dies out	pyrite	10031.7
175	46	<1	1	dies out	pyrite	10032

9	31	<1	1	dies out	pyrite	10032.3	
2	59	<1	1	icb, dies out	pyrite	10032.6	
11	95	<1	1	icb		10032.6	
172	94	<1	1	icb		10032.4	
176	94	<1	1	icb		10033.2	
2	92	<1	1	icb	pyrite	10034.2	
165	55	<1	1	icb	pyrite	10034.2	
171	94	<1	1	icb	pyrite	10034.2	
179	39	<1	1	icb		10034.4	
3	91	<1	1	icb	pyrite	10034.6	
4	56	<1	1	icb	pyrite	10034.7	
174	91	<1	1	icb		10034.8	
172	95	<1	1	icb	pyrite	10035.4	
1	74	<1	1	icb		10036.1	
177	61	<1	1	icb		10037.6	
176	53	<1	1	icb, dies out		10037.8	
179	94	<1	1	icb		10037.8	
4	94	<1	1	icb	calcite	10038.6	
165	51	<1	1	icb	calcite	10038.6	
8	31	<1	1	icb	calcite	10038.8	
29	42	<1	1	icb, dies out	calcite	10039.8	
3	41	<1	1	icb	calcite	10040.3	
13	67	<1	1	icb		10040.3	
166	22	<1	1	icb, dies out	calcite	10040.3	
171	25	<1	1	icb, dies out	calcite	10040.3	
18	94	<1	1	icb	calcite	10043.7	
0	94	<1	1	icb		10043.7	
2	83	<1	1	icb, dies out	calcite	10043.7	
4	91	<1	1	icb, dies out	calcite	10043.7	
18	76	<1	1	icb	calcite	10044.2	
0	40	<1	1	icb, dies out		10044.2	
5	94		4	icb		6770.8	Flatwillow 1-31H
0	94		4	icb		6770.8	
161	65		4	icb, dies out		6770.8	
175	93		4	icb		6770.8	
146	52	<1	1	icb, dies out	calcite	6771.4	
152	21	<1	1	icb, dies out	calcite	6771.4	
2	61		4	icb, dies out		6771.5	

171	94		4	icb		6771.6
4	94		4	icb		6771.7
161	79		4	icb		6771.8
5	94		4	icb		6772.1
4	84		4	icb, dies out		6772.2
175	94		4	icb		6772.4
0	23		4	icb, dies out		6772.6
5	69		4	icb, dies out		6772.6
81	74		4	icb, dies out		6773
164	90		4	icb		6775.1
2	81		4s	icb, dies out		6775.1
92	18	<1	1n	icb, dies out	calcite	6775.1
62	11	<1	1	icb, dies out	calcite	6775.4
61	98	<1	1	icb	calcite	6775.4
57	19	<1	1	dies out	calcite	6775.4
18	17	<1	1	if, icb	calcite	6775.4
35	29	<1	1	icb, dies out	calcite	6775.5
5	81	<1-1	1	icb, dies out	calcite	6775.5
90	21	<1	1	if, icb	calcite	6775.5
178	93		4	icb		6775.8
30	22	<1	1	dies out	calcite	6776.2
29	19	<1	1	dies out	calcite	6776.2
71	31	<1	1	icb	calcite	6776.2
11	6	<1	1	icb, dies out	calcite	6776.2
99	26	<1	1	dies out	calcite	6776.2
100	22	<1	1	if, dies out	calcite	6776.2
21	27	<1	1		calcite	6776.2
119	23	<1	1	dies out	calcite	6776.2
11	112	<1	1	icb	calcite	6776.2
7	20	<1	1	icb, dies out	calcite	6776.2
42	19	<1	1	icb, dies out	calcite	6776.2
18	21	<1	1	icb, dies out	calcite	6776.4
6	11	<1	1	dies out	calcite	6776.4
29	22	<1	1	dies out	calcite	6776.4
94	18	<1	1	dies out	calcite	6776.4
165	34	<1	4	dies out		6777.4
15	35	<1	1	dies out	calcite	6777.6
154	37	<1	1	dies out	calcite	6777.6

21	26	<1	1	dies out	calcite	6777.6
160	29	<1	1	icb, dies out	calcite	6777.8
98	18	<1	1	dies out	calcite	6777.8
8	46	<1	1	icb	calcite	6777.8
31	35	<1	1	icb	calcite	6777.8
103	40	<1	1	icb	calcite	6777.8
49	13	<1	1	icb, dies out	calcite	6778.3
157	31	<1	1	dies out	calcite	6778.3
61	14	<1	1	if, dies out	calcite	6778.3
8	32	<1	1	icb, dies out	calcite	6778.3
131	11	<1	1	if, icb	calcite	6778.3
156	35	<1	1	dies out	calcite	6778.3
9	59	<1	1	icb, dies out	calcite	6778.9
4	32	<1	1	icb, dies out	calcite	6778.9
106	85	<1	1	icb	calcite	6778.9
113	76	<1	1	icb	calcite	6778.9
43	6	<1	1	icb	calcite	6778.9
19	39	<1	1	if, icb	calcite	6778.9
5	41	<1	1	if, icb	calcite	6779.2
15	33	<1	1	if, icb	calcite	6779.2
12	18	<1	1	if, dies out	calcite	6779.2
10	32	<1	1	icb, dies out	calcite	6779.2
30	18	<1	1	icb, dies out	calcite	6779.4
31	56	<1	1	icb	calcite	6779.4
28	10	<1	1	icb, dies out	calcite	6779.6
21	56	<1	1	icb, dies out	calcite	6779.6
36	23	<1	1	icb	calcite	6779.6
111	11	<1	1	icb	calcite	6779.6
68	54	<1	1	if, icb	calcite	6780.3
59	31	<1	1	if	calcite	6780.3
32	16	<1	1	if, icb	calcite	6780.3
170	48	<1	1	if, icb	calcite	6780.3
18	33	<1	1	if, dies out	calcite	6780.3
68	45	<1	1	icb	calcite	6780.3
28	33	<1	1	icb	calcite	6780.3
162	9	<1	1	icb	calcite	6780.3
146	72	<1	1	icb	calcite	6780.6
6	21	<1	1	icb	calcite	6780.6

150	23	<1	1	icb, dies out		6780.6
10	22	<1	1	if, dies out	calcite	6780.6
0	46	<1	1	if, icb	calcite	6780.6
174	31	<1	1	if, icb	calcite	6780.6
85	42	<1	1n	if, icb	calcite	6782
89	61	<1	1n	if, icb	calcite	6782
2	24	<1	4s	icb		6782.2
89	14	<1	1	dies out	calcite	6782.2
55	95	<1	1	icb	calcite	6782.3
107	34	<1	1	icb, dies out	calcite	6782.6
167	76	<1	1	icb, dies out	calcite	6785.7
17	63		4	icb		6785.8
129	28	<1	1	icb, dies out	calcite	6785.8
91	18	<1	1	icb, dies out	calcite	6785.8
169	29		4	icb		6786.1
12	62		4	icb, dies out	calcite	6786.7
24	62	<1	1	icb	calcite	6786.9
18	43	<1	1	icb, dies out	calcite	6786.9
2	59	<1	1	if, icb	calcite	6786.9
11	21	<1	1	icb, dies out	calcite	6786.9
175	36	<1	1	icb, dies out	calcite	6786.9
118	55	<1	1	if, icb	calcite	6787.1
84	19	<1	1	if, dies out	calcite	6787.3
164	82	<1	1	icb	calcite	6787.3
177	32		4	dies out		6787.3
67	23	<1	1	dies out	calcite	6787.3
34	47		4	icb, dies out		6787.6
116	87	<1	1	dies out	calcite	6787.6
143	80	<1	4	icb	calcite	6787.9
61	30		4	if, icb		6788.6
163	22	<1	1	if, icb	calcite	6788.6
113	25	<1	1	if	calcite	6788.6
150	18		4	if, icb		6788.6
161	46		4	if, dies out		6788.6
164	78		4	icb		6788.6
39	15	<1	1	icb, dies out	calcite	6788.6
23	28	<1	1	dies out	calcite	6788.6
22	25	<1	1	icb, dies out	calcite	6788.6

32	22	<1	1	icb, dies out	calcite	6788.6	
36	19	<1	1	icb, dies out	calcite	6788.6	
17	13	<1	1	icb, dies out		6788.6	
152	22	<1	1	icb, dies out	calcite	6788.8	
113	77		4	icb		6788.8	
66	108	<1	1	icb, dies out	calcite	6015.5	
12	98		4	icb		6015.7	
159	47		4	icb, dies out		6015.8	
136	47		4	icb, dies out		6015.8	
176	34		4	icb, dies out		6016	
175	64		4	icb, dies out		6016	
39	29		1	icb, dies out	calcite	6016	
156	101		4	icb	pyrite	6016.3	
0	97	<1	1	icb	calcite	6017.2	
2	97	<1	1	icb	calcite	6017.2	
8	32	<1	1	icb, dies out	calcite	6017.2	
0	61	<1	1	icb, dies out	calcite	6017.2	
174	85	<1	1	icb	calcite	6017.4	
176	31	<1	1	icb, dies out	calcite	6017.4	
64	20	1	1	dies out	calcite	6017.5	
169	70	<1	1	dies out	calcite	6017.7	
92	80	<1-5	1	dies out	calcite	6018.3	Willowflats
113	46	<1-1	1	icb, dies out	calcite	6018.3	
4	97		4	icb		6018.7	
65	219	<1-2	1		calcite	6018.6	
52	11	<1	1	icb, dies out	calcite	6019.1	
60	26	<1	1	icb, dies out	calcite	6019.1	
51	9	<1	1	icb, dies out	calcite	6019.1	
60	34	<1	1	icb, dies out	calcite	6019.1	
140	13	<1	1	icb, dies out	calcite	6019.3	
21	95	<1	1	icb, dies out	calcite	6019.6	
15	71	<1	4	icb	calcite	6019.7	
4	32	<1	1	dies out	calcite	6019.8	
177	51	<1	1	icb, dies out	calcite	6019.8	
89	37	<1	1	dies out	calcite	6019.8	
178	42	<1	1	dies out	calcite	6020.2	
91	238	<1	1	dies out	calcite	6020.2	
3	74	<1	1	dies out	calcite	6020.4	

82	124	<1	1	dies out	calcite	6020.5
164	81	<1	1	icb, dies out	calcite	6020.5
178	51	<1	1	icb, dies out	calcite	6020.6
2	28	<1	1	dies out	calcite	6020.6
167	97		4	icb		6021.2
160	99	<1	4	icb		6021.2
110	21	<1	1	icb, dies out	calcite	6021.4
58	55	<1	1	icb, if	calcite	6021.6
51	25	<1	1	icb, if	calcite	6021.6
168	94	<1-1	1	icb	calcite	6021.7
7	18	<1	1	dies out	calcite	6021.4
172	18	<1	1	dies out	calcite	6021.4
161	27	<1	1	icb, dies out	calcite	6021.4
178	47	<1	1	icb	calcite	6022.3
78	24	<1	1	icb, dies out	calcite	6022.6
168	67	<1	1	icb, dies out	calcite	6022.7
158	101	<1	4	icb		6022.7
71	108	<1-4	1	icb, dies out	calcite	6022.7
4	35	<1	1	if, dies out	calcite	6023.1
22	29	<1	1	dies out	calcite	6023.2
175	97	<1	1	icb	calcite	6023.4
166	97	<1	1	icb	calcite	6023.6
69	63	<1	1	icb	calcite	6024.2
38	45	<1	1	icb		6024.2
165	46	<1	1	icb, dies out		6024.4
72	21	<1	1	icb, if		6024.7
174	94	<1-2	4	icb	calcite	6024.8
92	16	<1	1	icb		6024.8
90	19	<1-2	1	icb		6024.8
83	16	<1	1	icb	calcite	6024.8
76	18	<1	1	icb	calcite	6024.8
86	34	<1	1	if	calcite	6024.8
89	29	<1	1	if	calcite	6024.8
170	17	<1	1	if, dies out		6024.8
176	79	<1-1	4	icb		6024.8
69	83	<1	1	icb	calcite	6025.2
64	44	<1	1	icb, dies out	calcite	6025.3
14	43	<1	1	dies out	calcite	6025.3

62	25	<1	1	icb, dies out	calcite	6025.4
61	34	<1	1	icb	calcite	6025.4
110	45	<1	1	dies out	calcite	6025.4
64	35	<1	1	dies out	calcite	6025.4
92	63	<1	1	dies out	calcite	6025.6
24	19	<1	1	icb, if		6025.6
81	24	<1	1	icb	calcite	6025.7
23	34	<1	1	if	calcite	6025.7
88	6	<1	1	if	calcite	6025.7
103	18	<1	1	if, dies out	calcite	6025.7
18	39	<1	1	icb, dies out	calcite	6025.7
96	15	<1-1	1	icb	calcite	6025.7
84	15	<1	1	icb, dies out	calcite	6025.7
120	6	<1	1	icb, dies out	calcite	6025.7
122	127	<1	1	icb, dies out		6025.7
11	34	<1	1	icb, if	calcite	6025.7
175	12	<1	1	if	calcite	6025.7
162	19	<1	1	icb, dies out	calcite	6025.8
11	15	<1	1	icb, dies out	calcite	6025.8
11	23	<1	1	dies out	calcite	6026.1
10	11	<1	1	dies out	calcite	6026.1
9	11	<1	1	dies out	calcite	6026.1
11	7	<1	1	dies out	calcite	6026.1
9	51	<1	1	icb, dies out	calcite	6026.2
134	43	<1	1	icb, dies out	calcite	6026.2
6	41	<1	1	dies out	calcite	6026.2
97	75	<1	1	icb, dies out	calcite	6026.3
109	42	<1	1	icb, dies out	calcite	6026.4
178	78	<1	1	icb, dies out	calcite	6026.4
49	23	<1	1	icb, dies out	calcite	6026.4
122	19	<1	1	if, dies out		6026.4
177	56	<1	1	icb, dies out	calcite	6026.4
11	78	<1	1	dies out		6030.5
91	79	<1	1	icb		6032.5
85	149	<1	1	icb, dies out	calcite	6032.5
86	66	<1	1	icb		6033
89	44	<1	1	icb, dies out		6033.1
1	97	<1	4	icb		6033.1

40	92	<1	1	icb		6033.5
91	59	<1	1	icb, dies out	calcite	6033.6
4	36	<1	4	icb, dies out		6033.4
65	96	<1	1	icb	calcite	6033.4
173	25	<1-1	1	icb		6034.2
87	51	<1	1	icb, dies out		6034.2
86	39	<1	1	icb, dies out		6034.3
22	68	<1	4	icb		6035.6
32	53		4	icb, if		6035.7
22	94	<1	4	icb		6035.7
36	103	<1-1	4	icb		6035.8
34	61	<1-1	1	icb		6036
27	96	<1	1	icb		6036.4
3	72	<1	4	icb	calcite	6036.6
6	93		4	icb		6036.6
22	100		4	icb		6036.7
18	99		4	icb		6036.7
24	71		4	icb		6036.9
21	69		4	icb		6036.9
41	68		4	icb		6036.9
18	106	<1	4	icb	calcite	6036.9
30	13	<1	1	icb, dies out	calcite	6037.2
32	21	<1	1	icb, dies out	calcite	6037.2
149	27	<1	1	icb, dies out	calcite	6037.3
12	95	<1	1	icb	calcite	6037.3
19	99	<1	4	icb		6037.5
18	99	<1	1	icb		6037.5
19	97		4	icb		6037.6
21	99	<1	1	icb		6037.7
15	36	<1	1	icb, if	calcite	6037.7
166	35	<1	1	icb, if	calcite	6037.7
9	44	<1	1	icb, dies out		6037.9
31	25	<1	1	icb, dies out		6037.9
24	86		4	icb		6038.1
12	32	<1	1	dies out	calcite	6038.2
18	22	<1	1	icb, dies out	calcite	6038.3
20	7	<1	1	icb, dies out	calcite	6038.3
26	16	<1	1	icb, dies out	calcite	6038.3

28	24	<1	1	icb, dies out	calcite	6038.3
10	71	<1	1	icb, dies out	calcite	6038.3
104	29	<1	1	icb, if	calcite	6038.3
103	31	<1	1	icb, if	calcite	6038.3
18	28	<1	1	dies out	calcite	6038.4

APPENDIX B

FRACTURE DATA COLLECTED IN THE FIELD

Appendix B contains all of the fracture data collected in the field. QF: quality factor, ca: calcite, ca bl: blocky calcite, wtb: within the bed, itg: into the ground, bf: bedding fracture.

Strike	Dip	Dip Direction	Length (cm)	Aperture (mm)	Fill	QF	Arrest Behavior	Unit
274	25	NW	110	2 - 13		2	wtb	Antelope Valley Upper Sandstone
271	22	NW	70			3	wtb	
259	19	NW	37			3	wtb	
260	13	NW	39			2	wtb	
071	65	SE	9	1-2		3	wtb	
243	82	NW	4	2		2	wtb	
219	75	NW	11	3		2	wtb	
082	73	SE	10	2		3	wtb	
256	69	NW	3	2		2	wtb	
086	57	SE	8	1-12		3	wtb	
082	64	SE	5	< 1		3	wtb	
072	56	SE	6	< 1		2	wtb	
103	78	S	11	1-3		3	wtb	
006	89	E	12	< 1		2	wtb	
260	15	NW	125	< 1 - 9	ca blocky	3	wtb	
075	71	SE	12	< 1		2	wtb	
069	80	SE	8	1 -2		3	wtb	
241	87	NW	18	1		2	wtb	
087	78	SE	12	2		3	wtb	
081	82	SE	15	< 1		2	wtb	
080	76	SE	8	2		2	wtb	
254	65	NW	4	< 1		3	wtb	
178	82	W	64			4	wtb	
025	79	E	70	1-2		3	wtb	
201	76	NW	18	18		2	wtb	
033	61	E	27	2-3		3	wtb	
029	72	E	18	< 1		3	wtb	
183	84	W	13	1 - 2		2	wtb	
099	80	S	32	14		3	wtb	
265	86	N	27	11		2	wtb	
031	72	E	18	2		2	wtb	
023	69	E	12	< 1		2	wtb	

037	78	E	8	< 1 - 2		2	wtb	
024	71	E	4	< 1		2	wtb	
172	81	W	43	2		3	wtb	
028	69	E	32	1 - 3		2	wtb	
084	87	S	13	< 1		3	wtb	
095	78	S	11	< 1		2	wtb	
174	60	W	12	< 1		3	wtb	
028	78	E	16	< 1		2	wtb	
024	78	E	18	< 1		3	wtb	
031	82	E	11	1 -2		2	wtb	
306	28	NE	94	1 - 3	clay	2	wtb	
307	25	NE	85	1 - 2	clay	3	wtb	
310	21	NE	39	2 - 3	clay	2	wtb	
339	47	NE	161	2 - 20	clay	3	wtb	
159	81	W	10	1 - 7	ca	3	wtb	
304	34	NE	17	2 - 4	clay	3	wtb	
265	19	N	31	1 - 3	clay	3	wtb	
308	24	NE	28	1 - 2	clay	2	wtb	
162	87	W	52	1 - 4		2	wtb	
181	86	W	37	1 - 3		3	wtb	
101	82	S	17	< 1		2	wtb	
024	77	E	12	1 - 2		2	wtb	
031	81	E	23	< 1		3	wtb	
028	69	E	11	< 1		4	wtb	
038	71	E	8	1 - 3		3	wtb	
025	73	E	19	1 - 2		2	wtb	
271	32	N	37	1 - 5	clay	2	wtb	
161	83	W	23	< 1		2	wtb	
158	78	W	8	< 1 -2		2	wtb	
129	68	SW	94			3	wtb	
156	75	SW	73	2 - 8		3	wtb	
164	70	SW	37	1 - 5		2	wtb	
305	65	NE	21	< 1 - 2		3	wtb	
221	62	NW	58	< 1		3	wtb	
225	54	NW	23	< 1	clay	2	wtb	
235	61	NW	21	< 1	clay	3	wtb	
231	53	NW	28	< 1		2	wtb	
225	64	NW	13	1 - 2		2	wtb	

223	61	NW	33	1 - 3	clay	2	wtb	
231	51	NW	8	< 1		3	wtb	
228	57	NW	27	< 1		3	wtb	
224	55	NW	23	1 - 2		2	wtb	
227	49	NW	17	< 1		3	wtb	
238	67	NW	4	< 1 - 3		2	wtb	
231	52	NW	31	< 1		3	wtb	
209	54	W	11	< 1		3	wtb	
208	60	W	8	< 1		2	wtb	
210	55	W	12	< 1		3	wtb	
212	63	W	17	< 1		2	wtb	
207	51	W	8	< 1		2	wtb	
209	53	W	17	< 1		3	wtb	
211	57	W	16	< 1		2	wtb	
249	60	NW	13	< 1 - 2		2	wtb	
234	58	NW	22	< 1		3	wtb	
240	65	NW	13	< 1		3	wtb	
242	77	NW	4	< 1		2	wtb	
234	74	NW	11	< 1		3	wtb	
216	81	W	10	< 1		2	wtb	
244	71	NW	26	< 1		3	wtb	
241	71	NW	12			3	wtb	
238	62	NW	32	< 1 - 2		2	wtb	
199	68	W	34	< 1 - 3		3	wtb	
191	76	W	48	< 1 - 2		2	wtb	
237	59	NW	21			3	wtb	
224	85	NW	37	< 1 - 4		2	wtb	
011	87	E	25	< 1 - 5		3	wtb	
335	84	E	24	< 1 - 3		2	wtb	
010	89	E	18	< 1 - 2		2	wtb	
008	87	E	12	< 1 - 2		3	wtb	
001	78	E	16	1 - 3		2	wtb	
358	76	E	17	< 1		3	wtb	
004	82	E	8	< 1 - 2		2	wtb	
013	86	E	21	< 1 - 4		3	wtb	
351	71	E	18	< 1 - 2		2	wtb	
181	63	W	49			4	itg	
190	54	W	52			4	itg	

280	89	N	58			4	itg	
272	82	N	61			3	itg	
093	82	S	39			2	wtb	
340	41	E	85	< 1 - 4		3	wtb	
312	39	NE	64	< 1 - 3		2	wtb	
166	79	W	52	< 1 - 2		3	wtb	
350	42	E	36	< 1		2	wtb	
204	13	W	55	< 1		2	wtb	
071	61	S	27	1 - 4		2	wtb	
076	77	S	70	< 1 - 3		3	itg	
081	64	S	37	< 1 - 2		2	itg	
069	71	S	24	< 1		3	wtb	
318	27	NE	58	1 - 4		2	wtb	
309	31	NE	33	< 1 - 2		3	wtb	
071	83	S	73	< 1 - 2		2	itg	
083	89	S	18	2 - 3		2	itg	
271	87	N	40			2	itg	
283	79	N	55			3	itg	
069	81	S	23	1 - 3		2	wtb	
308	32	E	43	< 1 - 2		3	wtb	
312	39	E	64	1 - 4		2	wtb	
171	61	W	98			4	itg	Antelope Valley Lower Lodgepole
183	75	W	85			4	itg	
176	67	W	39			4	itg	
169	73	W	52			4	itg	
301	40	NE	70	< 1 - 4		3	wtb	
053	81	SE	23	< 1 - 2		2	wtb	
169	77	W	9	2 - 4		3	wtb	
173	82	W	38	< 1		2	wtb	
163	73	W	64	< 1 - 3		2	wtb	
312	38	NE	42	1 - 3		3	wtb	
309	35	NE	33	4		2	wtb	
176	78	W	55			3	itg	
187	81	W	17			2	wtb	
177	81	W	39	< 1 - 3		3	wtb	
168	72	W	22	< 1 - 2		2	wtb	
307	32	NE	94			3	wtb	
172	86	W	18	< 2 - 4		2	wtb	

186	78	W	43	< 1 - 2		2	itg	
072	76	SE	17	< 1		3	wtb	
164	79	W	37	1 - 3		3	wtb	
182	63	W	32	< 1 - 4		3	wtb	
311	41	NE	82	< 1 - 2		4	wtb	
069	75	SE	23	< 1 - 2		3	wtb	
177	69	W	37	< 1		4	itg	
078	70	SE	12	< 1		3	wtb	
169	84	W	21	< 1		2	wtb	
309	38	NE	81	< 1		2	wtb	
307	47	NE	60	< 1		3	wtb	
176	53	W	64	< 1		3	itg	
314	39	NE	54	< 1		2	wtb	
170	67	W	41	< 1 - 3		2	wtb	
298	41	NE	88	< 1 - 2		2	wtb	
166	78	W	31	< 1 - 4		3	wtb	
125	70	SE	24	< 1				Logan Gulch Sandstone
115	81	SE	12	< 1				
129	86	SE	11	< 1				
139	78	SE	34	< 1				
136	82	SE	5	< 1				
126	84	SE	5	< 1				
125	71	SE	6	< 1				
338	82	NE	7	< 1				
151	85	SE	48	1	ca			
270	80	N	12	< 1	ca			
091	89	S	18	< 1				
344	69	E	45	2 - 9				
248	29	NW	20	1 - 8				
324	70	NE	43	2 - 7				
301	71	NE	41					
141	71	SW	7	< 1				
325	80	NE	11	3				
309	80	NE	6	< 1				
335	76	NE	9	2				
324	78	NE	18	3				
331	66	NE	27	4				
337	79	NE	9	< 1				

331	78	NE	12	< 1				
311	66	NE	14.2	< 1				
203	38	W	16	2 - 4		2		
265	73	N	18	< 1 - 5		2	wtb	
206	61	W	15	< 1		2	wtb	
214	55	W	21	< 1		3	wtb	
359	70	E	17	< 1		4	wtb	
355	61	E	19			4	itg	
354	51	E	10		ca	2	wtb	
359	61	E	16	< 1 - 2		4	itg	
264	85	N	14			4	itg	
255	74	N	20			4	wtb	
011	62	E	14			3	wtb	
004	51	E	18	60		2	wtb	
006	40	E	21			1	wtb	
004	45	E	10			1	wtb	
095	69	E	32		ca	3	wtb	
219	45	NW	25	11		2	wtb	
325	62	NE	15	8		2	bf	
211	41	NW	44	< 1 - 9		1	wtb	
319	71	NE	14	< 1 - 3		2	wtb	
019	53	E	6			3	wtb	
089	65	S	8			1	wtb	
358	45	E	55	< 1		4	itg	
256	79	NE	49			3	itg	
005	52	E	38	< 1		4	itg	
010	67	E	43			3	itg	
241	51	NW	58			2	itg	
025	55	E	22	< 1 - 4		1	wtb	
091	70	S	48			2	itg	
072	79	SW	64			2	itg	
065	71	SW	21			1	itg	
003	74	E	17			2	itg	
358	59	E	21			4	itg	
011	63	E	14			3	itg	
355	55	E	27			4	itg	
300	77	NE	18			3	wtb	
210	57	NW	39	1	ca	3	wtb	

358	44	E	14	< 1 - 3	ca	2	wtb	
001	44	E	33			4	wtb	
259	72	N	10	2 - 8		2	wtb	
122	76	SW	13	8		2	wtb	
205	46	NW	17	< 1 - 3		2	wtb	
353	41	E	82			4	wtb	
151	66	SW	23			3	wtb	
356	55	E	28	< 1		4	bf	
211	47	NW	98	< 1 - 4		2	wtb	
109	50	S	85		ca	4	itg	
001	76	E	57	42 - 57	ca	2	itg	
120	61	SW	42		ca	3	itg	
222	41	NW	27	< 1		3	wtb	
005	41	E	11	< 1 - 3		2	wtb	
024	64	SE	15	50		1	wtb	
284	86	NE	16			3	wtb	
351	66	E	21			4	itg	
164	61	SW	17			3	wtb	
004	49	E	12	< 1 - 3		4	wtb	
358	61	E	23			3	wtb	
211	58	NW	43	< 1 - 3		2	wtb	
206	86	NW	82			3	wtb	
302	67	NE	16	12		3	bf	
106	76	SW	18	< 1		2	wtb	
128	86	SW	11	< 1 - 2		2	wtb	
119	88	SW	8	< 1		1	wtb	
111	73	SW	7	< 1		2	wtb	
299	32	N	6	< 1		3	wtb	
111	78	SW	5	< 1		2	wtb	
311	41	NE	6	< 1		2	wtb	
329	40	NE	8	< 1		3	wtb	
311	43	NE	5	< 1		2	wtb	
301	36	NE	7	< 1		3	wtb	
191	47	W	29	< 1		2	wtb	
314	43	NE	11	< 1 - 4		2	wtb	
189	50	W	15	< 1		2	wtb	
357	59	E	32			3	wtb	
334	61	NE	38	< 1 - 5		3	wtb	

306	76	NE	13	< 1 - 3		2	wtb	
295	06	NE	16	8		2	wtb	
205	37	NW	34	< 1		3	wtb	
203	32	NW	31	< 1		2	wtb	
207	34	NW	15	< 1		2	wtb	
211	41	NW	32	< 1		3	wtb	
201	36	NW	33	< 1		2	wtb	
206	37	NW	18	< 1		2	wtb	
205	42	NW	8	< 1		2	wtb	
208	38	NW	17	< 1		3	wtb	
207	48	NW	16	< 1		1	wtb	
210	33	NW	21	< 1		2	wtb	
203	34	NW	15	< 1		2	wtb	
205	34	NW	8	< 1		2	wtb	
330	61	NE	44			2	wtb	
180	87	W	32	9 - 22		2	wtb	
343	64	NE	51			3	itg	
326	87	NE	34			2	itg	
301	37	NE	15	< 1		2	wtb	
205	40	NW	23	< 1		3	wtb	
335	56	NE	16	< 1 - 2		2	wtb	
336	54	NE	15	< 1		2	wtb	
331	57	NE	23	< 1 - 2		3	wtb	
330	64	NE	18	< 1		2	wtb	
208	37	NE	31	< 1 - 3		2	wtb	
336	39	NE	12	< 1		3	wtb	
211	41	NW	29	< 1		3	wtb	
206	45	NW	18	< 1		2	wtb	
201	32	NW	17	< 1 - 2		3	wtb	
180	78	W	12	< 1- 3		2	wtb	
208	43	NW	23	< 1		3	wtb	
336	65	NE	37	< 1		2	wtb	
300	75	NE	34	< 1		3	bf	
084	83	W	27	< 1		2	wtb	
346	66	NE	32	< 1 - 4		2	bf	
206	41	NW	11	< 1 - 2		3	wtb	
121	75	SW	61			4	wtb	
005	75	SW	55	18 - 26		2	wtb	

004	40	E	52	< 1 - 22		3	wtb	
007	50	E	46		ca film	4	wtb	
290	85	N	21	2 - 4		3	wtb	
291	78	N	24	4 - 6		2	wtb	
204	50	NW	64	< 1		2	wtb	
206	48	NW	73	< 1 - 18		3	wtb	
203	43	NW	40	< 1		2	wtb	
026	44	SE	52	< 1		2	wtb	
123	85	SW	55	< 1		3	wtb	
212	48	NW	48	< 1		2	wtb	
215	41	NW	23	< 1		1	wtb	
119	81	SW	19			2	wtb	
358	47	E	47			3	itg	
001	53	E	18	< 1- 4		2	wtb	
221	37	NW	27	< 1		1	wtb	
218	42	NW	31	< 1		3	wtb	
211	48	NW	39	< 1		3	wtb	
007	47	E	43			2	itg	
131	81	SW	41			3	wtb	
128	76	SW	18	< 1 - 2		2	wtb	
357	51	E	14	< 1 - 3		3	wtb	
217	47	NW	37	< 1		2	wtb	
007	63	E	52			1	itg	
348	43	E	31			3	wtb	
211	38	NW	55	< 1		2	wtb	
118	68	SW	23	< 1 - 4		4	wtb	
286	75	N	17	< 1- 2		3	wtb	
218	39	NW	29	< 1		2	wtb	
357	41	E	85			4	itg	
207	43	NW	49	< 1		2	wtb	
213	33	NW	46	< 1 - 2		3	wtb	
219	14	NW	39	< 1		2	wtb	Logan Gulch Lodgpole Limestone
206	21	NW	43	< 1		3	wtb	
334	69	NE	52			4	wtb	
086	87	S	31			3	wtb	
212	36	NW	46	< 1		3	wtb	
010	89	E	58			2	wtb	
101	61	W	32	< 1 - 3		2	bf	

099	72	W	11	< 1- 2		3	bf	
356	81	E	29			4	wtb	
071	63	SE	36			2	wtb	
330	75	NE	48	13-15	breccia	3	wtb	
208	31	NW	38	< 1		2	wtb	
213	21	NW	21	< 1		2	wtb	
113	69	SW	18	< 1 - 2		2	wtb	
002	78	E	33	< 1 - 3		3	itg	
349	63	E	43	< 1 - 4		2	itg	
357	59	E	39			3	itg	
091	83	S	21			2	wtb	
211	23	NW	31	< 1		3	wtb	
221	19	NE	34	< 1		1	wtb	
329	68	NE	21	< 1		2	wtb	
359	76	E	43			4	itg	
008	69	E	21	< 1		3	wtb	
211	21	NW	37	< 1		2	wtb	
213	18	NW	22	< 1		2	wtb	
079	65	SE	12	< 1		2	wtb	
209	27	NW	38	< 1		3	wtb	
348	69	E	52			3	itg	
098	76	S	16	2 - 8		3	wtb	
211	24	NW	37	< 1 - 2		4	wtb	
201	19	NW	26	< 1		2	wtb	
207	17	NW	18	< 1		2	wtb	
002	67	E	39			3	wtb	
127	72	SW	17	< 1 - 3		2	wtb	
217	19	NW	33	< 1		2	wtb	
357	63	E	47			3	wtb	
010	71	E	31			2	wtb	
349	64	E	131	< 1		3	wtb	
219	46	NW	82	< 1		2	wtb	
347	71	E	104			3	wtb	
072	78	SE	146			4	wtb	
346	61	NE	124	< 1	ca	2	wtb	
331	49	NE	34	< 1	ca	3	wtb	
336	56	NE	31	< 1		3	wtb	
355	68	E	17			2	wtb	

081	61	S	82			4	wtb	
234	56	NW	147	< 1		3	wtb	
347	49	E	12	< 1		2	wtb	
356	59	E	31	< 1 - 3		3	wtb	
209	47	NW	94	< 1		2	wtb	
217	51	NW	70	< 1		3	wtb	
083	63	S	55	< 1		2	wtb	
079	73	S	48	< 1		3	wtb	
211	38	NW	42	< 1		2	wtb	
356	72	E	41			3	itg	
076	81	SE	82			4	itg	
349	61	NW	49	< 1		2	itg	
227	43	NW	39	< 1		1	wtb	
321	51	NE	16	< 1 - 2		3	bf	
219	36	NW	34	< 1		2	wtb	
352	67	E	49			4	itg	
088	83	S	23	< 1 - 3		2	wtb	
073	69	SE	17	< 1 - 2		3	wtb	
147	72	SW	12	< 1		3	wtb	
212	14	NW	27	< 1		1	wtb	
002	73	E	36			4	itg	
010	61	E	48			3	itg	
090	87	S	31			2	wtb	
219	42	NW	29	< 1		3	wtb	
223	32	NW	40	< 1		2	wtb	
076	81	SE	18	< 1 - 2		1	wtb	
081	84	SE	12	< 1		2	wtb	
349	71	E	27			3	wtb	
011	68	E	13	< 1 - 2		2	wtb	
213	41	NW	29	< 1		1	wtb	
218	49	NW	36	< 1		2	wtb	
153	61	SW	15	< 1 - 2		2	wtb	
091	83	S	26	< 1 - 4		3	wtb	
219	36	NW	45	< 1		2	wtb	
071	75	SE	25			4	wtb	Moose Creek Sandstone
065	79	SE	16	2		3	wtb	
051	80	SE	6	< 1		2	wtb	
066	74	SE	21			4	wtb	

325	46	NE	17	3		3	wtb	
321	30	NE	29	1		3	wtb	
321	37	NE	30	< 1		2	wtb	
044	83	SE	22	5		2	wtb	
010	48	E	18	4		2	wtb	
072	81	SE	21	3		2	wtb	
081	76	S	19			4	wtb	
179	66	W	11	< 1	ca b	3	wtb	
090	76	S	24	< 1	ca b	2	wtb	
072	44	SE	8	< 1	ca b	2	wtb	
331	36	NE	34	2		2	wtb	
337	29	NE	27	1		3	wtb	
081	77	SE	12	< 1	ca b	2	wtb	
066	79	SE	5	< 1		2	wtb	
086	19	SE	11	1		2	wtb	
018	70	E	5	2		2	wtb	
161	55	SW	7	< 1	ca b	3	wtb	
074	79	SE	58			4	wtb	
339	70	NE	7	3		3	wtb	
184	84	SW	52	12		2	wtb	
076	81	SE	11	< 1	ca b	3	wtb	
081	75	SE	15	2		2	wtb	
074	82	SE	21	3		2	wtb	
329	31	NE	32	2		3	wtb	
064	81	SE	18	< 1		3	wtb	
169	57	SW	9	2		2	wtb	
089	89	SE	12	1		3	wtb	
091	72	SE	15	2		2	wtb	
079	88	SE	17	3	ca b	2	wtb	
081	87	SE	12	2		3	wtb	
171	55	SW	17	< 1		2	wtb	
331	32	NE	39	2		4	wtb	
069	89	SE	11	2		3	wtb	
059	74	SE	19	< 1		2	wtb	
328	41	NE	27	1		3	wtb	
310	29	NE	33	2		3	wtb	
062	74	SE	7	2		2	wtb	
075	82	SE	11	< 1		3	wtb	

319	34	NE	21	2		3	wtb	
157	48	SW	47	3		4	itg	
011	72	E	18	4		2	wtb	
057	88	SE	13			3	wtb	
098	73	SE	27	2		2	wtb	
054	86	SE	11	< 1		3	wtb	
340	31	NE	48	2		3	wtb	
062	79	SE	24	1		2	wtb	
076	81	SE	64	< 1 - 2		3	wtb	
072	83	SE	49	< 1		3	wtb	
076	82	SE	24	< 1		2	wtb	
170	85	W	30	< 1 - 4		2	wtb	
170	85	W	64	2 - 5		3	wtb	
065	85	SE	116	< 1		4	wtb	
081	72	SE	42	< 1		3	wtb	
072	89	SE	18	2		2	wtb	
080	85	SE	46	4		3	wtb	
322	55	NE	43	1		2	wtb	
081	84	SE	37	< 1		3	wtb	
309	17	NE	140	2		3	wtb	
312	28	NE	87	< 1 - 4		2	wtb	
082	89	SE	12	2	ca b	3	wtb	
053	73	SE	17	2		2	wtb	
067	84	SE	23	< 1		2	wtb	
143	78	W	49	< 1		2	wtb	
318	46	NE	45	2		3	wtb	
177	64	W	16	< 1		3	wtb	Moose Creek Middle Shale
344	41	NE	11	< 1		2	wtb	
325	55	NE	15	1		2	wtb	
323	55	NE	13	4		3	wtb	
011	79	E	7	< 1		2	wtb	
355	73	NE	21	2		3	wtb	
069	77	SE	13	< 1		2	wtb	
064	65	SE	25	< 1		2	wtb	
024	80	E	5	< 1		2	wtb	
031	86	E	6	< 1		3	wtb	
020	72	E	5	< 1		2	wtb	
075	84	SE	14	< 1		3	wtb	

240	75	S	32	2		3	wtb	
238	88	S	21	2		2	wtb	
244	89	S	34	3		3	wtb	
220	80	S	17	2		2	wtb	
069	81	SE	42	1		3	wtb	
086	70	SE	14	< 1		2	wtb	
082	89	SE	23	< 1		2	wtb	
344	80	NE	17	2		2	wtb	
357	86	NE	8	1		3	wtb	
058	74	SE	12	< 1		2	wtb	
011	74	E	17	< 1	ca	2	wtb	
023	87	E	12	< 1	ca	3	wtb	
225	74	NW	21	< 1	ca	2	wtb	
174	74	W	10	< 1		2	wtb	
214	79	NW	11			3	wtb	
247	87	NW	15	< 1	ca	2	wtb	
256	77	N	16	1 - 2	ca	3	wtb	
220	75	NW	12	< 1	ca	2	wtb	
157	81	SW	25	< 1	ca	3	wtb	
243	82	NW	16	< 1 - 4		4	wtb	
054	84	SE	24	< 1		2	wtb	
029	85	E	16	< 1 - 3		2	wtb	
132	75	SW	18	< 1 - 2		3	wtb	
012	83	E	21	< 1	ca	2	wtb	
174	85	W	52	< 1		4	wtb	
196	82	W	31	< 1 - 2		3	wtb	
079	86	SE	11	2		2	wtb	
350	59	E	23	< 1		4	wtb	Moose Creek Siltstone
335	59	E	70	< 1		3	itg	
164	76	W	52	< 1		4	wtb	
335	88	E	20	2		3	wtb	
171	47	W	13	2		4	wtb	
002	62	E	6	< 1		3	wtb	
113	65	SW	7	< 1		2	wtb	
177	72	W	10	1		3	wtb	
197	65	W	7	< 1		3	wtb	
153	65	W	31	< 1		4	wtb	
173	58	W	12	< 1		3	wtb	

329	87	E	15	< 1		2	wtb	
184	63	W	27	1		3	wtb	
112	48	SW	5	< 1		2	wtb	
175	68	W	17	2		4	wtb	
151	51	W	24	< 1		3	wtb	
162	63	W	10	2		2	wtb	
138	74	W	13	< 1		3	wtb	
157	83	W	22	2		3	wtb	
184	44	W	29	< 1		2	wtb	
121	47	SW	11	1		3	wtb	
000	88	E	94	3		2	wtb	
171	80	W	34	< 1		3	wtb	
190	76	W	82	2		3	wtb	
187	78	W	58	3		2	wtb	
002	31	E	29	< 1		3	wtb	
178	82	W	70	2		3	wtb	
259	22	N	73	1		3	wtb	
072	76	SE	189	3		3	itg	
100	76	S	47	4		3	wtb	
151	69	SW	25	2	ca	2	wtb	
181	83	W	70	1		3	wtb	
092	68	S	85	< 1		2	itg	
345	35	E	131	< 1	ca	3	wtb	
359	71	E	43	1	ca	3	wtb	
176	59	W	43	1	ca	2	wtb	
182	87	W	52	2	ca	3	wtb	
358	85	E	198	1		3	itg	
266	88	N	223			2	itg	
000	84	E	253			3	itg	
085	84	S	98	2		3	wtb	
252	88	N	225	20-90		3	itg	
243	79	N	192			2	itg	
260	88	N	286	3		2	itg	
002	87	E	280			3	itg	
161	79	SW	101	2		2	wtb	
186	62	W	64	< 1		3	wtb	
182	75	W	13	< 1		3	wtb	
089	75	S	24	2		2	wtb	

072	83	S	37	1		3	wtb	
106	72	SW	49	4		3	wtb	
179	81	W	204		ca film	4	itg	
074	80	SE	32	< 1 - 2		2	wtb	
080	77	E	10	< 1		2	wtb	
089	84	SE	42	< 1		3	wtb	
086	69	SE	39	< 1 - 7	clay	2	wtb	
089	85	SE	36	< 1 - 2	clay	2	wtb	
081	80	SE	23	< 1		1	wtb	
084	71	SE	26	< 1		1	wtb	
255	79	NW	101			3	wtb	
002	71	E	12	< 1		2	wtb	
082	63	SE	57	< 1 - 12	ca	3	wtb	
175	76	W	> 366	< 1 - 20		4	wtb	
086	70	SE	36	< 1 - 2		2	bf	
085	75	SE	28	< 1 - 6		3	bf	
089	71	SE	32	< 1 - 4		1	bf	
324	27	NE	78	< 1 - 5		2	wtb	
304	51	NE	978	< 1 - 13		2	wtb	
061	72	SE	13	< 1		2	wtb	
011	89	E	12	< 1		3	wtb	
039	81	E	16	< 1		2	wtb	
021	84	E	14	< 1		1	wtb	
081	82	SE	24	< 1		2	wtb	
072	78	SE	21	< 1		2	wtb	
087	71	SE	14	< 1		1	wtb	
191	79	W	155		ca film	3	wtb	
068	75	SE	317			4	wtb	
123	64	SW	20	< 1 - 3		3	wtb	
284	87	N	16	< 1		2	wtb	
260	81	N	100	2 - 47		3	wtb	
269	88	N	66	< 1 - 3		3	wtb	
091	84	S	46	< 1 - 2		2	wtb	
119	87	SW	112	< 1 - 11		3	wtb	
116	81	SW	26	< 1		2	wtb	
257	85	NW	73	< 1 - 8		2	wtb	
082	80	S	38			3	wtb	
079	78	S	51	< 1 - 4		3	wtb	

071	85	S	57	< 1 - 2		2	wtb	
259	79	N	37	< 1 - 2		3	wtb	
069	86	SE	17	< 1 - 3	ca	2	wtb	
254	88	N	51	< 1 - 2	ca	2	wtb	
071	89	S	43	< 1		3	wtb	
265	86	N	29	< 1 - 4	iron	2	wtb	
091	84	S	62	< 1 - 3	iron	3	wtb	
261	76	N	186	< 1		2	wtb	
254	83	N	128	< 1		3	wtb	
256	86	N	119	< 1		4	wtb	
249	83	NW	265	< 1 - 3		3	wtb	
291	82	NE	38	< 1		4	wtb	
298	87	NE	155	< 1		3	wtb	
011	60	E	82	< 1		4	wtb	
271	87	N	> 243	< 1		3	wtb	
272	47	N	198	< 1		4	wtb	
260	88	N	140	< 1		4	wtb	
260	87	N	165	< 1		4	wtb	
259	86	N	79	< 1		4	wtb	
254	87	N	125	< 1		3	wtb	
248	86	NW	57	< 1		1	wtb	
261	88	N	171	< 1		4	wtb	
100	67	S	164	< 1		4	wtb	Moose Creek Lodgepole Limestone
101	65	S	48	< 1		4	bf	
301	25	NE	554	< 1 - 8		2	wtb	
215	86	NW	51	< 1 - 4		1	bf	
185	84	W	12	2		1	bf	
065	84	SE	17	< 1 - 2		2	bf	
186	84	W	43	< 1		3	bf	
115	61	SW	48	< 1 - 7		2	bf	
337	65	NE	46	< 1		3	bf	
051	84	SE	46	< 1 - 4		3	bf	
058	86	SE	42	< 1		3	bf	
332	23	NE	63	< 1		2	wtb	
023	81	SE	7	< 1		2	bf	
359	76	E	9	< 1		2	bf	
079	25	SE	17	< 1		2	bf	
088	82	S	71	< 1 - 3		3	bf	

054	81	SE	7	< 1		2	bf	
094	83	S	67			4	bf	
326	30	NE	48	< 1 - 23	ca	2	wtb	
003	81	E	31	< 1 - 12		3	bf	
099	74	S	25	< 1 - 4		4	itg	
184	72	W				2	wtb	Harscrabble Peak Siltstone
158	82	SW	30	1	ca	4	wtb	
160	76	SW	80	1 - 2	ca	2	wtb	
182	61	W	44	< 1	ca	4	wtb	
180	57	W	30	< 1		1	itg	
016	83	E	75	< 1		3	wtb	
004	64	E	32	< 1		4	wtb	
064	85	SE	78	< 1	ca	4	wtb	
071	79	SE	17	< 1	ca	2	wtb	
081	89	S	104	1 - 5		3	wtb	
019	85	E	23	< 1	ca	2	wtb	
179	61	W	81			4	itg	
070	51	SE	92		ca	3	itg	
171	89	W	48	< 1		2	itg	
347	87	E	42	< 1		2	wtb	
358	83	E	49	< 1		2	wtb	
158	75	SW	82			4	itg	
066	79	SE	71			4	itg	
239	79	NW	58			3	itg	
080	90		194	1 - 30		4	itg	Hardscrabble Peak Sandstone
071	85	SE	143	1 - 7	ca	4	wtb	
241	89	SW	97	2 - 11		3	wtb	
091	81	SE	23	< 1		2	itg	
066	83	SE	62	< 1		3	wtb	
049	90		22	< 1		2	wtb	
071	89	SE	42	< 1		4	wtb	
251	87	NW	46	< 1		4	wtb	
018	84	E	17	6		2	wtb	
056	89	SE	9	< 1		3	wtb	
069	87	SE	167	40		3	itg	
070	84	SE	119	1 - 80		2	itg	
073	86	SE	68		ca	3	itg	
287	36	NW	47	20		2	itg	

201	76	W	48	3		2	itg	
190	74	W	27	4		3	wtb	
255	83	NW	64	20		3	itg	
070	62	SE	32	2		2	itg	
072	58	SE	10	< 1	iron?	2	wtb	
063	68	SE	9	< 1		3	wtb	
251	85	NW	85			3	wtb	
011	75	E	67	4		2	wtb	
245	63	NW	29	1 - 4	ca	3	wtb	
059	79	SE	34	4		3	itg	
056	68	SE	16	< 1	ca	3	wtb	
086	73	S	28	< 1		2	wtb	
085	73	S	27	< 1		2	wtb	
159	72	SW	12	< 1	ca	2	wtb	
314	55	NE	17	< 1	ca	2	wtb	
254	88	NW	70	80		4	itg	
251	89	NW	33	< 1		4	itg	
246	89	NW	70	1		2	itg	
022	77	E	18	< 1	ca	3	wtb	
027	80	E	11	< 1	ca	2	wtb	
249	89	NW	32	1- 4	ca	3	wtb	
239	72	NW	47	12 - 30	ca	2	itg	
035	75	E	21	< 1	ca	3	wtb	
029	72	SE	44			3	wtb	
250	77	NW	216			2	itg	
054	80	SE	119	3 - 15		3	itg	
223	86	NW	28	2	ca	2	wtb	
231	69	NW	34	3		2	wtb	
081	11	S	10	2		3	wtb	
061	76	SE	21	< 1	ca	3	wtb	
049	85	SE	12	< 1	ca	2	wtb	
054	86	SE	31	< 1	ca	4	wtb	
053	81	SE	22	< 1	ca	3	wtb	
050	82	SE	51	< 1	ca	3	wtb	
321	41	NE	37	< 1		2	wtb	
025	71	E	11	< 1	ca	3	wtb	
029	76	E	13	< 1	ca	2	wtb	
035	76	SE	18	< 1	ca	4	wtb	

036	76	SE	24	< 1	ca	1	wtb	
244	70	NW	12	< 1	ca	3	wtb	
054	81	SE	3	< 1	ca	2	wtb	
055	85	SE	19	2	ca	3	wtb	
056	75	SE	7	< 1	ca	3	wtb	
061	80	SE	24	< 1		3	wtb	
076	76	SE	27	< 1		2	wtb	
141	78	SW	11	< 1	ca	3	wtb	
311	74	NE	19	< 1	ca	1	wtb	
023	85	E	65	< 1	ca	2	itg	
223	79	NW	32	< 1	ca	3	wtb	
243	74	NW	14	< 1	ca	2	wtb	
243	84	NW	11	< 1	ca	1	wtb	
315	46	NE	15	2		2	wtb	
324	31	NE	16	3		1	wtb	
276	20	N	20	3		2	wtb	
066	70	SE	106			3	itg	
229	69	NW	11	2		2	wtb	
234	69	NW	19	2		2	wtb	
250	21	NW	15	< 1		2	wtb	
342	43	E	22	< 1		3	wtb	
059	73	SE	7	< 1		2	wtb	
091	78	S	13			2	wtb	
359	17	E	27	< 1	ca	2	wtb	
357	27	E	25			3	wtb	
089	70	S	21	2	ca, iron	3	wtb	
219	71	NW	7	< 1	ca	2	wtb	
255	71	NW	13	< 1	ca	2	wtb	
296	55	NE	39	< 1		2	itg	
071	80	SE	177			2	wtb	
054	81	SE	158	67 - 132		3	itg	
032	83	E	131	1 - 26		2	wtb	
073	85	SE	229			3	itg	
325	44	NW	22	1 - 8		2	wtb	
329	35	NW	18	< 1 - 5		3	wtb	
331	40	NW	28	< 1		2	wtb	
336	41	NW	30	< 1		4	wtb	
081	81	SE	27	< 1 - 2	ca bl	3	itg	

072	81	SE	12			3	itg	
301	41	NE	70	2 - 9		3	wtb	
076	33	SE	10	2 - 4		2	wtb	
064	69	SE	20	< 1 - 3		3	wtb	
344	45	NW	55	< 1 - 4	ca	3	wtb	
076	66	SE	23	1 - 2	ca bl	2	wtb	
052	77	SE	43	< 1 - 8		2	wtb	
079	74	SE	8	< 1		3	wtb	
344	41	NE	27	< 1		2	wtb	
065	89	SE	146			4	itg	
321	38	NE	46	< 1 - 3		2	wtb	
311	28	NE	62	< 1 - 4		3	wtb	
164	54	W	39	< 1 - 5		3	wtb	
318	32	NE	47	1 - 4		2	wtb	
309	25	NE	34	< 1 - 2		2	wtb	
142	19	W	46	2 - 6		3	wtb	
174	38	W	64	3 - 7		3	wtb	
310	27	NE	27	< 1 - 2		3	wtb	
156	41	W	55	2 - 8		3	wtb	
139	21	W	47	1 - 6		2	wtb	
324	29	NE	42	< 1 - 3		2	wtb	
151	23	W	64	< 1 - 7		2	wtb	
163	24	W	40	2 - 8		3	wtb	
322	28	NE	38	< 1 - 3		2	itg	
315	27	NE	27	< 1 - 2		3	wtb	
307	31	NW	17	< 1 - 2		2	wtb	
169	51	W	14	2 - 4		3	wtb	
306	45	NE	37	2		2	wtb	
317	29	NE	12	< 1		2	wtb	
323	27	NE	52	< 1 - 3		3	wtb	
307	31	NE	32	< 1 - 4		2	wtb	
315	23	NE	29	< 1 - 2		3	wtb	
231	80	NW	5	4		2	bf	
309	34	NE	52	< 1 - 3		3	wtb	
312	40	NE	31	< 1		2	wtb	
306	24	NE	27	< 1 - 2		2	wtb	
085	73	S	70	4 - 7		3	bf	Hardscrabble Peak
076	80	S	18	< 1 - 2	ca	3	wtb	

076	69	S	34	< 1	ca	2	wtb	Lodgepole Limestone
255	85	NW	47	1 - 3	ca	2	wtb	
355	40	E	23	< 1	ca	3	wtb	
306	62	NE	38	< 1	ca	2	wtb	
042	86	SE	33	< 1	ca	3	wtb	
052	18	SE	13	< 1		2	wtb	
050	66	SE	23	< 1 - 2	ca	3	wtb	
262	66	NW	31	< 1		2	wtb	
298	67	NE	18	< 1 - 3		3	wtb	
058	70	SE	21	< 1 - 2	ca	2	wtb	
309	54	NE	32	< 1 - 4		2	wtb	
301	71	NE	12	< 1		2	wtb	
292	63	NE	17	< 1 - 2		3	wtb	
343	47	NE	42	< 1 - 2	ca	2	wtb	
296	78	NE	16	< 1		2	wtb	
069	69	S	41	< 1		3	wtb	
288	83	NE	24	< 1 - 3		2	wtb	
048	60	SE	12	< 1		4	wtb	
049	81	SE	27	< 1	ca	2	wtb	
071	83	S	24	< 1 - 2	ca	2	wtb	

APPENDIX C

SEISMIC ANISOTROPY CALCULATIONS

Appendix C contains the wave velocity min and maxes for anisotropy % calculations for each averaging model and Thompson Parameters for each model.

Sample	Clay (vol %)	Averaging Model	V_s min (km/s)	V_p max (km/s)	V_p min (km/s)	Anisotropy (%)
C605 A	8.72	Voigt	4.08	7.04	6.76	4.06
		Reuss	3.89	6.70	6.47	3.49
		Hill	3.99	6.87	6.62	3.71
		Geometric	3.97	6.90	6.63	3.99
C605 B	9.87	Voigt	4.03	7.01	6.75	3.78
		Reuss	3.82	6.65	6.39	3.99
		Hill	3.93	6.83	6.57	3.88
		Geometric	3.91	6.86	6.59	4.01
C605 C	4.92	Voigt	4.07	6.39	6.30	1.42
		Reuss	3.93	6.16	6.09	1.14
		Hill	4.00	6.28	6.20	1.28
		Geometric	3.99	6.29	6.20	1.44
R311 A	23.22	Voigt	3.81	6.97	6.49	7.13
		Reuss	3.50	6.39	6.12	4.32
		Hill	3.66	6.69	6.31	5.85
		Geometric	3.63	6.74	6.32	6.43
R311 B	47.19	Voigt	4.11	6.92	6.46	6.88
		Reuss	3.83	6.39	6.02	5.96
		Hill	3.97	6.66	6.25	6.35
		Geometric	3.95	6.69	6.24	6.96
R311 C	54.96	Voigt	3.91	7.35	6.19	17.13
		Reuss	3.55	6.66	5.82	13.46
		Hill	3.73	7.01	6.01	15.36
		Geometric	3.69	7.08	6.00	16.51
R311 D	15.92	Voigt	3.90	6.70	6.41	4.42
		Reuss	3.60	6.21	6.01	3.27
		Hill	3.75	6.46	6.21	3.95
		Geometric	3.73	6.49	6.21	4.41
R311 E	37.29	Voigt	4.00	7.12	6.34	11.59
		Reuss	3.71	6.55	5.99	8.93
		Hill	3.86	6.84	6.17	10.30
		Geometric	3.82	6.89	6.16	11.19
BND 1	53.55	Voigt	3.89	6.89	5.93	14.98

		Reuss	3.50	6.01	5.42	10.32
		Hill	3.70	6.61	5.68	15.13
		Geometric	3.65	6.64	5.65	16.11
BND 2	31.68	Voigt	3.66	6.82	6.16	10.17
		Reuss	3.22	6.09	5.58	8.74
		Hill	3.44	6.47	5.88	9.55
		Geometric	3.40	6.53	5.88	10.48
BMT 2	24.54	Voigt	3.75	6.73	6.04	10.81
		Reuss	3.55	6.33	5.91	6.86
		Hill	3.61	6.60	5.94	10.53
		Geometric	3.64	6.57	5.98	9.40
BMT 3	25.30	Voigt	4.04	6.91	6.67	3.53
		Reuss	3.75	6.43	6.23	3.16
		Hill	3.90	6.67	6.46	3.20
		Geometric	3.87	6.70	6.46	3.65
HSP U	28.61	Voigt	3.97	6.59	6.40	2.93
		Reuss	3.69	6.11	5.97	2.32
		Hill	3.83	6.36	6.19	2.71
		Geometric	3.81	6.38	6.19	3.02
HSP L	16.50	Voigt	4.17	6.38	6.36	0.31
		Reuss	4.01	6.12	6.10	0.33
		Hill	4.09	6.25	6.23	0.32
		Geometric	4.08	6.26	6.24	0.32
HH	6.05	Voigt	4.06	7.04	7.04	0.00
		Reuss	3.87	6.73	6.66	1.05
		Hill	3.96	6.89	6.85	0.58
		Geometric	3.96	6.92	6.89	0.43